Bio-Engineered Skeletal Muscle Tissue and the use of MRI for Cell Tracking and Functional Tissue Analyses

---

Dissertation

zur

Erlangung der naturwissenschaftlichen Doktorwürde
(Dr. sc. nat.)

vorgelegt der

Mathematisch-naturwissenschaftlichen Fakultät

der

Universität Zürich

von

Daniel Keller

aus

Buch (SH)

Promotionskommission

Prof. Dr. Dr. Daniel Eberli (Vorsitz)
Prof. Dr. Jan Krützfeldt
Prof Dr. Markus Rudin
Prof. Dr. Dr. Andreas Boss

Zürich, 2018

Acknowledgements

I would like to thank my family and friends for their support to during the last 3 years, 7 months and 22 days. Without them, a PhD would not have been doable. Special thanks go to Sarah Nötzli, M.Sc., Dr.Jakub Smolar and Dr. Christian Eberhardt who all not only have been great co-workers but also have become awesome friends. I also would like to thank Mara Dedual, M.Sc. and Dr. Tegnane Challa Delassa for the great talks during coffee breaks and lunch time and after work.

I cordially thank Prof. Dr. Dr Eberli and Prof. Dr. Andreas Boss for their commitment and support during my PhD thesis as well as for giving me the chance to enhance my scientific way of thinking. Further, Prof. Dr. Rudin and Prof. Dr. Krützfeldt for their support and inputs at the annual PhD commitee meetings.

Additional thanks go to all members of the Tissue Engineering Research Laboratory, Department of Urology, University Hospital Zurich for their engagement and inputs.

I as well want to thank all that have helped changing my way of thinking, because …

… "the important thing in science is not so much to obtain new facts as to discover new ways of thinking about them."

William Lawrence Bragg (1890 – 1971)

Summary

Urinary continence depends on urine storage in the bladder until voluntarily voidance through a sphincter system. Any interference may lead to involuntary urine leakage bringing along compromised daily activities in combination with exposure to the unpleasant sensation and odor. To date, external urethral sphincter or rhabdosphincter (RS) physiology and anatomy as well as the changes during aging and tissue regeneration are not fully understood. Molecular biology as well as non-invasive imaging might contribute to the full understanding of healthy and diseased tissue and therefore may add to the development of novel therapeutic options and diagnostic tools.

With two studies, we assessed muscle regeneration by multiparametric magnetic-resonance imaging (MRI) on a murine hind limb *tibialis anterior* (TA) muscle crush model, followed by an injection of collagen embedded human muscle precursor cells (MPCs) isolated from the *rectus abdominis* from different donors respectively of collagen only or PBS injection serving as control. MRI assessment of the hind limb using a 4.7T MR Scanner prior to surgery and on post-operatively quantified longitudinal and transverse relaxation times, and the magnetization-transfer ratio (MTR) as well as focusing on diffusion-tensor imaging (DTI) properties such as apparent diffusion coefficient (ADC) and fractional anisotropy (FA) off the regenerating TA muscle. Tissue specimens were histologically examined by hematoxylin-eosin staining and immunohistochemistry.

Neither collagen embedding of human MPCs during stem cell transplantation, nor collagen alone as widely applied scaffold in stem cell research did influence the retrieved MRI parameters delineating muscle regeneration of the TA with increasing longitudinal and transverse relaxation times as well as decreasing MTR. Injected haSSCs form *de novo* muscle tissue *in situ* following a defined pattern in DTI-MRI highlighting the direction of the newly formed fibers. Histological examination proved that all study groups concluded TA regeneration, suggesting that murine MPCs cells contributed significantly to the muscle restoration. Our results show, that this murine TA crush model, ideally with radiation depleted satellite cells, does lend itself for advancing MR methodology for monitoring of stem cell therapy as possible treatment for SUI. These results can easily be transferred to the clinical setting as a non-invasive biomarker for the assessment of muscle tissue regeneration in patients.

Table of Contents

1 Rhabdosphincter: The key element in stress urinary incontinence

This mansucript is ready for submission to Nature Reviews Urology.

Daniel Keller[1,2,3], Jakub Smolar[2,3], Christian Eberhardt[1],

Thomas M. Kessler[4], Andreas Boss[1] and Daniel Eberli[2,3]

*1 Institute of Diagnostic **and** Interventional Radiology, UniversityHospital Zurich, Rämistr. 100, 8091 Zurich, Switzerland;*

2 Department of Urology, UniversityHospital Zurich, Frauenklinikstr. 10, 8091 Zürich, Switzerland;

3 Zurich Center for Integrative Human Physiology (ZIHP), University of Zurich, Winterthurerstr. 190 8057 Zurich Switzerland

4 Department of Neuro-Urology, Balgrist University Hospital, University of Zurich, Forchstrasse 340, 8008 Zürich, Switzerland.

DK and DE contributed to the conception and design of the manuscript. DK performed literature research and wrote the mansuscript. JS, CE, TMK, AB and DE proof-read the manuscript. TMK, AB and DE are guarantors of integrity of the entire manuscript.

Urinary continence depends on urinary storage and voluntary voiding through a sphincter system. Any interference may lead to involuntary urinary leakage bringing along compromised daily activities in combination with exposure to the unpleasant sensation and odor. Conservatively evaluated, urinary incontinence (UI) affects approximately 20% all of women and may be as high as 50%[1–3] causing an estimated annual health care cost of $82.6 billion by 2020 just for the United States. These economic burdens on society and individual patients will increase with the rapidly aging societies[4].

To date, external urethral sphincter or rhabdosphincter (RS) physiology and anatomy as well as the changes during aging and tissue regeneration are not fully understood. Molecular biology as well as non-invasive imaging might contribute to the full understanding of healthy and diseased tissue and therefore may add to the development of novel therapeutic options and diagnostic tools.

1.1 Anatomy and physiology

Continence is achieved by a complex interplay of the internal and external urethral sphincter, bladder neck, urethral smooth muscle, pelvic floor, efferent and afferent nerves, vascular plexus and the surrounding connective tissue. Thereby, the human RS prevents involuntary urine release by providing both resting urethral tonus via slow-twitch fibers and rapid refractory contraction as the abdominal pressure rises. The bladder function is under control of the autonomic (sympathic and parasympathic) and somatic nervous system. The autonomic as well as the somatic nerves hold afferent (sensory) and efferent (motor) functions[5]. The neural component is controlled by cephalic control centers, spinal cord nuclei and infraspinal relay stations and peripheral ganglia terminating as intricate neuroplexuses within the vesicourethral muscle[6,7]. The act of micturition consists of filling, storage and voiding phases, which involve inverse functions of the bladder smooth muscle (detrusor) and the urethra (vesicourethral muscle)[6]: Detrusor relaxation allows urine storage, whereas the contraction leads to urine expel into the urethra[8]; while, the external an internal urethral sphincter relax.

It is still under discussion, whether a progressive, age-dependent decrease of striated muscle cell density followed by continuous loss of striated muscle cells leads to urinary incontinence mediated through apoptosis[9] or whether a compromised nervous control of RS function is the main cause[10] unless physical rupture of the tissue is given. Most common risk factors for female stress urinary incontinence (SUI) are aging, obesity, as well as pregnancy and child birth[11]. Especially the physical damage during vaginal birth,may lead to decreased urethral closure pressure due to damage to the pelvic nerves followed by delayed conduction

in the pudendal nerve or denervation of the pelvic musculature[12]. Whereas type 2 diabetes as well as smoking cause UI is still under discussion[13].

1.1.1 Rhabdosphincter

The human RS is sexually dimorphisitc: the male RS encircles the urethra forming a loop of continuous muscle bundles running along the anterior and lateral aspects of the prostate extending cranially to the bladder neck in a omega-like shape[14] whereas the female RS is semicircular[15] surrounding the middle third of the urethra and is located within the pelvic cavity in the urogenital hiatus of the pelvic diaphragm, and in the perineum[16]. RS is a striated and therefore under voluntary control. It surrounds the smooth muscle of the urethra[17] and contains both slow and fast-twitch fibers. Thereby type 1 muscle fibers are predominant over type 2 muscle fibers where 2A (fast fatigue resistant) fibers are more prevalent than 2B fibers (fast fatigable)[18]. Smooth muscle fibers may interlace the skeletal muscle fibers[16]. Abundant connective tissue and numerous intramuscular nerves without spindles indicate the capacity to produce sustained contractions and to react to stress[19].

Skeletal muscle, is composed of longitudinally aligned cylindrical, multinucleated bundles, so called myofibers, arrayed within sheaths of connective tissue and extracellular matrix (ECM) [20]. The endomysium surrounding single myofibers; the perimysium around muscle bundles and epimysium covering the entire tissue[21]. Main skeletal muscle functions are movement, heat production and energy storage as well as protection of inner organs from physical trauma. Function-specific physiological and biochemical tissue variances control contraction speed, fatigue-resistance and metabolism, mainly through myosin heavy chain isoforms: type I (oxidative slow-twitch), IIA (oxidative fast-twitch), and type IIB (glycolytic fast-twitch); Types IIA / B are the rodent equivalent to human type IIX (glycolytic fast-twitch). In concerns of contraction speed, type I is the slowest, followed by type IIA and IIX/B the fastest[18]. During micturition fiber elasticity and contraction force is reduced for both type I and IIA fibers[22]. Age-related changes in RS anatomy show pathophysiological implications due to decreased urethral support similar to changes in levator ani defects[23]. Different hormonal backgrounds lead to gender-specific fiber architecture and quantity of elastic fibers of the endopelvic fascia. The male endopelvic fascia is multilayered and contains abundant smooth muscle fibers, whereas the female endopelvic fascia is solid, thick, and contains abundant elastic fibers rather than smooth muscle[24].

While little tissue turnover occurs under homeostatic conditions *in vivo*, muscle fibers undergo physiological changes (atrophy, hypertrophy, or fiber type switch) when exposed to excessive physical stress, such as tearing or blunt trauma. Generally, skeletal muscle is able to regenerate from damage to the sarcolemma or myofibrils inflicted by muscle contraction

without inducing an inflammatory response, thus preserving morphological and functional features[25,26]. On contrary, volumetric muscle loss, causes destruction of whole muscle fibrils, fibers or entire muscle segments leading to hypercontraction and followed by muscles loss due to necrosis, apoptosis or autophagy making lager injuries non-reversible as they are often replaced by non-functional fibrotic tissue[27]. Muscle regeneration after injury and necrosis can be separated into three tightly timed phases. Within minutes after the injury, acute inflammation is initiated, lasting for up to 14 days during which invading granulocytes and macrophages secrete chemokines, cytokines, growth factors and potentially damaging cell substrates, such as NO, reactive oxygen species and proteases, therewhile initiating regeneration[28–30]. In parallel, injury-related destruction of the dense vascular network normally supplying the tissue with oxygen and nutrients whilst discarding metabolites direct crosstalk between satellite stem cells (SSC) and the endothelium, ensures a proper coordination of angiogenesis and myogenesis during regeneration[25,31,32]. During this phase angiogenic capillary sprouts invade the damaged muscle tissue to vascularize newly formed myofibers and support their growth orchestrated by activated SSCs (aSSC) and newly emerging myofibers themselves as well as endothelial cells that provide growth factors[33,34], chemokines[35] as well as cytokines[36] while pericytes surround the endothelial cells to stabilize forming neo-vasculature[25]. Vascular endothelial growth factor (VEGF), one of the major factors of angiogenesis[32], which is produced by a variety of cell types is up-regulated during hypoxia in the regenerating muscle and drives endothelial cell chemotaxis, differentiation, proliferation as well as survival. Resident quiescent SSCs (qSSC)[37], located between the sarcolemma and the basal membrane of muscle fibers[38,39] thereby play a regulatory role in the differentiation of committed SSCs and promote their proliferation and myogenic commitment after activation. The differences in the qSSC commitment are controlled by SSCs and niche factors. Responsible for the maintenance of SSC commitment diversity is the orientation of the cell division plane in the SSC niche, e.g. between basal lamina of the muscle fibers and sarcolemma. Planar diffusion herbeby generates two daughter qSSCs, while apical division gives rise to a qSSC and, in case of the daughter cell losing contact with the basal lamina, aSSC[25,40,41]. This process is tightly regulated by the Notch signaling pathway[42] and is important for the maintenance of SSC self-renewal as the lack of Notch signaling leads to myogenic commitment of the SSCs and their transformation into myoblasts. The activation of SSCs can be induced intrinsically[43] or by extrinsic signals, such as muscle injury, leading to the initiation of myogenesis. The activation and subsequent myogenic differentiation of qSSCs is controlled by myogenic regulatory factors (MRFs), such as MYF5, MyoD, myogenin and MRF4. Upon activation, committed SSCs start expressing markers of myogenic commitment, followed by cell migration out of the sub-laminar niche and their differentiation into the fast proliferating myoblasts[44]. After reaching terminal

differentiation, myoblasts withdraw from the cell cycle, elongate and start expressing myosin heavy chain and α-actin. These terminally differentiated myocytes fuse to multinucleated myotubes, further aligning to myofibers and finally forming mature skeletal muscle[45].

Muscle regeneration can be impaired by tissue microenvironment changes, such as chronic inflammation, fibrosis or ageing[40,46] causing a loss of qSSC leading to disturbed self-renewal or loss of tissue homeostasis in response to injury. However, little is known about tissue repair and inflammatory processes in specialized skeletal muscle tissue, such as the RS. Further research performing proteomics and substantial quantification during regeneration using RS biopsies from cystectomy patients or animal models simulating childbirth injuries via vaginal distension (VD), pudendal nerve injuries, anatomic support damage of the pelvic floor including urethrolysis, pubourehtral ligament damage, intraurethral damage such as sphincterectomy or pudendal nerve transaction[47] may help to understand the tissue-specific physiology in future.

1.1.2 Extracellular matrix

The endopelvic fascia and other connective tissue elements of the pelvic floor are at risk of stretch and detachment after childbirth. During pregnancy, the pelvic floor undergoes hormone-mediated physiological changes in its biomechanical properties, resulting in an increased distensiblity of the vagina. Animal models have shown that the vaginal wall and its supportive tissue complex is more distensible and less stiff during pregnancy[48]. This process is mediated by increased synthesis of collagen and elastin by fibroblasts. Collagen and elastin are two main components of the extracellular matrix of the connective tissue. Collagen determines the tensile strength while elastin contributes to the tissues' stretch ability. Collagen is the major structural component contributing to 1-10% of the tissue dry weight. Type I and fibrillar types I and III collagens are predominate in adult endo-, peri-, and epimysium[20]. Fibroblasts, sensitive to mechanical stretch, adapt connective tissue synthesis proportional to the degree of stretch.

Connective tissue remodeling after vaginal delivery is mediated via the upregulation of ECM genes, such as elafin (a elastase-specific protease inhibitor), keratin 16, collagen type XVII, plakophilin 1 (a desmosome-related protein)in vaginal tissue of women with stress urinary incontinence[49]. These changes in collagen and elastin synthesis and degradation influence tissue stiffness. However, it is yet unanswered, whether these changes are the cause or the result of SUI[48] and must be investigated with specific gene knockout animal model. Excessive stretching of the vaginal wall initiates a degradative response mediated by release of collagenases from activated fibroblasts. This results in increased degradation of collagen, as well as other constituents of the vaginal wall. Thus, difficult or prolonged labor may

exceed the stretch limits of the soft tissue, causing imbalance in the reparative and degradative processes and increasing susceptibility of pelvic floor supportive structures to birth trauma[50]. Allover, the content and spatial organization of collagen subtypes are the key factors of tissue strength and elasticity and therefore, collagen synthesis and metabolism likely has a effect on tissue functionality, micturition control and continence[51]. Besides giving organizational support to the skeletal muscle architecture, the ECM plays an important biomechanicistic role participating in the signaling cascade connecting the neuromuscular junctions[52] and protecting remaining muscle mass after overload injury via increased mechanical stability[53]. Despite the many biological adaptions to vaginal childbirth including muscle fiber elongation, increased collagen synthesis in the intramuscular ECM[54] and changes in pelvic floor muscle tissue stiffness due to glycosylated crosslink changes[55], the pelvic floor tissue is prone to injury as delivery-related mechanical strains cause acute sarcomere elongation[56]. Women with SUI have lower endopelvic collagen content[57]. Collagen is cleaved extracellularly from pro-collagen precursor molecules[58]. It is under discussion whether lower collagen levels in SUI arise from increased degradation, decreased biosynthesis, or both. Whilst Rechenberger et al. suggest lower collagen content due to a decrease in collagen biosynthesis[57], Chen et. al. indicate that lower collagen content in the endopelvic fascia and skin of women with SUI is not due to changes in collagen synthesis[58] and Kushner et al. suggest increased collagenolytic activity compared to healthy controls[59]. Periurethral vaginal tissues from incontinent women expresses less tissue inhibitors of metalloproteinase (TIMPs) compared to healthy tissue whereas active metalloproteinases (MMPs) are expressed similarly. Interestingly the TIMP expression from fibroblasts correlates with estradiol levels whereas MMP expression is not altered by estradiol levels[60]. As ECM metabolism is modulated by reproductive hormones[61–63] the phase of menstrual cycle in which biological specimens are collected is of crucial importance to be able to differentiate between hormonal and disease-derived alterations[64] which may explain the different findings on collagen expression and turnover: Lower gene expression of fibrillin-1 in SUI whereas no significant changes for collagen I, collagen III, fibromodulin and fibulin-5 occurred[65]. Comparison of rat urethral striated muscle and ECM morphological characteristics has shown that mild diabetes mellitus and pregnancy can lead to a time-dependent disorder and tissue remodeling compared to virgin animals[66] seen by the increase in total collagen area, fibrosis and loss of total fiber number and fast twitch fibers amongst other morphological changes. Chen et al. reported, that the balance between MMPs and TIMPs defining collagen turnover is in favour of protein expression in the vaginal wall of SUI and pelvic prolapse patients[67]. Urinary proteomics in female SUI patients revealed an overexpression of plasma serine protease inhibitor, leucine-rich alpha-2-glycoprotein, lysosomal alpha-glucosidase, and peptidyl-prolyl-cis-trans isomerase A, and lower expression of uromodulin, which forms

forms high-molecular weight filaments that constitute the matrix of hyaline casts[68], and TALPID3, a regulator of centrosome and cell polarity[69] as well as collagen I (strength), III (elasticity) and V (function unknown), which are cleaved by MMP-1,8-13 (interstitial collagen / type I and III) and MMP-2 and 9 which degrade elastin and cleaved collagen into amino acids[46]. Analysis of vaginal wall tissue from SUI patients compared to menstrual-cycle matched withc continent women shows changes in decorin, fibromodulin an biglycan. In addtion para-urethral ECM proteoglycans binding to collagen and growth factors, further play a crucial role in cell proliferation, migration and adhesion and tissue elasticity, in a hormonal and continence dependent manner[70]. Protein and gene expression analysis support the nerve-mediated pelvic tissue degeneration as a cause of SUI development as neurodegeneration-linked proteins APOE, GRB2, and GBA are upregulated in post-menstrual SUI patients compared to continent women[64]. Collagen synthesis in endopelvic fascia is not altered in female stress urinary incontinence[58] while collagen marker levels in women with SUI suggest a reduced collagen turnover[51]. Cohort analysis of primiparous female rats with experimentally induced SUI showed an increase of Smad2, mmp13 and smooth muscle inhibitor Rgs2 in the incontinent rats further highlighting the roles of inflammation, collagen breakdown, and smooth muscle inhibition as important factors in SUI development[71]. Moreover, the expression of elastin and lysyl oxidase family genes in murine urogenital tissues of decreases with aging[72].

1.1.3 Innervation and functionality

Skeletal muscle contraction is known to be controlled by a calcium-dependent structural change in the actin-containing thin filaments. The action potential in a motor nerve that triggers an action potential in a muscle cell membrane at the neuromuscular junction leads to an intracellular calcium concentration increase: calcium binds to troponin in the actin-containing thin filaments and the resulting structural changes in the thin filament allow myosin motors from the thick filaments to bind to actin and generate muscle contraction[73,74]. Deficient RS activity may be of neurological or non-neurological origin[75]. During muscle regeneration, re-innervation of the damaged tissue begins from the surrounding healthy tissue and directly defines the type of myofibers to emerge during the tissue regeneration, e.g. either slow- or fast-twitch fibers[76]. Motor neurons control the contraction of skeletal muscle via neuromuscular junctions (NMJ) and neurotransmitter release, such as acetylcholine[37]. Furthermore, motor neurons are responsible for growth factor production, especially via the NMJ that are capable of governing the behavior of SSCs in their activation and proliferation[77]. Motor axons in peripheral nerves have the capacity to regenerate after injury, but fully functional motor recovery rarely occurs in clinics. Recent findings suggest a critical time window of 1 month after injury in which full neuronal functionality may be

restored[78]. Electrical stimulation, exercise or their combination may enhance peripheral nerve regeneration after injury[79,80]. The urethral pressure as defined by the International Continence Society as the fluid pressure needed to just open a closed urethra[81] and hence, the urethral pressure profile (UPP) indicates RS activity. In SUI, the lower pressure required for urine outflow is an indicator for unvoluntary leakages. Both passive urethral pressure profile measures as well as the valsalva leak point pressures correlate with some severity measures of stress incontinence[82]. Another method to assess the functionality and therefore the innervation of the RS is video-urodynamics, wherein filling and voiding of the bladder is measured. However, even when performed under "good urodynamic practice", urodynamics is prone to false positve results showin pathological findings in symptom-free healths subjects[83]. RS electromyography (EMG) of the striated urethral sphincter permits detection of individual motor unit action potentials and is a valuable diagnostic tool in the evaluation of voiding disorders[84]. The EMG of the pelvic floor to assess RS neurophiosology can either be performed using patch electrodes but also EMG of the rhabdosphincter using needle electrodes. Whilst the urinary bladder and urethra are innervated by all three neural systems – sympathetic, parasympathetic and somatic – the RS is under control of the somatic nervous system. The pudendal nerve is a mixed nerve composed of sensory, motor, and autonomic fibers[85]. After the release of norephidrine, a excitatory α-adrenergic response leads to an increase in muscular tonus, whereby the bladder outflow is inhibited[86]. In humans, the RS gets its input through somatic and autonomic pathways. Besides voluntary control, there is evidence of a sympathetic reflex whereby bladder stretching results in the stimulation of β-adrenergic receptors in the detrusor that enhance bladder relaxation and inhibit parasympathetic activity. The question, whether this bilateral innervations is crucial for proper functioning remains unclear to date. Originating from the Onuf nucleus in the sacral spinal cord from the S2–S4 nerve roots via the pudendal nerve, signal transduction in men follows nerve of the penis after it splits from the pudendal nerve[87,88]. In the female RS, the intrapelvic somatic fibers along the anterior vaginal wall supply the pelvic floor[89]]. The urethral muscles receive somatic information from the pudendal nerve entering from the perineum. Dual somatic innervation of the RS is suggested as are branches from the perineal nerve and an intrapelvic component that course nearby to the pelvic nerve[90] so that the afferent nerve fibers from the proximal urethra mainly pass through the pelvic plexus, whereas the afferent innervation of the distal urethra is provided by the pudendal nerve[91].

In both females and males, the striated muscle tissue is intervened by the vagina and prostate, respectively[92]. To date, the precise innervation of the RS in either sex remains particularly unclear. However, it is well confirmed that the internal urinary sphincter (smooth muscle tissue) and the RS get dual response from the pelvic and pudendal nerve. Descriptive anatomical studies on the male RS shows innervation via axons from the pelvic

nerve and dual innervation from an intrapelvic branch and a perineal branch of the pudendal nerve[92,93]. Large axon bundles surrounded by perineurium have been detected within the RS. These bundles are themselves encircled by Schwann cells, contain between 1 and 3 axons forming autonomic adrenergic nerve ends and surface junctions with the striated muscle of the RS[94].

Pudendal nerve transections (PNT) decrease contraction amplitude and voided volume, and increase in contraction duration and residual volume[95]. Pudendal nerve is particularly vulnerable to injury during VD[96]. Compression and stretching, damage to the fascia, ligaments and pelvic floor muscles during childbirth are a result of neuropathic changes. As a result levator ani muscle may fail to reflexively contract and elevate sphincter pressure during a cough or sneeze[97]. PNT unlike VD shows no recovery of leak-point pressure (LPP) whereas striated muscle tissue does not alter significantly[98]. In females suffering from urinary retention, which contrary to SUI is described as voiding difficulty, urethral closure pressure and urethral sphincter volume are increased[99]. Histopathological examination of women with SUI in combination with pelvic floor prolapse revealed an increased density of collagen, decreased hexosaminidase activity without changes in glycosaminoglycans[100]. However, to date it is not possible to argue that a change in collagen structure or quantity by itself cause SUI.

1.2 Therapeutic options

Currently rehabilitation of skeletal muscle function includes vaginal pressaries[101] physical, pharmaceutical or interventional treatment options[102,103]. However, these methods show tremendous patient-to-patient variability and only limited success. Whilst interventional attempts relying on synthetic materials have been heavily condemned due to severe complications and limited success. The field of tissue engineering (TE) combining materials science, chemistry, biology and medicine[104–108] in order to develop tissue-like structures[109] in vitro with the aim to implant these constructs into the body to repair an injury or replace the function of a failing organ may solve the problem.

Conservative treatment options for SUI includes injectable or implantable bulking agents (e.g.[110,111]) or sling surgery but risk of reoperation is common[112,113] and certain materials such as Mersilene may cause a chronic inflammatory response[114] of the surrounding tissue showing an increased risk of rejection.

Pelvic floor muscle exercise or physiotherapy is a preferred frontline therapy as it strengthens the pelvic floor muscle and improves RS efficiency non-invasively[115] either through voluntary contractions[116], vaginal weight cones[117] or electromagnetic stimulation[118].

Exercise can reduce severity of SUI symptoms in conceiving women[119]. However, the variances between the applied exercise protocols complicate comparisons. Success therefore may be enhanced through telephone calls or feedback of exercising effectiveness[120]. Animal studies suggest that immediate electromagnetic stimulation after denervation leads to more effective recovery than delayed application[121]. In case of VD, this would suggest that immediate post-delivery intervention might prevent neurodegeneration. However, this assumption must be tested in a clinical environment.

1.2.1 Tissue Engineering and cell therapy

The overall goal of TE is to incorporate the bioengineered tissue into the surrounding tissue to form a functional unit and result in a final, purely biological substitute to re-establish tissue function[4,104,105]. For instance, injection of autologous cartilage cells as bulking agents into the bladder neck and trigone region to correct anatomical deformities has been performed successfully in patients with urinary incontinence[106] and vesicoureteral reflux[107]. Notexin injection into the female rat RS and subsequent analysis of cells, has shown that satellite cells within the RS contribute to tissue regeneration in the same manner as in other skeletal muscle tissue[122].

The majority of SSCs are committed to the myogenic lineage[123] and are therefore most suitable for muscle bioengineering. These cells can be isolated from muscle biopsies, grown in culture and re-implanted into an injured or weakened muscle, where they lead to structural reconstruction and improve contractile function[124,125]. SSCs can be isolated from patients of all ages and both sexes, forming new muscle tissue in a time-dependent manner[126]. Depending on the patterns of cell division in stem cell lineages, a mother cell can divide into two cells of the same fate (symmetric division) or to two daughter cells of separate fate (asymmetric division)[127]. In contrary to embryonic stem cell (ESC) or induced pluripotent stem cells (ipSC), for adult stem cells there is no tumorogenicy documented and compared to ESC no ethical concerns exist[128,129].

Besides finding a suitable cell source, appropriate scaffolds for the extracellular environment is required. The scaffold should serve as a temporary structure that will degrade or resorb and become replaced by the host[109]. Tissue scaffolds typically purposes on or several of the following characteristics providing a surface for cell attachment or migration, an assembly of biochemical factors enhancing growth, innervation or cell guidance; porosity enabling diffusion of nutrients and stability mimicking the critical aspects of the *in vivo* setting[130]. aSSCs treatment has the potential to become the first treatment to restore RS muscle function[123,131,132] by mimicking the tissue response upon injury. Animal studies have demonstrated the applicability of cell therapy for the treatment of SUI and other acquired

myopathies[131–136] and ongoing clinical trials are trying to confirm these results for patient application using both muscle[137–144] and adipose[145–148] tissue- derived stem cells in women and men. Clinical trials with UI patients, using autologous cells showed no signs of rejection or other side effects so far, proving that the application of for skeletal muscle regeneration is feasible, safe and ready for the “bench to bedside” transfer. A comparison of male RS muscle cells and other skeletal muscle tissue has shown high degree of similarity in membrane properties[149].

The proof of long term sphincter restoration or even the replenishment of the stem cell pool; that tissue homeostasis and response to recurring tissue damage and acute inflammation will be guaranteed, is still undescribed. Moreover, it still is under debate, whether improved continence after cell therapy is due to functional differentiation of injected stem cells or whether a systemic cytokine-controlled effects triggers the regeneration of the RS[150]: Besides improved continence measured after injection of stem cells[139,140,143,151] homing of stem cells after perineal application or directly due to injury-related signaling factors has been emphasized. The combination of physical therapy, such as by electrical stimulation, might enhance the outcome of cell therapy due to upregulation of the cytokines CXCL12 and CCL7 resulting in an increase of muscle regeneration in a model of a chronic large anal sphincter injury[152]. To ensure muscle functionality and to obtain complete muscle regeneration, muscle tissue has to be properly re-innervated after damage as lack of innervation leads to progressive muscle atrophy. It has been shown that myoblast differentiation and subsequent fusion into myotubes occurs faster when the neuronal network controlling muscle contraction is undamaged compared to non-functional motor neurons[153].

1.3 Imaging

The best spatial resolution and contrast to image cells in a biological environment is provided microscopy imaging. However, most such methods require a post-biopsy processed tissue sample and therefore are invasive. Furthermore current microcopy technology is limited by tissue penetration depth below millimeter-range. The few devices available for clinics focus on imaging of ectopic easy accessible tissues such as skin, cornea or retina. Hence, access to both healthy and diseased tissue via cadavers[154] or suitable animal models are needed to overcome this issue. However, for the comparison of human tissue with animal models, normalization tools such as architectural difference indexes parameterizing a combined measure are required. Parameters such as sarcomere-length-to-optimal-sarcomere ratio, fiber-to-muscle-length ratio, and fraction of total pelvic floor muscle mass and physiological cross-sectional area are used full tools[155] besides standardized termiology, testing procedures and well matched diagnostic instruments[156]. Alternatively, non-invasive imaging

may be used. However, X-ray and computed tomography (CT), because of low sotft tissue contrast, as well as positron emission tomography (PET) and single-photon emission computed tomography (SPECT) due to radioligand accumulation in the urinary bladder, are unsuitable despite the general potential to asses skeletal muscle physiology such as insulin sensitivity, VO_2 max[157] or glucose metabolism[158] but also cell tracking[159–162] and viability[163] detection after myoblast transfer therapy(MTT). In comparison, modern magnetic resonance imaging (MRI) and ultrasound (US) scanner technology, allow the tracking of cells in clusters allowing the imaging of unlabeled single cells and small cell aggregates[164] or the study of ECM and describe the tissue anatomy.

T1, T2 weighted as well as dynamic MRI allow to post-operatively asses the position of the slings, but contrast is dependent on the sling material[165,166] or bulking agents and allow the assessment of structural changes[167] as well as the visualization of pelvic floor anatomy through multiplanar localizer, axial and coronal T2 fast spin echo (FSE)[168] or damage after childbirth and allows an association with SUI[169,170]. Using T2-weighted MRI of the urethra and the surrounding ligaments as example, we are able to distinguish whether SUI in any given patient is due failure of the supporting tissue or sphincter deficiency[171]. Diffusion-weighteed MRI (DW-MRI) with the thereon computed apparent diffusion coefficient (ADC) maps may allow the detection of ischemia and may be used to identify edemas after surgical intervention. Anatomical findings by MRI or neurophysiological findings by EMG indicate, a connection of RS shortening and poorer pelvic floor muscle function such as shorter amplitude, duration of motor unit action potentials (MUP) with decreased turns and worse MUP recruitment during bladder filling[23,172,173]. Intravaginal EMG (partially in combination with endorectal probes) has enabled the mapping of the innervation zones of the pelvic floor and RS muscles[174]. MR neurography sequences applied to fresh cadaver specimen before and after surgical marking of different nerve segments could easily detect the proximal pudendal nerve. However, MR pudendal nerve neurography is prone to poor spatial resolution and signal to noise ratio on wide field-of-view imaging, inhomogeneous fat suppression, nerve branching variations, and surrounding vessels, especially in the setting of pelvis venous congestion[85] but still can be interpreted by experienced radiologist[175]. Van der Jagt et. al. have shown feasibility of diffusion tensor imaging (DTI) and fiber tractography to study the nerves of the sacral plexus in humans *in vivo* and to assess the architectural configuration and microstructural properties of these peripheral nerves including the pudendal nerve[176]. MR angiography, such as time-of-flight, phase-contrast, or contrast-enhanced methods, such as susceptibility weighted imaging or blood-oxygen-level dependent functional MRI have not been tested for RS imaging to date.

Imaging after cell therapy is the most demanding, as not only the anatomical restoration is of interest, but also the fate of the cells or the implant. Magnetizaiton Tranfer imaging (MT) has been demonstrated to be of value for a variety of applications including the evaluation of skeletal muscle pathologies[177] muscle damage and repair over time upon myotoxin injection in the mouse hind leg[178] and can be used to follow-up differentiation of injected muscle precursor cells[179] as a biomarker of the quantity and quality of muscle fiber formation[179]. Furthermore, superparamagnetic iron oxide nanoparticles, can be used track muscle regeneration after cell therapy without negative effects on the functionality of the bioengineered muscle[180] while applications of DWI and DTI represent promising tools to monitor including the muscle[181–184] visualization of variations in diffusion reveals tissue microstructure and its architectural organization, which allows following fiber-tract trajectories in fibrous tissues[185]. MR imaging relaxation and diffusion measurements can be used as potential biomarkers for non-invasive in vivo monitoring of the myogenic differentiation process from muscle precursor cells to mature skeletal muscle tissue in muscle cell therapy[186]. Age-related changes in tissue composition can be shown via high-resolution MR spectroscopy (MRS) as demonstrated in mice[187] but to date, there is no data available on MR spectrcopic studies for the RS metabolism. Whilst tissue stiffness has been documented for various skeletal muscle tissue[188], the pelvic floor has not been analyzed to date, elastin specific MR contrast agents (ESMA)[189,190], DW-MRI and dynamic contrast-enhanced MRI (DCE-MRI)[191] might upbring new insights.

Transurethral US enables the visualization the anatomical arrangement and contractions of the RS loop, scar formation for patients with postoperative SUI[14]. Intraurethral US allows clear visualization of voluntary contractions and RS configuration during micturition including measurement of RS thickness and estimate the grade of fibrosis and lipomatosis[192,193]. Overall, US corresponds to urodynamic parameters giving rise to new diagnostic tools[194] as it has shown that primi- and multipara have decreased numbers of elastic fibers compared to nullipara, most probably as an effect from severe tissue damage after childbirth in combination with impaired regeneration[195]. Data about vascularization of the RS and the surrounding tissue has been obtained from the use of US contrast agents and intraurethral US devices allowing the estimation of blood volume and flow[196]. Furthermore, Doppler US enables visualizing the urethral vasculature involved in the mechanism of urethral closure[197]. Thereby it could be shown that compared to continent nullipara, continent multipara have a significant reduction in vascularity[198]. Siracusano et al. showed blood volume and blood flow decreased with age but no changes in velocity in pre- and postmenopausal women after contrast-agent enhanced US[196]. In future, elastography either using US or MRI might be established for the pelvic floor and help to give information on tissue inflammation, and fibrosis as well as changes in stiffness of tissue by assessing the propagation of mechanical

waves through the tissue with a special magnetic resonance imaging technique. In case of US[199] and MR elastography shear waves generated within the tissue are acquired via MRI and post-processed to generate quantitative maps of tissue stiffness, the so called elastograms[200]. Shear wave US elastography[201] may give further insights into, ECM changes and measurement of tissue elasticity with reflecting collagen contents[202]. This may be supported with elastin-specific MR contrast agents[203] or endoruethral sonography similarly performed as endoanal US[204]. Considering the emerging role of the pelvic floor ECM in SUI, imaging the mechanical properties of the tissue surrounding the RS may be important to track the disease progression, recognize indications of disease development and monitor the progression of recovery.

1.4 Outlook

Besides conservative approaches, several clinical trials on myoblast transfer therapy (e.g. [138,140]) in order to overcome SUI have been performed during the last decade or are currently being performed currently. These studies focus surgical attempts using novel slings, pharmaceuticals, physiotherapy or cell therapy. According to clinicaltrials.gov currently arround 70 studies are ongoing or rectruiting patients for various therapeutics inverventions. However, the outcome of these trials is difficult to compare due to small cohort size, short evaluation periods or different cell sources (muscle-derived stem cells, adipose tissue-derived stem cells, cord blood stem cells or total nucleated cells) and number of injected cells [205]. Furthermore all those clinical studies have different parameters to evaluate the outcome of their trial. Hence, it is important to introduce a standard evaluation systems followed strictly by all clinical trials and basic research projects focusing on SUI.

1.5 Conclusions

The RS is the key element in SUI which affects the lives of millions of people worldwide and imposes a substantial economic burden on every health care system. It is still unclear which is the key factor causing RS deficiency as innervation, stem cell senesence as well as the ECM contribtue to healthy tissue homeostasis and are altered in disease state such as SUI. Due to the high impact on tissue functionality, neither genomics, transcriptomic, proteomic or metabolic data is available for healthy and injured RS at any age class, sex or type of functionality loss and hinder detailed research to date. Besides getting tissue samples en passant of cystectomy or prostatectomy, non-invasive imaging could support the understanding of disease development and the processes of subsequent therapy. Therapeutics interventions vary from surgical applications of slings supporting the pelvic floor structures, pharmaceuticals physioherapy and tissue engineering approaches. However, due

to no standarisation in the evaluation of the trials, it is difficult to compare the success of these studies.

1.6 References

1. Brown JS, Nyberg LM, Kusek JW, et al. Proceedings of the national institute of diabetes and digestive and kidney diseases international symposium on epidemiologic issues in urinary incontinence in women. *Am J Obstet Gynecol*. 2003;188(6):S77-S88.
2. Nygaard IE, Heit M. Stress urinary incontinence. *Obstet Gynecol*. 2004;104(3):607-620.
3. Dooley Y, Kenton K, Cao G, et al. Urinary incontinence prevalence: results from the National Health and Nutrition Examination Survey. *J Urol*. 2008;179(2):656-661.
4. Coyne KS, Wein A, Nicholson S, Kvasz M, Chen C-I, Milsom I. Economic burden of urgency urinary incontinence in the United States: A systematic review. *J Manag Care Pharm*. 2014;20(2):130-140.
5. Miftahof RN, Nam HG. *Biomechanics of the Human Urinary Bladder*. Berlin, Heidelberg: Springer Berlin Heidelberg; 2013.
6. Elbadawi A. Functional anatomy of the organs of micturition. *Urol Clin North Am*. 1996;23(2):177-210.
7. Elbadawi A, Resnick NM, Dörsam J, Yalla S V, Haferkamp A. Structural basis of neurogenic bladder dysfunction. I. Methods of prospective ultrastructural study and overview of the findings. *J Urol*. 2003;169(2):540-546.
8. Tasian G, Cunha G, Baskin L. Smooth muscle differentiation and patterning in the urinary bladder. *Differentiation*. 2010;80(2-3):106-117.
9. Strasser H, Tiefenthaler M, Steinlechner M, Eder I, Bartsch G, Konwalinka G. Age dependent apoptosis and loss of rhabdosphincter cells. *J Urol*. 2000;164(5):1781-1785.
10. Gössl C, Miller K. Urinary incontinence and the rhabdosphincter. Lancet. 2000; 355(9203):578.
11. Luber KM. The definition, prevalence, and risk factors for stress urinary incontinence. *Rev Urol*. 2004;6 Suppl 3: S3-9.
12. Ashton-Miller JA, Howard D, DeLancey JO. The functional anatomy of the female pelvic floor and stress continence control system. *Scand J Urol Nephrol Suppl*. 2001;(207):1-7; 106-25.
13. Danforth KN, Townsend MK, Lifford K, Curhan GC, Resnick NM, Grodstein F. Risk factors for urinary incontinence among middle-aged women. *Am J Obstet Gynecol*. 2006;194(2):339-345..
14. Strasser H, Frauscher F, Helweg G, Colleselli K, Reissigl A, Bartsch G. Transurethral Ultrasound: Evaluation of anatomy and function of the rhabdosphincter of the male urethra. 1998:100-105.
15. Colleselli K, Stenzl A, Eder R, Strasser H, Poisel S, Bartscg G. The female urethral sphincter: a morphological and topographical study. *J Urol*. 1998;160(1):49-54.
16. Oelrich TM. The striated urogenital sphincter muscle in the female. *Anat Rec*. 1983;205(2):223-232.
17. Keane DP, O'Sullivan S. Urinary incontinence: anatomy, physiology and pathophysiology. *Best Pract Res Clin Obstet Gynaecol*. 2000;14(2):207-226.
18. Sumino Y, Sato F, Kumamoto T, Mimata H. Striated muscle fiber compositions of human male urethral rhabdosphincter and levator ani. *J Urol*. 2006;175(4):1417-1421..
19. Schrøder HD, Reske-Nielsen E. Fiber types in the striated urethral and anal sphincters. *Acta Neuropathol*. 1983;60(3-4):278-282.
20. Gillies AR, Lieber RL. Structure and function of the skeletal muscle extracellular matrix. *Muscle Nerve*. 2011;22(2):1-23.
21. Zhang C, Gao Y. Finite element analysis of mechanics of lateral transmission of force in single

muscle fiber. *J Biomech*. 2012;45(11):2001-2006.

22. Ochala J, Frontera WR, Dorer DJ, Hoecke J V., Krivickas LS. Single Skeletal Muscle Fiber Elastic and Contractile Characteristics in Young and Older Men. *Journals Gerontol Ser A Biol Sci Med Sci*. 2007;62(4):375-381.

23. Morgan DM, Umek W, Guire KE, Morgan HK, Garabrant A, DeLancey JO. Urethral sphincter morphology and function with and without stress incontinence. *J Urol*. 2009;182(1):203-209.

24. Hinata N, Murakami G. The Urethral Rhabdosphincter , Levator Ani Muscle , and Perineal Membrane : A Review. *Biomed Res Int*. 2014;2014.

25. Ceafalan LC, Popescu BO, Hinescu ME. Cellular players in skeletal muscle regeneration. *Biomed Res Int*. 2014;2014:957014.

26. Siegel AL, Atchison K, Fisher KE, Davis GE, Cornelison DDW. 3D timelapse analysis of muscle satellite cell motility. *Stem Cells*. 2009;27(10):2527-2538.

27. Sicari BM, Rubin JP, Dearth CL, et al. An acellular biologic scaffold promotes skeletal muscle formation in mice and humans with volumetric muscle loss. *Sci Transl Med*. 2014;6(234):234-58.

28. Huard J, Li Y, Fu FH. Muscle injuries and repair: current trends in research. *J bone Jt Surg*. 2002;84-A(5):822-832.

29. Stratos I, Rotter R, Eipel C, Mittlmeier T, Vollmar B. Granulocyte-colony stimulating factor enhances muscle proliferation and strength following skeletal muscle injury in rats. *J Appl Physiol*. 2007;103(5):1857-1863.

30. Eming SA, Wynn TA, Martin P. Inflammation and metabolism in tissue repair and regeneration. *Science*. 2017;356(6342):1026-1030.

31. Tonnesen MG, Feng X, Clark R a F. Angiogenesis in wound healing. *J Investig Dermatol Symp Proc*. 2000;5(1):40-46.

32. Kleinheinz SJ and J. *Regenerative Medicine and Tissue Engineering*. (Andrades JA, ed.). InTech; 2013.

33. Ten Broek RW, Grefte S, Von den Hoff JW. Regulatory factors and cell populations involved in skeletal muscle regeneration. *J Cell Physiol*. 2010;224(1):7-16.

34. Christov C, Chrétien F, Abou-Khalil R, et al. Muscle Satellite Cells and Endothelial Cells: Close Neighbors and Privileged Partners. *Mol Biol Cell*. 2007;18(4):1397-1409.

35. Deshmane SL, Kremlev S, Amini S, Sawaya BE. Monocyte chemoattractant protein-1 (MCP-1): an overview. *J Interferon Cytokine Res*. 2009;29(6):313-326.

36. Abou-Khalil R, Mounier R, Chazaud B. Regulation of myogenic stem cell behavior by vessel cells: the “ménage à trois” of satellite cells, periendothelial cells and endothelial cells. *Cell Cycle*. 2010;9(5):892-896.

37. Mauro A. Satellite cell of skeletal muscle fibers. *J Biophys Biochem Cytol*. 1961;9:493-495.

38. Schultz E, Gibson MC, Champion T. Satellite cells are mitotically quiescent in mature mouse muscle: an EM and radioautographic study. *J Exp Zool*. 1978;206(3):451-456.

39. Ontell M, Feng KC, Klueber K, Dunn RF, Taylor F. Myosatellite cells, growth, and regeneration in murine dystrophic muscle: a quantitative study. *Anat Rec*. 1984;208(2):159-174.

40. Bentzinger CF, Wang YX, Dumont N a, Rudnicki M a. Cellular dynamics in the muscle satellite cell niche. *EMBO Rep*. 2013;14(12):1062-1072.

41. Wang YX, Rudnicki M a. Satellite cells, the engines of muscle repair. *Nat Rev Mol Cell Biol*. 2012;13(2):127-133.

42. Brack AS, Conboy IM, Conboy MJ, Shen J, Rando T a. A temporal switch from notch to Wnt signaling in muscle stem cells is necessary for normal adult myogenesis. *Cell Stem Cell*. 2008;2(1):50-59.

43. Danieli-Betto D, Peron S, Germinario E, et al. Sphingosine 1-phosphate signaling is involved in skeletal muscle regeneration. *Am J Physiol Cell Physiol*. 2010;298(3):C550-8.

44. Beauchamp JR, Heslop L, Yu DS, et al. Expression of CD34 and Myf5 defines the majority of quiescent adult skeletal muscle satellite cells. *J Cell Biol*. 2000;151(6):1221-1234.

45. Tidball JG, Villalta SA. Regulatory interactions between muscle and the immune system during muscle regeneration. *Am J Physiol Regul Integr Comp Physiol*. 2010;298(5):R1173-87.

46. Mann CJ, Perdiguero E, Kharraz Y, et al. Aberrant repair and fibrosis development in skeletal muscle. *Skelet Muscle*. 2011;1(1):21.

47. Jiang H-H, Damaser MS. Animal Models of Stress Urinary Incontinence. In: *Handbook of Experimental Pharmacology*. NIH Public Access; 2011:45-67.

48. Memon HU, Handa VL. Vaginal childbirth and pelvic floor disorders. *Womens Heal (l Engl)*. 2013;9(3):1883-1889.

49. Chen B, Wen Y, Zhang Z, Guo Y, Warrington JA, Polan ML. Microarray analysis of differentially expressed genes in vaginal tissues from women with stress urinary incontinence compared with asymptomatic women. *Hum Reprod*. 2006;21(1):22-29.

50. Cannon TW, Wojcik EM, Ferguson CL, Saraga S, Thomas C, Damaser MS. Effects of vaginal distension on urethral anatomy and function. *BJU Int*. 2002;90(4):403-407.

51. Edwall L, Carlström K, Jonasson AF. Markers of collagen synthesis and degradation in urogenital tissue from women with and without stress urinary incontinence. *Neurourol Urodyn*. 2005;24(4):319-324.

52. Purslow PP. The structure and functional significance of variations in the connective tissue within muscle. *Comp Biochem Physiol A Mol Integr Physiol*. 2002;133(4):947-966.

53. Corona BT, Wu X, Ward CL, McDaniel JS, Rathbone CR, Walters TJ. The promotion of a functional fibrosis in skeletal muscle with volumetric muscle loss injury following the transplantation of muscle-ECM. *Biomaterials*. 2013;34(13):3324-3335.

54. Alperin M, Lawley DM, Esparza MC, Lieber RL. Pregnancy-induced adaptations in the intrinsic structure of rat pelvic floor muscles. *Am J Obstet Gynecol*. 2015;213(2):191.e1-191.e7.

55. Alperin M, Kaddis T, Pichika R, Esparza MC, Lieber RL. Pregnancy-induced adaptations in intramuscular extracellular matrix of rat pelvic floor muscles. *Am J Obstet Gynecol*. 2016;215(2):210.e1-210.e7.

56. Catanzarite T, Bremner S, Barlow CL, Bou-Malham L, O'Connor S, Alperin M. Pelvic muscles' mechanical response to strains in the absence and presence of pregnancy-induced adaptations in a rat model. *Am J Obstet Gynecol*. 2018;218(5):512.e1-512.e9.

57. Rechberger T, Postawski K, Jakowicki JA, Gunja-Smith Z, Woessner J. Role of fascial collagen in stress urinary incontinence. *Am J Obstet Gynecol*. 1998;179(6 I):1511-1514.

58. Chen Y, DeSautel M, Anderson A, Badlani G, Kushner L. Collagen synthesis is not altered in women with stress urinary incontinence. *Neurourol Urodyn*. 2004;23(4):367-373.

59. Kushner L, Mathrubutham M, Burney T, Greenwald R, Badlani G. Excretion of collagen derived peptides is increased in women with stress urinary incontinence. *Neurourol Urodyn*. 2004;23(3):198-203.

60. Chen B, Wen Y, Wang H, Polan ML. Differences in estrogen modulation of tissue inhibitor of matrix metalloproteinase-1 and matrix metalloproteinase-1 expression in cultured fibroblasts from continent and incontinent women. *Am J Obstet Gynecol*. 2003;189(1):59-65.

61. Jackson S, James M, Abrams P. The effect of oestradiol on vaginal collagen metabolism in postmenopausal women with genuine stress incontinence. *BJOG An Int J Obstet Gynaecol*. 2002;109(3):339-344.

62. Wen Y, Polan ML, Chen B. Do extracellular matrix protein expressions change with cyclic reproductive hormones in pelvic connective tissue from women with stress urinary incontinence? *Hum Reprod*. 2006;21(5):1266-1273.

63. Shynlova O, Bortolini MAT, Alarab M. Genes responsible for vaginal extracellular matrix metabolism are modulated by women's reproductive cycle and menopause. *Int braz j urol*. 2013;39(2):257-267.

64. Tong J, Lang J, Zhu L. Microarray analysis of differentially expressed genes in vaginal tissues in postmenopausal women. The role of stress urinary incontinence. *Int Urogynecol J*. 2010;21(12):1545-1551.

65. Westergren Söderberg M, Byström B, Hammarström M, Malmström A, Ekman-Ordeberg G. Decreased Gene Expression of Fibrillin-1 in Stress Urinary Incontinence. *Neurourol Urodyn*. 2010;29:476-481.

66. Piculo F, Marini G, Barbosa AMP, et al. Urethral striated muscle and extracellular matrix morphological characteristics among mildly diabetic pregnant rats: Translational approach. *Int Urogynecol J*. 2014;25(3):403-415.

67. Chen B, Yeh J. Alterations in connective tissue metabolism in stress incontinence and prolapse. *J Urol*. 2011;186(5):1768-1772.

68. Devuyst O, Olinger E, Rampoldi L. Uromodulin: from physiology to rare and complex kidney disorders. *Nat Rev Nephrol*. 2017;13(9):525-544.

69. Koch M, Mitulovic G, Hanzal E, et al. Urinary proteomic pattern in female stress urinary incontinence: a pilot study. *Int Urogynecol J*. 2016;27(11):1729-1734.

70. Wen Y, Zhao YY, Li S, Polan ML, Chen BH. Differences in mRNA and protein expression of small proteoglycans in vaginal wall tissue from women with and without stress urinary incontinence. *Hum Reprod*. 2007;22(6):1718-1724.

71. Lin G, Shindel AW, Banie L, et al. Molecular mechanisms related to parturition-induced stress urinary incontinence. *Eur Urol*. 2009;55(5):1213-1222.

72. Jiang Y, Zong W, Luan H, et al. Decreased expression of elastin and lysyl oxidase family genes in urogenital tissues of aging mice. *J Obstet Gynaecol Res*. 2014;40(8):1998-2004.

73. Irving M. Regulation of Contraction by the Thick Filaments in Skeletal Muscle. *Biophys J*. 2017;113(12):2579-2594.

74. Linari M, Brunello E, Reconditi M, et al. *Force Generation by Skeletal Muscle Is Controlled by Mechanosensing in Myosin Filaments*. Nature Publishing Group; 2015.

75. De Leval J, Chantraine A, Penders L. [The striated sphincter of the urethra. 3: Urodynamic and physiopathologic study of the striated sphincter]. *J Urol (Paris)*. 1984;90(8-9):529-551.

76. Zhou Z, Cornelius CP, Eichner M, Bornemann A. Reinnervation-induced alterations in rat skeletal muscle. *Neurobiol Dis*. 2006;23(3):595-602.

77. Hawke TJ, Garry DJ. Myogenic satellite cells: physiology to molecular biology. *J Appl Physiol*. 2001;91(2):534-551. http://www.ncbi.nlm.nih.gov/pubmed/11457764. Accessed April 20, 2015.

78. Sakuma M, Gorski G, Sheu SH, et al. Lack of motor recovery after prolonged denervation of the neuromuscular junction is not due to regenerative failure. *Eur J Neurosci*. 2016;43(3):451-462.

79. Gordon T, English AW. Strategies to promote peripheral nerve regeneration: Electrical stimulation and/or exercise. *Eur J Neurosci*. 2016;43(3):336-350.

80. Xu C, Kou Y, Zhang P, et al. Electrical stimulation promotes regeneration of defective peripheral nerves after delayed repair intervals lasting under one month. *PLoS One*. 2014;9(9):e105045.

81. Klarskov N, Loses G. Urethral Pressure Reflectometry and Pressure Profilometry in Health Volunteers ans Stress Urinary Incontinent Women. *Neurourol Urodyn*. 2008;27:807-812.

82. Theofrastous JP, Bump RC, Elser DM, Wyman JF, McClish DK. Correlation of urodynamic measures of urethral resistance with clinical measures of incontinence severity in women with pure genuine stress incontinence. The Continence Program for Women Research Group. *Am J Obstet Gynecol*. 1995;173(2):407-12; discussion 412-4

83. Leitner L, Walter M, Sammer U, Knüpfer SC, Mehnert U, Kessler TM. Urodynamic Investigation: A Valid Tool to Define Normal Lower Urinary Tract Function? Shore N, ed. *PLoS One*. 2016;11(10):e0163847.

84. Olsen AL, Benson JT, McClellan E. Urethral sphincter needle electromyography in women:

comparison of periurethral and transvaginal approaches. *Neurourol Urodyn*. 1998;17(5):531-535

85. Wadhwa V, Hamid AS, Kumar Y, Scott KM, Chhabra A. Pudendal nerve and branch neuropathy: Magnetic resonance neurography evaluation. *Acta radiol*. 2017;58(6):726-733.

86. Nambiar AK, Lucas MG. Pathophysiology of urinary incontinence. *Surg*. 2014;32(6):279-285.

87. Binder MD, Hirokawa N, Windhorst U, eds. Pelvic Floor. In: *Encyclopedia of Neuroscience*. Berlin, Heidelberg: Springer Berlin Heidelberg; 2009:3097.

88. Martellucci J, Weil EHJ, Matzel K. *Electrical Stimulation for Pelvic Floor Disorders*.; 2015.

89. Thor KB, de Groat WC. Neural control of the female urethral and anal rhabdosphincters and pelvic floor muscles. *Am J Physiol Regul Integr Comp Physiol*. 2010;299(2):R416-38.

90. Heesakkers JPFA, Gerretsen RRR. Urinary incontinence: sphincter functioning from a urological perspective. *Digestion*. 2004;69(2):93-101.

91. Kessler TM, Studer UE, Burkhard FC. Increased proximal urethral sensory threshold after radical pelvic surgery in women. *Neurourol Urodyn*. 2007;26(2):208-212.

92. Hollabaugh RS, Steiner MS, Dmochowski RR. Neuroanatomy of the female continence complex: Clinical Implications. *Urology*. 2001;57(2):382-388.

93. Hollabaugh RS, Dmochowski RR, Steiner MS. Neuroanatomy of the male rhabdosphincter. *Urology*. 1997;49(3):426-434.

94. Kumagai A, Koyanagi T, Takahashi Y. The innervation of the external urethral sphincter; An ultrastructural study in male human subjects. *Urol Res*. 1987;15(1):39-43.

95. Peng C, Chen JJ, Chang H, Groat WC de, Cheng C. External Urethral Sphincter Activity in a RatModel of Pudendal Nerve Injury. *Neurourol Urodyn*. 2006;25:388-396.

96. Damaser MS, Broxton-King C, Ferguson C, Kim FJ, Kerns JM. Functional and neuroanatomical effects of vaginal distention and pudendal nerve crush in the female rat. *J Urol*. 2003;170(3):1027-1031.

97. Fonti Y, Giordano R, Cacciatore A, Romano M, La Rosa B. Post partum pelvic floor changes. *J Prenat Med*. 2009;3(4):57-59.

98. Lin Y-H, Liu G, Li M, Xiao N, Daneshgari F. Recovery of continence function following simulated birth trauma involves repair of muscle and nerves in the urethra in the female mouse. *Eur Urol*. 2010;57(3):506-512.

99. Wiseman OOJ, Swinn MMJ, Brady CMC, Fowler CCJ. Maximum urethral closure pressure and sphincter volume in women with urinary retention. *J Urol*. 2002;167(3):1348-51; discussion 1351-2.

100. Suzme R, Yalcin O, Gurdol F, Gungor F, Bilir A. Connective tissue alterations in women with pelvic organ prolapse and urinary incontinence. *Acta Obstet Gynecol Scand*. 2007;86(7):882-888.

101. Al-Shaikh G, Syed S, Osman S, Bogis A, Al-Badr A. Pessary use in stress urinary incontinence: a review of advantages, complications, patient satisfaction, and quality of life. *Int J Womens Health*. 2018;Volume 10:195-201.

102. Baoge L, Van Den Steen E, Rimbaut S, et al. Treatment of Skeletal Muscle Injury: A Review. *ISRN Orthop*. 2012;2012:1-7.

103. Bø K. Pelvic floor muscle training in treatment of female stress urinary incontinence, pelvic organ prolapse and sexual dysfunction. *World J Urol*. 2012;30(4):437-443.

104. Atala A. Tissue engineering for the replacement of organ function in the genitourinary system. *Am J Transplant*. 2004;4:58-73.

105. De Filippo R, Yoo JJ, Atala A. Engineering of Vaginal Tissue in Vivo. *Tissue Eng Part A*. 2003;9(2):301-306.

106. Cols AA y. De novo reconstitution of a functonal mamilian urinary bladder by tissue engineering". *Nat Biotechnol*. 1999;17(2):144-155.

107. Kershen RT, Fefer D, Atala A. Tissue-engineered therapies for the treatment of urinary incontinence and vesicoureteral reflux. *World J Urol*. 2000;18:51-55.

108. Paltiel HJ, Diamond DA, Zurakowski D, Drubach LA, Atala A. Endoscopic Treatment of Vesicoureteral Reflux with Autologous Chondrocytes: Postoperative Sonographic Features 1. *Radiology*. 2004;232:390-397.

109. Atala A, Kasper FK, Mikos AG. Engineering complex tissues. *Sci Transl Med*. 2012;4(160):160rv12.

110. Lightner D, Calvosa C, Andersen R, et al. A new injectable bulking agent for treatment of Stress Urinay Incontinence: Results of a Mulitcenter, randomized, controlled, double-blind study of Durasphere, Urology. 2001 Jul;58(1):12-5.

111. Pycha A, Klingler CH, Haitel A, Heinz-Peer G, Marberger M. Implantable Microballoons: An Attractive Alternative in the Management of Intrinsic Sphincter Deficiency. *Eur Urol*. 1998;33(5):469-475.

112. Olsen AL, Smith VJ, Bergstrom JO, Colling JC, Clark AL. Epidemiology of surgically managed pelvic organ prolapse and urinary incontinence. *Obstet Gynecol*. 1997;89(4):501-506.

113. Clark AL, Gregory T, Smith VJ, Edwards R. Epidemiologic evaluation of reoperation for surgically treated pelvic organ prolapse and urinary incontinence. *Am J Obstet Gynecol*. 2003;189(5):1261-1267.

114. Falconer C, Söderberg M, Blomgren B, Ulmsten U. Influence of different sling materials on connective tissue metabolism in stress urinary incontinent women. *Int Urogynecol J*. 2001;12(SUPPL. 2):S19-S23.

115. Berghmans LCM, Hendriks HJM, Bø K, et al. Conservative treatment of stress urinary incontinence in women: a systematic review of randomized clinical trials. *Br J Urol*. 1998;82:181-191.

116. Hay-Smith E, Bø K, Berghmans L, Hendriks H, de Bie R, van van Waalwijk DE. Pelvic floor muscle training for urinary incontinence in women. In: Hay-Smith J, ed. *Cochrane Database of Systematic Reviews*. Chichester, UK: John Wiley & Sons, Ltd; 2001:CD001407.

117. Bo K. Vaginal weight cones. Theoretical framework, effect on pelvic floor muscle strength and female stress urinary incontinence. *Acta Obs Gynecol Scand*. 1995;74(2):87-92.

118. Voorham-van der Zalm PJ, Pelger RCM, Stiggelbout AM, Elzevier HW, Lycklama à Nijeholt GAB. Effects of magnetic stimulation in the treatment of pelvic floor dysfunction. *BJU Int*. 2006;97(5):1035-1038.

119. Sangsawang B, Serisathien Y. Effect of pelvic floor muscle exercise programme on stress urinary incontinence among pregnant women. *J Adv Nurs*. 2012;68(9):1997-2007.

120. Haddow G, Watts R, Robertson J, et al. Effectiveness of a pelvic floor muscle exercise program on urinary incontinence following childbirth. *Int J Evid Based Healthc*. 2005;3(5):103-146..

121. Koh ES, Kim HC, Lim JY. The effects of electromyostimulation application timing on denervated skeletal muscle atrophy. *Muscle and Nerve*. 2017;56(6):E154-E161.

122. Yiou R, Lefaucheur JP, Atala A. The regeneration process of the striated urethral sphincter involves activation of intrinsic satellite cells. *Anat Embryol (Berl)*. 2003;206(6):429-435.

123. Benchaouir R, Rameau P, Decraene C, et al. Evidence for a resident subset of cells with SP phenotype in the C2C12 myogenic line: a tool to explore muscle stem cell biology. *Exp Cell Res*. 2004;294(1):254-268.

124. Eberli D, Aboushwareb T, Soker S, Yoo JJ, Atala A. Muscle precursor cells for the restoration of irreversibly damaged sphincter function. *Cell Transpl*. 2012;21(9):2089-2098.

125. Stölting M, Hefermehl L, Tremp M, Azzabi F, Sulser T, Eberli D. 173 Impact of patient age or gender on bioengineering of functional muscle tissue using muscle precusor cells. *J Urol*. 2011;185(4):e72.

126. Stolting MN, Hefermehl LJ, Tremp M, et al. The role of donor age and gender in the success of human muscle precursor cell transplantation. *J Tissue Eng Regen Med*. 2017;11(2):447-458.

127. Morrison SJ, Shah NM, Anderson DJ. Regulatory Mechanisms in Stem Cell Biology. *Cell*. 1997;88:287-298.

128. Liu Z, Tang Y, Lü S, et al. The tumourigenicity of iPS cells and their differentiated derivates. *J Cell Mol Med*. 2013;17(6):782-791.

129. Stölting MNL, Ferrari S, Handschin C, et al. Myoblasts inhibit prostate cancer growth by paracrine secretion of tumor necrosis factor-α. *J Urol*. 2013;189(5):1952-1959.

130. Berthiaume F, Maguire TJ, Yarmush ML. Tissue engineering and regenerative medicine: history, progress, and challenges. *Annu Rev Chem Biomol Eng*. 2011;2(1):403-430.

131. Nikolavasky D, Stangel-Wójcikiewicz K, Stec M, Chancellor MB. Stem cell therapy: a future treatment of stress urinary incontinence. *Semin Reprod Med*. 2011;29(1):61-70.

132. Yiou R, Yoo JJ, Atala A. Restoration of functional motor units in a rat model of sphincter injury by muscle precursor cell autografts. *Transplantation*. 2003;76(7):1053-

133. Gussoni E, Soneoka Y, Strickland CD, et al. Dystrophin expression in the mdx mouse restored by stem cell transplantation. *Nature*. 1999;401(6751):390-394.

134. Léobon B, Garcin I, Menasche P, et al. Myoblasts transplanted into rat infarcted myocardium are functionally isolated from their host. *Proc Natl Acad Sci USA*. 2003;100(13):7808-7811.

135. Jin M-H, Yokoyama U, Sato Y, et al. DNA microarray profiling identified a new role of growth hormone in vascular remodeling of rat ductus arteriosus. *J Physiol Sci*. 2011;61(3):167-179.

136. Lee JY, Cannon TW, Pruchnic R, Fraser MO, Huard J, Chancellor MB. The effects of periurethral muscle-derived stem cell injection on leak point pressure in a rat model of stress urinary incontinence. *Int Urogynecol J Pelvic Floor Dysfunct*. 2003;14(1):31-37.

137. Gerullis H, Eimer C, Georgas E, et al. Muscle-Derived Cells for Treatment of Iatrogenic Sphincter Damage and Urinary Incontinence in Men. *Sci World J*. 2012;2012:1-6. 138. Peters KM, Dmochowski RR, Carr LK, et al. Autologous muscle derived cells for treatment of stress urinary incontinence in women. *J Urol*. 2014;192(2):469-476.

139. Carr LK, Steele D, Steele S, et al. 1-Year Follow-Up of Autologous Muscle-Derived Stem Cell Injection Pilot Study To Treat Stress Urinary Incontinence. *Int Urogynecol J Pelvic Floor Dysfunct*. 2008;19(6):881-883.

140. Carr LK, Robert M, Kultgen PL, et al. Autologous muscle derived cell therapy for stress urinary incontinence: a prospective, dose ranging study. *J Urol*. 2013;189(2):595-601.

141. Sèbe P, Doucet C, Cornu J-N, et al. Intrasphincteric injections of autologous muscular cells in women with refractory stress urinary incontinence: a prospective study. *Int Urogynecol J*. 2011;22(2):183-189.

142. Cornu J-N, Lizée D, Pinset C, Haab F. Long-term Follow-up After Regenerative Therapy of the Urethral Sphincter for Female Stress Urinary Incontinence. *Eur Urol*. 2014;65(1):256-258. doi:10.1016/J.EURURO.2013.09.022.

143. Stangel-Wojcikiewiczellor MB. Cellular therapy for treatment of stress urinary incontinence. *Curr Stem Cell Res Ther*. 2010;5(1):57-62.

144. Blas myoblast injections with electrical stimulation for stress urinary incontinence. *Int J Gynecol Obstet*. 2012;117(2):164-167.

145. Yamamoto T, Gotoh M, Kato M, et al. Periurethral injection of autologous adipose-derived regenerative cells for the treatment of male stress urinary incontinence: Report of three initial cases. *Int J Urol*. 2012;19(7):652-659.

146. Kuismanen K, Sartoneva R, Haimi S, et al. Autologous Adipose Stem Cells in Treatment of Female Stress Urinary Incontinence: Results of a Pilot Study. *Stem Cells Transl Med*. 2014;3(8):936-941.

147. Choi JY, Kim TH, Yang JD, Suh JS, Kwon TG. Adipose-Derived Regenerative Cell Injection Therapy for Postprostatectomy Incontinence: A Phase I Clinical Study. *Yonsei Med J*. 2016;57(5):1152-1158.

148. Gotoh M, Yamamoto T, Kato M, et al. Regenerative treatment of male stress urinary

incontinence by periurethral injection of autologous adipose-derived regenerative cells: 1-year outcomes in 11 patients. *Int J Urol*. 2014;21(3):294-300.

149. Berjukow S, Margreiter E, Marksteiner R, Strasser H, Bartsch G, Hering S. Membrane properties of single muscle cells of the rhabdosphincter of the male urethra. *Prostate*. 2004;58(3):238-247.

150. Gill BC, Sun DZ, Damaser MS. Stem Cells for Urinary Incontinence: Functional Differentiation or Cytokine Effects? *Urology*. 2018..

151. Cornu JN, Doucet C, Sèbe P, et al. Évaluation prospective du traitement de l'incontinence urinaire post-prostatectomie par injections intrasphinctériennes de cellules musculaires autologues. *Prog en Urol*. 2011;21(12):859-865.

152. Sun L, Yeh J, Xie Z, Kuang M, Damaser MS, Zutshi M. Electrical Stimulation Followed by Mesenchymal Stem Cells Improves Anal Sphincter Anatomy and Function in a Rat Model at a Time Remote from Injury. In: *Diseases of the Colon and Rectum*.Vol 59.; 2016:434-442.

153. Czerwinska AM, Streminska W, Ciemerych MA, Grabowska I. Mouse gastrocnemius muscle regeneration after mechanical or cardiotoxin injury. *Folia Histochem Cytobiol*. 2012;50(1):144-153.

154. Chen BH, Wen Y, Li H, Polan ML. Collagen metabolism and turnover in women with stress urinary incontience and pelvic prolapse. *Int Urogynecol J Pelvic Floor Dysfunct*. 2002;13(2):80-87.

155. Alperin M, Tuttle LJ, Conner BR, et al. Comparison of pelvic muscle architecture between humans and commonly used laboratory species. *Int Urogynecol J*. 2014;25(11):1507-1515.

156. Luginbuehl H, Baeyens J-P, Taeymans J, Maeder I-M, Kuhn A, Radlinger L. Pelvic Floor Muscle Activation and Strength Components Influencing Female Urinary Continence and Stress Incontinence: A Systematic Review. *Neurourol Urodyn*. 2015;34(5):498-506.

157. Nuutila P, Knuuti MJ, Mäki M, et al. Gender and insulin sensitivity in the heart and in skeletal muscles. Studies using positron emission tomography. *Diabetes*. 1995;44(1):31-36.

158. Müller MJ, Selberg O, Burchert W. Use of positron emission tomography (PET) in the assessment of skeletal muscle glucose metabolism. *Z Ernahrungswiss*. 1997;36(4):359-363.

159. Haralampieva D, Salemi S, Dinulovic I, et al. Human muscle precursor cells overexpressing PGC-1 α enhance early skeletal muscle tissue formation. *Cell Transplant*. 2017;26(6):1103-1114.

160. Haralampieva D, Betzel T, Dinulovic I, et al. Noninvasive PET Imaging and Tracking of Engineered Human Muscle Precursor Cells for Skeletal Muscle Tissue Engineering. *J Nucl Med*. 2016;57(9):1467-1473. doi:10.2967/jnumed.115.170548.

161. Haralampieva DG, Ametamey SM, Sulser T, Eberli D. Non-Invasive Imaging Modalities for Clinical Investigation in Regenerative Medicine. In: *Cells and Biomaterials in Regenerative Medicine*.; 2014.

162. Elster JL, Rathbone CR, Liu Z, et al. Skeletal muscle satellite cell migration to injured tissue measured with 111In-oxine and high-resolution SPECT imaging. *J Muscle Res Cell Motil*. 2013;34(5-6):417-427.

163. Smith GT, Wilson TS, Hunter K, et al. Assessment of skeletal muscle viability by PET. *J Nucl Med*. 1995;36(8):1408-1414.

164. Chen Y, Dodd SJ, Tangrea MA, Emmert-Buck MR, Koretsky AP. Measuring collective cell movement and extracellular matrix interactions using magnetic resonance imaging. *Sci Rep*. 2013;3:1-9.

165. Giri SK, Drumm J, Wallis F, Flood H. Postoperative magnetic resonance imaging characterization of slings for female stress urinary incontinence. *Neurourol Urodyn*. 2011;30(1):108-112.

166. Rinne K, Kainulainen S, Aukee S, Heinonen, S, Nilsson, CG. Dynamic MRI confirms support of the mid-urethra by TVT and TVT-O surgery for stress incontinence. *Acta Obstet Gynecol Scand*. 2011;90(6):629-635.

167. Tunn R, Schuettoff SA, Gauruder-Burmester A, Beyersdorff D. Changes in the MRI morphology of the stress continence control system after TVT (tension-free vaginal tape) insertion. *Eur J Obstet Gynecol Reprod Biol*. 2007;131(2):209-213.

168. Macura KJ, Genadry R, Borman TL, Mostwin JL, Lardo AC, Bluemke DA. Evaluation of the female urethra with intraurethral magnetic resonance imaging. *J Magn Reson Imaging*. 2004;20(1):153-159.

169. Kearney R, Miller JM, Ashton-Miller JA, DeLancey JOL. Obstetric factors associated with levator ani muscle injury after vaginal birth. *Obstet Gynecol*. 2006;107(1):144-149.

170. Ashton-Miller JA, Delancey JOL. On the biomechanics of vaginal birth and common sequelae. *Annu Rev Biomed Eng*. 2009;11:163-176.

171. Macura KJ. Magnetic resonance imaging in assessment of stress urinary incontinence in women: Parameters differentiating urethral hypermobility and intrinsic sphincter deficiency. *World J Radiol*. 2015;7(11):394.

172. Kenton K, Mueller E, Brubaker L. Continent women have better urethral neuromuscular function than those with stress incontinence. *Int Urogynecol J*. 2011;22(12):1479-1484.

173. Takahashi S, Homma Y, Fujishiro T, Hosaka Y, Kitamura T, Kawabe K. Electromyographic study of the striated urethral sphincter in type 3 stress incontinence: evidence of myogenic-dominant damages. *Urology*. 2000;56(6):946-950.

174. Peng Y, He J, Khavari R, Boone TB, Zhang Y. Functional mapping of the pelvic floor and sphincter muscles from high-density surface EMG recordings. *Int Urogynecol J*. 2016;27(11):1689-1696.

175. Chhabra A, McKenna CA, Wadhwa V, et al. 3T magnetic resonance neurography of pudendal nerve with cadaveric dissection correlation. *World J Radiol*. 2016;8(7):700.

176. van der Jagt PKN, Dik P, Froeling M, et al. Architectural configuration and microstructural properties of the sacral plexus: A diffusion tensor MRI and fiber tractography study. *Neuroimage*. 2012;62(3):1792-1799.

177. McDaniel JD, Ulmer JL, Prost RW, et al. Magnetization transfer imaging of skeletal muscle in autosomal recessive limb girdle muscular dystrophy. *J Comput Assist Tomogr*. 1999;23(August):609-614.

178. Feng S, Chen D, Kushmerick M, Lee D. Multiparameter MRI analysis of the time course of induced muscle damage and regeneration. *J Magn Reson imaging*. 2014;40(4):779-788.

179. Rottmar M, Haralampieva D, Salemi S, et al. Imaging to Monitor Muscle Tissue Formation during Myogenic in Vivo Differentiation of Muscle Precursor Cells 1. *Radiology*. 2016;281(2):436-443.

180. Azzabi F, Rottmar M, Jovaisaite V, et al. Viability, Differentiation Capacity, and Detectability of Super-Paramagnetic Iron Oxide-Labeled Muscle Precursor Cells for Magnetic-Resonance Imaging. *Tissue Eng Part C*. 2015;21(2):182-191.

181. Rousset P, Delmas V, Buy J-N, Rahmouni A, Vadrot D, Deux J-F. In vivo visualization of the levator ani muscle subdivisions using MR fiber tractography with diffusion tensor imaging. *J Anat*. 2012;221(3):221-228.

182. Sinha S, Sinha U, Malis V, Bhargava V, Sakamoto K, Rajasekaran M. Exploration of male urethral sphincter complex using diffusion tensor imaging (DTI)-based fiber-tracking. *J Magn Reson Imaging*. 2018:1-10.

183. Zijta FM, Froeling M, van der Paardt MP, et al. Feasibility of diffusion tensor imaging (DTI) with fibre tractography of the normal female pelvic floor. *Eur Radiol*. 2011;21(6):1243-1249.

184. Okamoto Y, Kemp GJ, Isobe T, et al. Changes in diffusion tensor imaging (DTI) eigenvalues of skeletal muscle due to hybrid exercise training. *Magn Reson Imaging*. 2014;32(10):1297-1300.

185. Basser PJ, Basser PJ, Jones DK, Jones DK. Diffusion-tensor MRI: theory, experimental design and data analysis - a technical review. *NMR Biomed*. 2002;15(7-8):456-467.

186. Chuck NC, Azzabi Zouraq F, Rottmar M, et al. MR Imaging Relaxometry Allows Noninvasive Characterization of in Vivo Differentiation of Muscle. *Radiology*. 2015;000(0):1-10.

187. Sobolev AP, Mannina L, Costanzo M, Cisterna B, Malatesta M, Zancanaro C. Age-related changes in skeletal muscle composition: A pilot nuclear magnetic resonance spectroscopy study in mice. *Exp Gerontol*. 2017;92:23-27.

188. Ringleb SI, Bensamoun SF, Chen Q, Manduca A, An K-N, Ehman RL. Applications of magnetic resonance elastography to healthy and pathologic skeletal muscle. *J Magn Reson Imaging*. 2007;25(2):301-309.

189. Makowski MR, Anne Preissel Þ, von Bary C, et al. Three-Dimensional Imaging of the Aortic Vessel Wall Using an Elastin-Specific Magnetic Resonance Contrast Agent. 2012.

190. Protti A, Lavin B, Dong X, et al. Assessment of Myocardial Remodeling Using an Elastin/Tropoelastin Specific Agent with High Field Magnetic Resonance Imaging (MRI). *J Am Heart Assoc*. 2015;4(8):e001851.

191. Wegner CS, Gaustad J-V, Andersen LMK, Simonsen TG, Rofstad EK. Diffusion-weighted and dynamic contrast-enhanced MRI of pancreatic adenocarcinoma xenografts: associations with tumor differentiation and collagen content. *J Transl Med*. 2016;14(1):161.

192. Klauser A, Frauscher F, Strasser H, et al. Age-related rhabdosphincter function in female urinary stress incontinence: assessment of intraurethral sonography. *J Ultrasound Med*. 2004;23(5):631-7; quiz 638-9.

193. Reimers K, Reimers CD, Wagner S, Paetzke I, Pongratz DE. Skeletal muscle sonography: A correlative study of echogenicity and morphology. *J Ultrasound Med*. 1993;12(2):73-77.

194. Heit M. Intraurethral Ultrasonography: Correlation of Urethral Anatomy with Functional Urodynamic Parameters in Stress Incontinent Women. *Int Urogynecol J*. 2000;11:204-211.

195. Hirata E, Koyama M, Murakami G, et al. Comparative histological study of levels 1-3 supportive tissues using pelvic floor semiserial sections from elderly nulliparous and multiparous women. *J Obstet Gynaecol Res*. 2011;37(1):13-23.

196. Siracusano S, Bertolotto M, Cucchi A, et al. Application of Ultrasound Contrast Agents for the Characterization of Female Urethral Vascularization in Healthy Pre- and Postmenopausal Volunteers: Preliminary Report. *Eur Urol*. 2006;50(6):1316-1322.

197. Siracusano S, Bertolotto M, D'Aloia G, Silvestre G, Stener S. Colour doppler ultrasonography of female urethral vascularization in normal young volunteers: A preliminary report. *BJU Int*. 2001;88(4):378-381.

198. Lone F, Sultan AH, Stankiewicz A, Thakar R, Wieczorek A. Vascularity of the urethra in continent women using colour doppler high-frequency endovaginal ultrasonography. *Springerplus*. 2014;3(1):619.

199. Gennisson J-L, Deffieux T, Macé E, Montaldo G, Fink M, Tanter M. Viscoelastic and Anisotropic Mechanical Properties of in vivo Muscle Tissue Assessed by Supersonic Shear Imaging. *Ultrasound Med Biol*. 2010;36(5):789-801.

200. Mariappan YK, Glaser KJ, Ehman RL. Magnetic resonance elastography: A review. *Clin Anat*. 2010;23(5):497-511.

201. Arda K, Ciledag N, Aktas E, Aribas BK, Köse K. Quantitative assessment of normal soft-tissue elasticity using shear-wave ultrasound elastography. *Am J Roentgenol*. 2011;197(3):532-536.

202. Hauge A, Wegner CS, Gaustad J-V, Simonsen TG, Andersen LMK, Rofstad EK. Diffusion-weighted MRI-derived ADC values reflect collagen I content in PDX models of uterine cervical cancer. *Oncotarget*. 2017;8(62):105682-105691.

203. Makowski MR, Wiethoff AJ, Blume U, et al. Assessment of atherosclerotic plaque burden with an elastin-specific magnetic resonance contrast agent. *Nat Med*. 2011;17(3):383-388.

204. Albuquerque A. Endoanal ultrasonography in fecal incontinence: Current and future perspectives. *World J Gastrointest Endosc*. 2015;7(6):575-581..

205. Aragón IM, Imbroda BH, Lara MF. Cell Therapy Clinical Trials for Stress Urinary Incontinence: Current Status and Perspectives. *Int J Med Sci*. 2018;15(3):195-204.

References

References

2 Non-invasive monitoring of skeletal muscle regeneration after human-derived myoblast transfer therapy in mouse hind limb via diffusion-tensor imaging

Submitted to PlosOne. The manuscript is currently under revision by the journal.

Daniel Keller[1,2,3], Christian Eberhardt[1], Marc Vollenweider[2], Jakub Smolar[2,3], Deana Haralampieva[2], Souzan Salemi[2], Andreas Boss[1] and Daniel Eberli[2]

*1 Institute of Diagnostic **and** Interventional Radiology, UniversityHospital Zurich, Rämistr. 100, 8091 Zurich, Switzerland;*

2 Department of Urology, UniversityHospital Zurich, Frauenklinikstr. 10, 8091 Zürich, Switzerland;

3 Zurich Center for Integrative Human Physiology (ZIHP), University of Zurich, Winterthurerstr. 190 8057 Zurich Switzerland

DK, CE and AB contributed to the conception and design of research. DK, MV, and JS performed the experiments. DK and CE analyzed the data, interpreted the results, and prepared the figures. DK and SS wrote the animal license application. DK and AB wrote the manuscript. DK, DH and DE contributed to the ethical license application. AB and DE acquired research funding and are guarantors of integrity of the entire study. All authors approved final version of the manuscript.

2.1 Abstract

Purpose: In this study, we show that the measurement of tissue water diffusion properties using magnetic resonance imaging (MRI) enables the monitoring of skeletal muscle tissue regeneration after injection of human activated satellite stem cells (haSSC) in an athymic mouse model.

Methods: haSSCs were isolated, characterized and expanded before injection into a crushed mouse tibialis anterior muscle. *In situ* differentiation was followed up via MRI (4.7 T scanner) for 21 days by focusing on diffusion-tensor imaging (DTI) properties such as apparent diffusion coefficient (ADC) and fractional anisotropy (FA) of the *de novo* tissue. The results were confirmed by histology and immunohistochemistry.

Results: Mice treated with haSSCs showed similar regeneration as mice treated with collagen or PBS. DTI revealed that *de novo* generated muscle fibers were orientated in the same direction as the fibers in the surrounding healthy tissue that were not affected by the initial muscle crush injury. An increase in muscle specific markers confirmed cell differentiation and myofiber formation. In all study cohorts, similar patterns for diffusion values were observed. The ADC (10^{-3} mm^2/s) increased in all groups, reaching its maximum on post-operative day (POD) 1 (haSSCs 1.47 ± 0.12, PBS 1.48 ± 0.09, collagen 1.40 ± 0.11); FA reached minimum values on POD 1 (haSSCs 0.17 ± 0.04, PBS 0.16 ± 0.03, collagen 0.19 ± 0.05), approximating baseline values thereafter.

Conclusions: Injected haSSCs form *de novo* muscle tissue *in situ* following a defined pattern in DTI-MRI highlighting the direction of the newly formed fibers. These results can easily be transferred to the clinical setting as a non-invasive biomarker for the assessment of muscle tissue regeneration in patients.

Keywords: human activated satellite stem cell (haSSC) ■ myoblast transfer therapy (MTT) ■ stress urinary incontinence (SUI) ■ diffusion tensor imaging (DTI) ■ magnetic resonance imaging (MRI)

2.2 Introduction

The quality of life of patients with urinary incontinence (UI) is significantly reduced [1,2]. UI may affect 20-50% of all women [3], with health care expenditures of $65.9 billion in 2007 and projected costs of $82.6 billion in 2020 in the United States alone [4,5]. Urinary continence is achieved by a complex interplay between the urethra, the rhabdosphincter, bladder neck position, detrusor muscle, nerve integrity, vascular plexus and the connective tissue support. Thereby, the rhabdosphincter prevents urine outflow by providing both resting urethral tone via slow-twitch fibers and rapid refectory contraction if the abdominal pressure rises. Any damage to the sphincter muscle, linked nerves or the surrounding tissue, e.g. during childbirth, by surgical treatments of the lower urinary tract or aging, may result in UI. While current treatment options, e.g. physical exercise, medication or surgery only show limited success as well as extensive variability within the patient population [1,2], bioengineering of tissues might meet those challenges.

Muscle regeneration after injury and necrosis follows strictly regulated, time-dependent steps. Minutes after the injury, an acute inflammation is initiated, which lasts for about 2 weeks. The injured area is invaded by polymorphonuclear leukocytes and macrophages. These cells actively secrete chemokines, cytokines, growth factors and NO, reactive oxygen species and proteases. This mix of cell- and ECM-derived substrates released during the inflammation process leads to the initiation of muscle regeneration [6,7]through resident satellite stem cells (SSCs) [8]. SSCs are considered a heterogeneous, quiescent adult stem cell population located between the sarcolemma and the basal membrane of muscle fibers and account for 2-5% of identifiable nuclei in muscle tissue [9,10]. After trauma or damage, SSCs participate in tissue regeneration by proliferating and differentiating into myoblasts and later fuse to form new myofibers.

Engineered tissues generated from harvested stem cells, such as skeletal muscle precursor cells and activated SSCs (aSSC), that were injected directly or implanted into the body in combination with a biocompatible carrier material, have been investigated as a treatment for stress UI (SUI) and other (genetically) acquired myopathies [11–15]. Ongoing clinical trials are trying to confirm these results for patient application. Clinical trials with UI patients showed no signs of rejection or other side effects, proving that the application of autologous cells for skeletal muscle regeneration is feasible, safe and ready for the “bench to bedside” transfer.

SSC transplantation imitates the tissue response upon injury. Nonetheless, for long-term functional tissue restoration, myofiber restoration is not sufficient, but self-restoration upon recurring damage must also be secured. The use of injectable cultured aSSCs for the treatment of SUI has been investigated in rodent and canine models, where its potential to

become the first treatment to restore sphincter muscle function has been shown [12,14,16]. These cells provide overall safe muscle regeneration even for patients with previous medical history of cancer, preventing cancer recrudescence by secretion of paracrine TNFα and through inhibition of tumor growth [17]. First clinical studies revealed no negative side effects after myoblast transfer therapy (MTT) [18,19,7]. These cells can be isolated from patients of all ages and both sexes, forming new skeletal muscle tissue over time [6]. Their *in vitro* growth potential and functional output after transplantation permits autologous transplantation within 3 weeks after muscle biopsy [6]. The majority of SSCs are committed to the myogenic lineage [16] and are therefore most suitable for muscle engineering: Investigations on the use of injectable cultured human aSSCs (haSSC) for the treatment of SUI in small animal models were highly promising [8,10,9,20].

However, cell follow-up after transplantation and the training of the engineered muscle tissue are necessary to ensure a consistent and long-lasting therapeutic benefit. Unfortunately, the evaluation of MTT (and any other cell therapy approach) is challenging, as it mainly relies on indirect measures, e.g. pre- and post-injection pad tests, diary of incontinence episodes and quality of life surveys. Evidently, a non-invasive monitoring system for reliable treatment monitoring is highly desirable. Magnetic resonance imaging (MRI) techniques bear the potential to monitor tissue regeneration and determine efficiency and functionality of matured tissue without destructive and invasive tissue sampling.

In biological tissue, water diffusion is restricted by cell membranes as well as intracellular structures, which can be measured using MR diffusion-weighted imaging (DWI). DWI is based on the addition of two equal magnetic field gradients with opposite orientation, where the first gradient de-phases and the second gradient re-phases the proton spins. With no or only limited movement of the spins, a high signal can be observed due to an almost complete refocusing of the spin signal. However, diffusion of the spins between the two gradients will eventually result in an attenuated signal as not all spins can be refocused by the latter gradient [21]. Moreover, water diffusion in structured tissue, such as neurons or skeletal muscle, is anisotropic. MR diffusion-tensor imaging (DTI), an extension of DWI, measures anisotropy per pixel and provides the directional information relevant for MR tractography or fiber tracking *in vivo* [22]. While applications of DWI and DTI have always been largely focused on neurological disorders [23,24] they represent promising tools to monitor a wide variety of diseases in regions outside of the brain including the spinal cord [25], liver [26] or muscle [27–30]. Both, DTI and tractography can easily be combined with other MR imaging techniques and modalities to obtain comprehensive tissue characterization [31].

In tissues such as brain grey matter, apparent diffusivity is largely independent of the orientation of the tissue and therefore isotropic. In oriented tissues, such as the skeletal muscle or brain white matter, however, measured diffusion depends on the structural organization of the tissue [32]. Since water diffusion is restricted by cell membranes in healthy tissue, the apparent diffusion coefficient (ADC) of the water compartment is expected to be increased when cellularity is reduced [33]. After skeletal muscle tissue damage, the diffusion of water, proteins and cells into the damage site influence the anisotropy of muscle architecture, which is defined through the diffusion tensor eigenvalues (λ1, λ2, λ3), and indices of diffusion anisotropy such as fractional anisotropy (FA). They provide information on the local tissue microstructure and geometry change [34]. Our study investigated the potential of DTI to determine the regeneration after myoblast transfer therapy. DTI has proven invaluable for the study of skeletal muscle fiber architecture in humans and small rodents [29,35,36]. Furthermore, DTI has proven to be applicable to show tissue recovery after femoral artery ligation and ischemia-reperfusion in mouse skeletal muscle [30,34] as well as in tissue denervation [37]. However, to our knowledge, this is the first study to utilize DTI and fiber tracking in order to follow skeletal muscle tissue regeneration after aSSCs treatment of an injured muscle. In this study, we aimed to monitor skeletal muscle regeneration after MTT, using DTI and MR Tractography measuring the integrity and length of regenerating muscle fibers in a small animal muscle crush model.

2.3 Materials and Methods

Study design

To apply DTI for the monitoring of stem cell supported muscle fiber regeneration in an *in vivo* muscle crush model, haSSCs were injected in a model of acute muscle injury. Regeneration was examined via MRI after 1, 3, 7, 14 and 21 days, with succeeding tissue harvest of the de-novo muscle tissue at days 3, 7, 14 and 21 (**Figure 1**). Tissue samples were analyzed by immunohistochemistry and haematoxylin-eosin staining. Injections were performed in three groups: haSSCs (n=9), collagen (n=3) and phosphate buffered saline (n=3) in mice that previously underwent a standardized muscle crush treatment of the tibialis anterior (TA) muscle.

Cell culture

We derived haSSCs from rectus abominis samples obtained of female patients (n=3, age 55±5) undergoing abdominal surgery after providing informed consent. Tissue isolation was approved by the local ethics committee (Kantonale Ethikkommission Zürich, license no StV 01/2008 and 2016-02171). The cells were isolated and cultured as described previously [38].

Briefly, muscle biopsies were soaked in iodine (3 min), iodine-PBS (1:1; 3 min) and washed in PBS until all iodine was removed. After macroscopic dissection of adipose tissue, the muscle biopsies were minced with a surgical scissor in 0.4% dispase (Gibco, Grand Island, NY, US) / 0.2% collagenase type I (Worthington Biochemical, Lakewood, NJ, US) and digested (60 min, 37°C). Dispase / collagenase activity was blocked with Dulbecco's Modified Eagle's Medium / F12 (Gibco) supplemented with 10% Fetal Bovine Serum (FBS; Sigma, St. Louis, MO, US). The cell suspension was filtered through a 100 µm cell strainer (Corning, Corning, NY, US) and transferred into collagen type 1 pre-coated cell culture dish (Corning). After 24 h, the non-adherent cells were transferred to a second pre-coated culture dish in order to remove fibroblasts. The growth media for the cell isolation and expansion consisted of DMEM/F12 supplemented with 18% FBS (Sigma), 1% penicillin / streptomycin (Gibco and Invitrogen, Carlsbad, CA, US), human epidermal growth factor (10 µg/ml, Sigma), human basic fibroblast growth factor (1 µg/ml, Sigma), human insulin (10 µg/ml, Sigma), and dexamethasone (0.4 µg/ml, Sigma). The cells were subcultivated on standard tissue culture polystyrene dishes and passaged when reaching 80%–90% confluency.

Surgery and cell injection

The local veterinary authorities (Veterinary Office of the Department of Health of the Canton of Zurich, license no. 99/2013) approved all animal experiments. We injected haSSCs into the crushed TA muscle of female nude mice (Crl:CD1-Foxn-1^{nu}; Charles River Laboratories, Sulzfeld, De). The animals were anesthetized with 3% isoflurane (1-Chlor-2,2,2-trifluorethyl-difluoromethylether; Attane, Provet, Lyssach, CH), and received Buprenorphine; (0.1 mg/kg BW s.c., Temgesic, Reckitt Benckiser Healthcare, Wallisellen, Switzerland) pre-operative (15 min) and again if signs of post-operative pain occurred (as defined by the score sheet).

After cell expansion (passage 4), cells were labelled with PKH-67 (PKH67GL-1KT, Sigma) according to the manufacturer's recommendation. The reaction was blocked by FBS [1:1]. The cells were washed twice with culture medium and in 1xPBS in order to remove surplus dye material. Cells were resuspended in 1.5% collagen type I solution (Corning): (7:10) + MEM (1:10) + $NaHCO_3$ [23.4 mg/ml] (2:10).

Prior to the injection, the animals were subjected to a mechanical muscle crush injury of the anterior tibialis muscle [39]. For the crush injury, a lateral incision through skin and fascia lata, starting from the talocrural region up to the knee was made with an iris scissor (Wagner KG Klinikbedarf, Remscheid, DE). The coronal plane between the TA and the extensor digitorum longus (EDL) was separated. The lower jaw of an artery forceps was inserted between the TA and the EDL, so that the top jaw rested on the superior surface of the TA. The crush injury was then performed by pressing the forceps until reaching a given mark on the holders

for 3 s. The haSSC-collagen solution (6*10^7 cells / ml collagen type 1; injection volume 30 µl) was injected into the left and right TA. Control animals received an equal volume of either PBS or collagen type 1 without cells. The site of injury and the wound was closed with Ethikon Vicryl 5-0 resorbable suture material. The crush injury was applied to both hind limbs of each mouse. After surgery, animals were placed in a warmed cage for recovery.

MR imaging

Mice were subjected to MR imaging analysis post-operative day POD 0 (=baseline) and POD 1, 3, 7, 14 and 21. During the imaging process, mice were anesthetized with 1.8-3.0% isoflurane and placed in prone position on a respiratory sensor (SA Instruments, Stony Brook, NY, USA) located in a plastic holder with nose cone and covered by a warming pad to maintain body temperature. Vitamin A ointment was used to prevent dryness of the eyes during the imaging process. All measurements were performed with a Bruker 4.7-T Pharmascan 47/16 unit (Bruker BioSpin MRI GmbH, Ettlingen, Germany).

Subsequent to a gradient-echo localizer scan in three spatial directions, an axial and sagittal T2-weighted, two-dimensional fast spin-echo sequences (2D-RARE) imaging protocol with time-to-echo (TE) = 33 ms/ time-to-repetition (TR) = 2500 ms, number of averages (AVG) = 2, receiver bandwidth (BW) = 50000 Hz, echo train length = 8, echo spacing = 11.0 ms, field of view (FoV) = 40 x 40 mm, slice thickness = 1.5 mm, matrix 256 x 256, voxel size = 0.156 x 0.156 x 1 mm was recorded to cover the leg in 20 slices. The duration of the scan was 1 min 20 s.

A diffusion-weighted spin-echo MR sequence was used for DTI and tractography. The diffusion gradients were applied in six non-collinear directions, and one reference image was obtained without diffusion weighting. The in-plane resolution was 0.3125 mm. Imaging parameters were as follows: FOV = 40 x 40 mm^2, TE = 22.8 ms / TR = 6000 ms, matrix 128 x 64, 1 mm section thickness, 1 mm intersection gap, four sections, two acquired signals, diffusion gradient separation time = 13 ms, diffusion gradient duration = 8 ms, and a b-value of 450 s/mm^2. The duration of the scan was 90 min.

DTI parameters

For every muscle eigenvalues (λ_1, λ_2 and λ_3), mean diffusivity (MD), and fractional anisotropy (FA), according to (1) and (2) (D=diffusion tensor were calculated:

$$ADC = \frac{1}{3}\,Trace(D) = \frac{\lambda 1 + \lambda 2 + \lambda 3}{3} = \langle \lambda \rangle \qquad (1)$$

Apparent Diffusion Coefficient (ADC) measures the diffusion of water molecules within tissue. A low mobility of water molecules corresponds to a low ADC value [40].

$$FA = \sqrt{\frac{(\lambda 1 - \lambda 2)^2 + (\lambda 2 - \lambda 3)^2 + (\lambda 1 - \lambda 3)^2}{2 * (\lambda 1^2 + \lambda 2^2 + \lambda 3^2)}} \quad (2)$$

Fractional anisotropy (FA) represents the anisotropy of water motion ranging from 0 (isotropic movement of water) to 1 (anisotropic movement of water molecules), ($\lambda_1 >> \lambda_2 = \lambda_3$) [41].

$$RA = \frac{\lambda 2 + \lambda 3}{2} \quad (3)$$

Radial anisotropy (RA), the average of the second and third eigenvector, represents the flow perpendicular to the major structure, e.g. an axon or a muscle fiber, representing the magnitude of the shortest axes of the elliptical area of diffusion [42].

$$AA = \lambda 1 \quad (4)$$

Axial anisotropy (AA) or first eigenvector, represents the flow in parallel along the major structure, e.g. an axon or a muscle fiber, representing the magnitude of longest axes of the elliptical area of diffusion [42].

Region of interest (ROI) selection and fiber tracking

MR data analysis was done using DTI-Studio (http://dsi-studio.labsolver.org/). Paravision files were converted to an NIFTI image format. For three-dimensional visualization of the regenerated muscle, a region of interest (ROI) was manually drawn in the axial, coronal and/or sagittal planes.

For each muscle or muscle group, the DTI parameters were calculated at multiple points per fiber along the fiber tracts. The corresponding T2w anatomical image was used as a reference. A deterministic fiber tracking algorithm [43] was used. The anisotropy threshold was 0.04. The angular threshold was 30 degrees and, step size was 0.3 mm. The fiber trajectories were smoothed by averaging the propagation direction with 80% of the previous direction. The seed points were set as follows: tracking index = 0, FA threshold = 0.04, turning angle = 30°, step size = 0.3, smoothing = 0.8, min length = 5, maximal length = 50, initial direction = 0, seed plan = 1. Tracks with a length less than 16 mm were discarded. A total of 10’000 tracts were calculated.

Morphological analysis

Dissected tissue of *de novo*-formed muscle was placed in tissue optimum cutting temperature (OCT) compound embedding medium (Cell Path; VWR, Zurich, Switzerland) immediately after isolation. Tissues were cut into 12 µm cryostat sections (CM1850, Leica Biosystems, Wetzlar, DE); average blade temperature was -20 °C and the sample temperature was around -20 °C. Cryosections were placed onto Superfrost Plus slides

(Thermo Scientific) and stored at -20 °C until use. Images were acquired with Leica DFC7000T (Leica Microsystems, Wetzlar, DE) at 20x or 40x magnification.

Immunofluorescence

Cryosections were air-dried for 30 min at 37 °C and fixed (4% PFA in PBS for 20 min), permeabilized (0.5% Triton X-100 in PBS; 15 min) and blocked (3% BSA + 0.1% Triton X-100 in PBS; 60 min). Cryosections were stained with anti-MyHC (1:5; NA4; Developmental Studies Hybridoma Bank, University of Iowa, Iowa City, IA, US) or anti-α-sarcomeric actinin (1:100; A7811, Sigma) overnight at 4 °C. After washing with PBS, the tissues were incubated with Cy3 anti-mouse IgG secondary antibody (1:1000; C2181, Sigma) and 4',6-Diamidin-2-phenylindol (DAPI; 1:200; D9542, Sigma) for 1 h at room temperature, washed again, and finally mounted (Dako). For image acquisition, exposures were normalized to unstained controls (secondary antibody and DAPI only).

Haematoxylin and eosin staining

Cryosections were air-dried for 30 min at 37 °C, fixed in 4% PFA-PBS solution for 20 min, and rinsed in PBS. The tissue samples were placed in haematoxylin for 10 min and thereafter rinsed with cold water for 2 min. The slides were dipped in HCl-EtOH (1% in 70% EtOH) before placing them in Eosin for 30 sec. The Cryosections were dehydrated in 70% EtOH, 96% EtOH, absolute EtOH and cleared in Xylol. The slides were covered with Pertex (Histolab, Gothenburg, SWE).

Statistics

Experiments were repeated with three human muscle biopsies. Data was analyzed by one-way analysis of variance (ANOVA) test. The results are presented as mean values ± standard deviations, and P values below 0.05 were considered to indicate a significant difference. The parameters were considered as normally distributed data. From these data points, the mean value for each of the parameters was calculated. Per muscle data set, all subjects were combined to express a mean value ± standard deviation (SD). Percentage changes of values are expressed as mean value ± error propagation of SD.

2.4 Results

We assessed the changes of tissue water diffusion properties (described by FA and ADC values as well as fiber tract number, volume and length) over time (21 days) in a haSSCs supported small animal muscle crush model. The MRI data were compared with histology and immunofluorescence imaging. The three applied treatment options were injections at the

site of the injury with 1) haSSCs in a collagen type 1 carrier solution, 2) collagen type 1 or 3) PBS.

Tissue formation

Tissue regeneration was shown in all three-study groups. During regeneration, the changes in tract volume, tract number and tract length were recorded by computer tractography of the same individual for up to 21 days. Tractography of healthy TA (n = 36) shows an initial tract number of 198 ± 56, a tract volume of 35.75 ± 9.06 mm3 and a tract length of 9.08 ± 1.13 mm. During the period of tissue regeneration, breathing and movement artefacts had a negative influence on subsequent fiber tractography. Exemplary longitudinal tractography of the regeneration TA muscle (**Figure 2**). The haematoxylin eosin staining to assess the tissue formation after therapeutic intervention showed no significant differences between the three treatment options when compared to corresponding time points of the other treatment groups (**Figure 3b and 4**). At POD 3, all samples exhibited a high presence of immunomodulatory cells, decreasing at POD 7. The region of injury showed no presence of skeletal muscle fibers at day 3 and 14. On POD 14 regenerated skeletal muscle fibers at the region of injury were present together with a population of infiltrating cells, which were absent as of POD 21. The expression of skeletal muscle associated proteins myosin heavy chain and alpha-sarcomeric actinin could be detected for all three conditions on POD 14. The expression of these proteins is maintained onwards during the remaining regeneration period until day 21 as shown by indirect labelling with corresponding primary and secondary antibodies (emitting red light after excitation). The detection of haSSCs at the site of regeneration was possible due to the initial PKH-67 membrane labelling (emitting green light when excited). haSSCs have fused either with existing unharmed myofibers after the injury or with host satellite cells resulting from self-regeneration.

Diffusion tensor imaging

To characterize the diffusion characteristics of healthy and regenerating mouse TA muscle, the mean FA and ADC parameters were calculated from the DTI datasets. Baseline values of intact TA muscle was determined in all animals. The initial FA was 0.251 ± 0.047 mm^2/s and ADC was 1.182 ± 0.094 $x10^{-3}$ mm^2/s (n=36).

Upon application of injury and the subsequent treatment intervention, ADC values increased from the initially measured values on POD 0 (in $x10^{-3}$ mm^2/s: collagen 1.174 ± 0.077, haSSCs 1.197 ± 0.094 and PBS 1.129 ± 0.106) across all experimental cohorts on POD 1 (in $x10^{-3}$ mm^2/s: collagen 1.401 ± 0.077, haSSCs 1.473 ± 0.120 and PBS 1.480 ± 0.094). The values remained increased on POD 3 compared to healthy muscle; however, they were approaching baseline measurements compared to POD 3 (in $x10^{-3}$ mm^2/s: collagen 1.353 ±

0.077 haSSCs 1.332 ± 0.111 and PBS 1.358 ± 0.117) approximating baseline values on POD7 (in $x10^{-3}$ mm^2/s: collagen 1.200 ± 0.108, PBS 1.235 ± 0.115) or falling below (in $x10^{-3}$ mm^2/s: haSSC 1.176 ± 0.094). Values in all study groups fell below initial values of healthy muscle on POD 14 (in $x10^{-3}$ mm^2/s: collagen 1.119 ± 0.105, haSSC 1.163 ± 0.129 and PBS 1.121 ± 0.034). On POD 21 values remained below POD 0 when treated with collagen (in $x10^{-3}$ mm^2/s: 1.110 ± 0.072) and haSSC (in $x10^{-3}$ mm^2/s: 1.166 ± 0.103) but increase when treated with PBS (in $x10^{-3}$ mm^2/s: 1.173 ± 0.088) (Table 2).

Percentagewise, the change in ADC in relation to healthy muscle was +23.03% ± 11.61 after haSSCs treatment, and +31.13% ± 9.26 or 19.3 % ± 11.44 after PBS or collagen treatment, respectively. On POD 3, these values remained increased (haSSCs: 11.25 ± 14.91%, PBS: 20.26% ± 21.10, and collagen: 15.27 ± 11.29%). While deviation from healthy tissue was lowest on POD 1 when treated with haSSCs, the PBS and collagen treated animals expressed similar values. Changes from POD 1 to POD 3 were 3.32% ± 8.09 for collagen treatment, 9.67 % ± 13.31 after MTT and 8.24% ± 21.08 when PBS was injected into the injury site (Table 1).

Post-operative FA values decreased in all three study groups. Percentagewise, FA changes in relation to healthy muscle were -29.5% ± 7.58 after haSSCs treatment and -43.54% ± 8.18 or -25.31% ± 8.03 after PBS or collagen treatment, respectively. On POD 3, these values remained lower compared to POD 0 (haSSCs: -8.21% ± 4.18, PBS: -25.35% ± 5.02 and collagen: -17.51% ± 3.9). Changes from POD 1 to POD 3 were 9.83% ± 15.46 for collagen treatment, 29.61% ± 14.99 after MTT and 35.49% ± 26.87 when PBS was injected into the injury site (Table 1).

In absolute terms, FA values decreased from baseline values measured on POD 0 (collagen 0.254 ± 0.035, haSSCs 0.240 ± 0.031 and PBS 0.291 ± 0.085) to POD 1 (collagen 0.190 ± 0.049, haSSCs 0.169 ± 0.040 and PBS 0.164 ± 0.030). Values remained lower on POD 3 compared to healthy muscle, but higher in comparison to POD 1 (collagen 0.210 ± 0.026, haSSC 0.220 and PBS 0.217 ± 0.056). On POD 7, collagen equaled baseline measurements (0.253 ± 0.041) while mice receiving MTT had a higher FA value than measured initially (0.278 ± 0.039) and FA values remained lower after treatment with PBS (0.245 ± 0.042).

On POD 14, the FA value for collagen treated mice remained at the level of POD 7 (0.253 ± 0.046). Measurements in haSSC treated mice showed a decline on POD 14 (0.273 ± 0.048) while PBS treated mice now showed an increased value compared to baseline (0.288 ± 0.018). On POD 21, FA values fell in all conditions (collagen: 0.249 ± 0.056; haSSCs: 0.270 ± 0.026; PBS: 0 0.235 ± 0.033 [mean ± SD] (Table 2). The values for collagen-treated mice

remained near POD 0, while those for haSSC treated mice remained increased and the values for PBS treatment fell below POD 0.

Although no significant differences could be observed amongst the investigated study groups, there were time-dependent and statistically significant differences among PODs within each study group (Table 3).

2.5 Discussion

The rhabdosphincter, like any other skeletal muscle tissue, is a highly ordered, dynamic, structurally stable tissue, composed of longitudinally aligned contractile fibers arrayed within sheaths of connective tissue and extracellular matrix [16]. It is supplied with oxygen and nutrients by a dense network of blood vessels. While little tissue turnover occurs under homeostatic conditions *in vivo*, the muscle fibers undergo physiological changes (atrophy, hypertrophy, or fiber type switch) under physical activity. Adult skeletal muscle is able to regenerate from damage to sarcolemma or myofibrils inflicted by muscle contraction, without inducing an inflammatory response and under preservation of morphological and functional features [17,18]. However, when exposed to high forces, destruction of muscle fibrils, fibers or entire tissue segments occur. In this case, native tissue regeneration undergoes a second / inflammatory phase as well as a repair and remodeling phase. Although skeletal muscle shows remarkable regeneration capability, it is unable to cope with larger injuries, such as focal and volumetric loss [19], resulting from chronic inflammation / fibrosis or aging [44,45]. This issue may be overcome by injection of stem cells, which allows structural reconstruction and improves contractile function [8,46].

The activation of SSCs can be induced intrinsically [47] or by extrinsic signals, e.g. muscle injury, initiating myogenesis. The activation and subsequent myogenic differentiation of quiescent SSCs (qSSC)is controlled by diverse myogenic regulatory factors (MRFs) initiating the transformation to aSSCs. Upon activation, committed aSSCs migrate out of the sub-laminar niche and the differentiation into fast proliferating myoblasts [48] begins. After reaching terminal differentiation, myoblasts withdraw from the cell cycle, elongate and start expressing myosin heavy chain and sarcomeric α-actinin. These terminally differentiated myocytes fuse to multinucleated myotubes, further align to myofibers and finally form mature skeletal muscle [49]. In addition, the initial increase of ADC may be accelerated by local inflammation or edema [50].

The FA and ADC values of the healthy TA measured in our study are in line with previous literature. However, to our knowledge, we are the first group to investigate the MTT-mediated tissue regeneration using DTI. Heemskerk et al. extensively described the application of DTI

in human and murine skeletal muscle (reference number here?). Their study was the first study of its kind and showed the applicability of DTI when studying the mouse hind limb anatomy [29]. The extent of changes of FA and ADC in the injured muscle area depends on type of injury and extent of inflammation (swelling, edema and the infiltration of immune cells). As described by Heemskerk et al. and others, diffusion properties to some extent are not only defined by tissue properties but also by cell size and morphology [30,52]. Time course of injury progression and initiation of tissue regeneration until POD 3, for both histological as well as MRI measurements, correlate with findings (e.g. [53,54]). Compared to healthy skeletal muscle, the FA values decreased and ADC increased in all three injury/treatment conditions to a similar extent as the tissue architecture and therefore spatial anisotropy was disrupted: Without the spatial restriction of the muscle fibers, the environment switched from anisotropic to isotropic. This observation goes hand in hand with the influx of immune cells and the expansion of local cells due to inflammatory processes, cell proliferation and osmosis to maintain physiological molecule concentrations within the tissue. Changes in FA and ADC after muscle crush injury are similar to those of ligation or denervation injury [51]. As reviewed by Sotak, diffusion changes are a function of intracellular-extracellular water homeostasis, and therefore are a sensitive marker of ionic equilibrium[55]. This changes upon tissue rupture, cell membrane depolarization and cell volume changes such as cellular swelling, growth during cell cycle or loss of cell volume [56]. Hence, presence and orientation of barriers are due to translational motion, extracellular space tortuosity, and the integrity of cellular membrane [57,58].

Tractography shows a one-directional tissue development in line with histological findings, indicating that this is an important factor for the *de novo* synthesis of muscle fibers, and therefore also essential to establish a functional bioengineered skeletal muscle tissue.

Potential shortcomings of this study

As mentioned by Heemskerk et al. [35] inconsistency in the DTI parameters may be the result of different DWI acquisition protocols (coil positioning, B0 drift, gradients, shimming) as well as differences in tissue water diffusion, architecture and physiological conditions. Nevertheless, clinical feasibility and repeatability of DTI-based skeletal muscle imaging and especially of the female pelvic floor has been shown previously [24,32,52].

Although the echo planar imaging MRI modality as used in this study is of short duration, image artefacts such as blurring, signal dropout, and ghosting due to either its sensitivity to magnetic susceptibility contrast or the eddy currents generated by its rapid gradient switching, occur [62]. Furthermore, possibly due to variation in analytical methods, there is a heterogeneity in skeletal muscle DTI parameters [63].

Moreover, the applied injury model used in this study imitates acute muscle associated with fast self-regeneration of 21-28 days. We observed this process in our study in all three experimental groups. The muscle crush lesion performed in this study causes a blunt trauma without any laceration along the sarcolemma of the TA. Therefore, the muscle extracellular matrix remains intact and may serve as a template for endogenous muscle regeneration [59–61]. Nevertheless, our standard animal model mimics the rhabdosphincter destruction (resulting e.g. from childbirth) more closely than other injury models. Laceration for instance would not have caused damage to the muscle fibers, while cardiotoxin requires long recovery and volumetric muscle loss as well as ischemia is not described for urinary incontinence. In order to realize the full potential of rhabdosphincter cell therapy, optimized animal models such as cre-flox-mediated $Pax7^+$ cell depletion to inhibit self-regeneration must be considered. Furthermore, functional data (e.g. myography) might allow a correlation of DTI and functional regeneration.

Future directions / practical application

The use of aSSCs in human patients to treat SUI is considered save [19]. Our results reveal a non-invasive monitoring tool for the analysis of skeletal muscle bioengineering in human patients, where other imaging tools do not allow sufficient access. These findings will soon be applied in a clinical phase 1 trial performed by our research group. Unlike several previously performed studies without longitudinal *in vivo* imaging[18,19,7], the DTI in our study might help to find the optimal method for myoblast transfer, considering the various approaches in clinical trials (e.g. minced muscle tissue [64] vs. expanded myoblast [18,19,7]). This will be one of the first in man applications of non-invasive imaging in rhabdosphincter cell therapy.

DTI and tractography may not only enable direct visualization of tissue regeneration but also offer insight into microstructural anomalies in the pelvic floor. This will allow to determine the clinical applications as well as the time point of intervention with the best outcome for the patients. So far, DTI and fiber tractography have been applied only in grey and white matter tracts of the spine and the cerebellum, but they may bear the potential as diagnostic tools also for other biological tissues. DTI and fiber tractography-visualization of the female pelvic floor using standard clinical MRI-device has been proven feasible [27]. However, limitations due to gas artefacts, bowel movement or imaging repeatability (imaging protocol, noise and artefact characteristics, and the fiber tracking algorithm [35]) must be overcome. Differences in endpoint values may be due to physiological properties of the tissue. Zijta et al. showed, that within a patient, FA and ADC properties differ between different skeletal muscle tissues of

the pelvic floor [27] and Sinha et al showed [65] that DTI-based fiber tracking of the male urethral sphincter is feasible.

2.6 Conclusion

In summary, we could show that DTI not only allows imaging of healthy skeletal muscle but also permits the monitoring of self- / cell therapy-mediated tissue regeneration of anisotropic tissues. The technology is suitable to follow regeneration in animal models but most importantly can also be applied in clinical trials, e.g. for the follow up after treatment of UI with MTT.

2.7 References

1. Holroyd-Leduc JM, Mehta KM, Covinsky KE. Urinary incontinence and its association with death, nursing home admission, and functional decline. *J Am Geriatr Soc*. 2004;52(5):712-718.
2. Holroyd-Leduc JM, Straus SE. Management of urinary incontinence in women: Scientific Review. *J Am Med Assosciation*. 2004;291(8):986-955.
3. Brown JS, Nyberg LM, Kusek JW, et al. Proceedings of the national institute of diabetes and digestive and kidney diseases international symposium on epidemiologic issues in urinary incontinence in women. *Am J Obstet Gynecol*. 2003;188(6):S77-S88.
4. Dooley Y, Kenton K, Cao G, et al. Urinary incontinence prevalence: results from the National Health and Nutrition Examination Survey. *J Urol*. 2008;179(2):656-661.
5. Wilson L, Brown JS, Shin GP, Luc KO, Subak LL. Annual direct cost of urinary incontinence. *Obstet Gynecol*. 2001;98(3):398-406.
6. Stolting MN, Hefermehl LJ, Tremp M, et al. The role of donor age and gender in the success of human muscle precursor cell transplantation. *J Tissue Eng Regen Med*. 2017;11(2):447-458.
7. Carr LK, Steele D, Steele S, et al. 1-Year Follow-Up of Autologous Muscle-Derived Stem Cell Injection Pilot Study To Treat Stress Urinary Incontinence. *Int Urogynecol J Pelvic Floor Dysfunct*. 2008;19(6):881-883.
8. Eberli D, Aboushwareb T, Soker S, Yoo JJ, Atala A. Muscle precursor cells for the restoration of irreversibly damaged sphincter function. *Cell Transpl*. 2012;21(9):2089-2098.
9. Yokoyama T, Huard J, Pruchnic R, et al. Muscle-derived cell transplantation and differentiaon into lower urinary tract smooth muscle. *Gene Ther*. 2002;9(23):1617-1626.
10. Yokoyama T, Huard J, Pruchnic R, et al. Muscle-derived cell transplantation and differentiation into lower urinary tract smooth muscle. *Urology*. 2001;57(4):826-831.
11. Gussoni E, Soneoka Y, Strickland CD, et al. Dystrophin expression in the mdx mouse restored by stem cell transplantation. *Nature*. 1999;401(6751):390-394.
12. Yiou R, Yoo JJ, Atala A. Restoration of functional motor units in a rat model of sphincter injury by muscle precursor cell autografts. *Transplantation*. 2003;76(7):1053-1060.
13. Léobon B, Garcin I, Menasche P, et al. Myoblasts transplanted into rat infarcted myocardium are functionally isolated from their host. *Proc Natl Acad Sci USA*. 2003;100(13):7808-7811..
14. Nikolavasky D, Stangel-Wójcikiewicz K, Stec M, Chancellor MB. Stem cell therapy: a future treatment of stress urinary incontinence. *Semin Reprod Med*. 2011;29(1):61-70. doi:10.1055/s-0030-1268705.
15. Jin M-H, Yokoyama U, Sato Y, et al. DNA microarray profiling identified a new role of growth

hormone in vascular remodeling of rat ductus arteriosus. *J Physiol Sci*. 2011;61(3):167-179. doi:10.1007/s12576-011-0133-3.

16. Benchaouir R, Rameau P, Decraene C, et al. Evidence for a resident subset of cells with SP phenotype in the C2C12 myogenic line: a tool to explore muscle stem cell biology. *Exp Cell Res*. 2004;294(1):254-268.

17. Stölting MNL, Ferrari S, Handschin C, et al. Myoblasts inhibit prostate cancer growth by paracrine secretion of tumor necrosis factor-α. *J Urol*. 2013;189(5):1952-1959.

18. Carr LK, Robert M, Kultgen PL, et al. Autologous muscle derived cell therapy for stress urinary incontinence: a prospective, dose ranging study. *J Urol*. 2013;189(2):595-601..

19. Peters KM, Dmochowski RR, Carr LK, et al. Autologous muscle derived cells for treatment of stress urinary incontinence in women. *J Urol*. 2014;192(2):469-476.

20. Chancellor MB, Yokoyama T, Tirney S, et al. Preliminary results of myoblast injection into the urethra and bladder wall: A possible method for the treatment of stress urinary incontinence and impaired detrusor contractility. *Neurourol Urodyn*. 2000;19(3):279-287..

21. Bydder GM, Rutherford M a., Hajnal J V. How to perform diffusion-weighted imaging. *Child's Nerv Syst*. 2001;17(4-5):195-201.

22. Basser PJ, Basser PJ, Jones DK, Jones DK. Diffusion-tensor MRI: theory, experimental design and data analysis - a technical review. *NMR Biomed*. 2002;15(7-8):456-467.

23. Burlina ABP, Manara R, Calderone M, et al. Diffusion-weighted imaging in the assessment of neurological damage in patients with methylmalonic aciduria. *J Inherit Metab Dis*. 2003;26(5):417-422.

24. Exhibit E, Lee S-K, Kim DISJ, et al. Imaging and Fiber Trac- tography : A New Method of Describing Aberrant Fiber Connections in Developmental CNS Anomalies 1. *RadioGraphics*. 2005;25(1):53-65.

25. Demir A, Ries M, Moonen C, Vital J. Diffusion-weighted MR Imaging with Apparent Diffusion Coefficient and Apparent Diffusion Tensor Maps in Cervical Spondylotic Myelopathy 1. *Radiology*. 2003:37-43.

26. Patel J, Sigmund EE, Rusinek H, Oei M, Babb JS, Taouli B. Diagnosis of cirrhosis with intravoxel incoherent motion diffusion MRI and dynamic contrast-enhanced MRI alone and in combination: preliminary experience. *J Magn Reson imaging*. 2010;31(3):589-600..

27. Zijta FM, Froeling M, van der Paardt MP, et al. Feasibility of diffusion tensor imaging (DTI) with fibre tractography of the normal female pelvic floor. *Eur Radiol*. 2011;21(6):1243-1249.

28. Rousset P, Delmas V, Buy J-N, Rahmouni A, Vadrot D, Deux J-F. In vivo visualization of the levator ani muscle subdivisions using MR fiber tractography with diffusion tensor imaging. *J Anat*. 2012;221(3):221-228.

29. Heemskerk AM, Strijkers GJ, Vilanova A, Drost MR, Nicolay K. Determination of mouse skeletal muscle architecture using three-dimensional diffusion tensor imaging. *Magn Reson Med*. 2005;53(6):1333-1340. doi:10.1002/mrm.20476.

30. Heemskerk AM, Strijkers GJ, Drost MR, van Bochove GS, Nicolay K. Skeletal Muscle Degeneration and Regeneration after Femoral Artery Ligation in Mice: Monitoring with Diffusion MR Imaging. *Radiology*. 2007;243(2):413-421.

31. Bammer R, Acar B, Moseley ME. In vivo MR tractography using diffusion imaging. *Eur J Radiol*. 2003;45(3):223-234.

32. Basser PJ, Jones DK. Diffusion-tensor MRI: theory, experimental design and data analysis - a technical review. *NMR Biomed*. 2002;15(7-8):456-467.

33. Machann J, Stefan N, Schick F. (1)H MR spectroscopy of skeletal muscle, liver and bone marrow. *Eur J Radiol*. 2008;67(2):275-284.

34. Heemskerk AM, Drost MR, Van Bochove GS, Van Oosterhout MFM, Nicolay K, Strijkers GJ. DTI-based assessment of ischemia-reperfusion in mouse skeletal muscle. *Magn Reson Med*. 2006;56(2):272-281.

35. Heemskerk AM, Sinha TK, Wilson KJ, Ding Z, Damon BM. Repeatability of DTI-based skeletal muscle fiber tracking. *NMR Biomed*. 2010;23(3):294-303.

36. Heemskerk AM, Sinha TK, Wilson KJ, Ding Z, Damon BM. Quantitative assessment of DTI-based muscle fiber tracking and optimal tracking parameters. *Magn Reson Med*. 2009;61(2):467-472.

37. Ha D-H, Choi S, Kang E-J, Park HT. Diffusion tensor imaging and T2 mapping in early denervated skeletal muscle in rats. *J Magn Reson imaging*. 2014;42(3):1-7. doi:10.1002/jmri.24818.

38. Haralampieva D, Betzel T, Dinulovic I, et al. Noninvasive PET Imaging and Tracking of Engineered Human Muscle Precursor Cells for Skeletal Muscle Tissue Engineering. *J Nucl Med*. 2016;57(9):1467-1473.

39. Haralampieva D, Salemi S, Betzel T, et al. Injected human muscle precursor cells overexpressing pgc-1 enhance functional muscle regeneration after trauma. *Stem Cells Int*. 2018;2018:1-11.

40. Sener RN. Diffusion MRI: apparent diffusion coefficient (ADC) values in the normal brain and a classification of brain disorders based on ADC values. *Comput Med Imaging Graph*. 2001;25(4):299-326..

41. Basser PJ, Pierpaoli C. Microstructural and physiological features of tissues elucidated by quantitative-diffusion-tensor MRI. *J Magn Reson - Ser B*. 1996;111(3):209-219.

42. Karlsgodt KH, Rosser T, Lutkenhoff ES, Cannon TD, Silva A, Bearden CE. Alterations in White Matter Microstructure in Neurofibromatosis-1. Buratti E, ed. *PLoS One*. 2012;7(10):e47854.

43. Yeh FC, Verstynen TD, Wang Y, Fernández-Miranda JC, Tseng WYI. Deterministic diffusion fiber tracking improved by quantitative anisotropy. Zhan W, ed. *PLoS One*. 2013;8(11):e80713.

44. Mann CJ, Perdiguero E, Kharraz Y, et al. Aberrant repair and fibrosis development in skeletal muscle. *Skelet Muscle*. 2011;1(1):21.

45. Bentzinger CF, Wang YX, Dumont N a, Rudnicki M a. Cellular dynamics in the muscle satellite cell niche. *EMBO Rep*. 2013;14(12):1062-1072.

46. Stölting M, Hefermehl L, Tremp M, Azzabi F, Sulser T, Eberli D. 173 Impact of patient age or gender on bioengineering of functional muscle tissue using muscle precusor cells. *J Urol*. 2011;185(4):e72.

47. Danieli-Betto D, Peron S, Germinario E, et al. Sphingosine 1-phosphate signaling is involved in skeletal muscle regeneration. *Am J Physiol Cell Physiol*. 2010;298(3):C550-8.

48. Beauchamp JR, Heslop L, Yu DS, et al. Expression of CD34 and Myf5 defines the majority of quiescent adult skeletal muscle satellite cells. *J Cell Biol*. 2000;151(6):1221-1234.

49. Tidball JG, Villalta SA. Regulatory interactions between muscle and the immune system during muscle regeneration. *Am J Physiol Regul Integr Comp Physiol*. 2010;298(5):R1173-87.

50. Hoerr V, Faber C. Magnetic resonance imaging characterization of microbial infections. *J Pharm Biomed Anal*. 2014;93:136-146.

51. Zhang J, Zhang G, Morrison B, Mori S, Sheikh K. Magnetic resonance imaging of mouse skeletal muscle to measure denervation atrophy. *Exp Neurol*. 2008;212(2):448-457.

52. Anderson A., Xie J, Pizzonia J, Bronen R., Spencer D., Gore J. Effects of cell volume fraction changes on apparent diffusion in human cells. *Magn Reson Imaging*. 2000;18(6):689-695.

53. Huard J, Li Y, Fu FH. Muscle injuries and repair: current trends in research. *J bone Jt Surg*. 2002;84-A(5):822-832.

54. Ju YM, Atala A, Yoo JJ, Lee SJ. In situ regeneration of skeletal muscle tissue through host cell recruitment. *Acta Biomater*. 2014;(June).

55. Schlaug G, Siewert B, Benfield A, Edelman RR, Warach S. Time course of the apparent diffusion coefficient (ADC) abnormality in human stroke. *Neurology*. 1997;49(1):113-119.

56. Bortner CD, Cidlowski JA. Uncoupling cell shrinkage from apoptosis reveals that Na+ influx is

required for volume loss during programmed cell death. *J Biol Chem*. 2003;278(40):39176-39184.

57. Sotak CH. Nuclear magnetic resonance (NMR) measurement of the apparent diffusion coefficient (ADC) of tissue water and its relationship to cell volume changes in pathological states. *Neurochem Int*. 2004;45(4):569-582.

58. Patterson DM, Padhani AR, Collins DJ. Technology Insight: Water diffusion MRI - A potential new biomarker of response to cancer therapy. *Nat Clin Pract Oncol*. 2008;5(4):220-233.

59. Stratos I, Graff J, Rotter R, Mittlmeier T, Vollmar B. Open blunt crush injury of different severity determines nature and extent of local tissue regeneration and repair. *J Orthop Res*. 2010;28(7):950-957.

60. Mourikis P, Relaix F. Activated Muscle Satellite Cells Chase Ghosts. *Cell Stem Cell*. 2016;18(2):160-162.

61. Webster MT, Manor U, Lippincott-Schwartz J, Fan CM. Intravital Imaging Reveals Ghost Fibers as Architectural Units Guiding Myogenic Progenitors during Regeneration. *Cell Stem Cell*. 2016;18(2):243-252.

62. Damon BM, Froeling M, Buck AKW, et al. Skeletal muscle diffusion tensor-MRI fiber tracking: Rationale, data acquisition and analysis methods, applications and future directions. *NMR Biomed*. 2016;(April).

63. Damon BM, Buck AKW, Ding Z. Diffusion-Tensor MRI Based Skeletal Muscle Fiber Tracking. *Imaging Med*. 2011;3(6):675-687.

64. Gräs S, Klarskov N, Lose G. Intraurethral Injection of Autologous Minced Skeletal Muscle: A Simple Surgical Treatment for Stress Urinary Incontinence. *J Urol*. 2014;192(3):850-855.

65. Sinha S, Sinha U, Malis V, Bhargava V, Sakamoto K, Rajasekaran M. Exploration of male urethral sphincter complex using diffusion tensor imaging (DTI)-based fiber-tracking. *J Magn Reson Imaging*. 2018:1-10.

2.8 Tables

Table 1:

Percentagewise changes of fractional anisotropy (FA) and apparent diffusion coefficient (ADC) of the assessed TA muscles on POD 1 and POD 3 compared to values prior to intervention

	Δ FA			Δ ADC		
	Collagen	haSSC	PBS	Collagen	haSSC	PBS
$\Delta_{POD0:POD\ 1}$	25.31%	33.44%	35.33%	19.30%	25.46%	26.09%
$\Delta_{POD\ 0:POD3}$	17.51%	13.34%	14.49%	15.27%	13.45%	15.63%
$\Delta_{POD\ 1\ :POD\ 3}$	28.06%	40.93%	23.95%	11.36%	11.70%	9.01%

Table 2:

Mean and standard deviation (SD) after computation of fractional anisotropy [mm^2/s] (FA) and apparent diffusion coefficient (ADC) of the assessed TA muscles.

	FA									ADC								
	collagen			hSSC			PBS			collagen			hSSC			PBS		
	Mean	SD	p-value from previous POD	Mean	SD	p-value from previous POD	Mean	SD	p-value from previous POD	Mean	SD	p-value from previous POD	Mean	SD	p-value from previous POD	Mean	SD	p-value from previous POD
POD 0	0.254	0.035		0.240	0.031		0.291	0.085		1.174	0.077		1.197	0.094		1.129	0.106	
POD 1	0.190	0.049	0.3735	0.169	0.040	<0.0001	0.164	0.030	<0.0001	1.401	0.112	0.0332	1.473	0.120	<0.0001	1.480	0.094	<0.0001
POD 3	0.210	0.026	>0.9999	0.220	0.042	0.0032	0.217	0.056	0.7245	1.353	0.077	>0.9999	1.332	0.111	0.0012	1.358	0.177	0.8727
POD 7	0.253	0.041	0.9320	0.278	0.039	>0.0.003	0.245	0.042	0.9995	1.200	0.108	0.5434	1.176	0.094	0.0001	1.235	0.115	0.8755
POD 14	0.253	0.046	>0.9999	0.273	0.048	>0.9999	0.288	0.018	>0.9999	1.119	0.105	0.998	1.163	0.129	>0.9999	1.121	0.034	0.9173
POD 21	0.249	0.056	>0.9999	0.270	0.026	>0.9999	0.235	0.033	0.7354	1.110	0.072	>0.9999	1.166	0.103	>0.9999	1.173	0.088	>0.9999

2.9 Figures

Fig. 1:

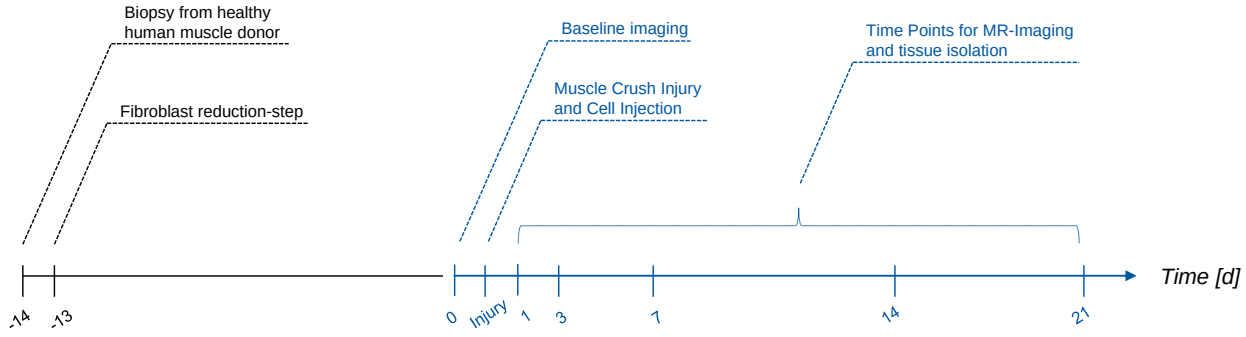

Scheme with time axis showing the experimental setup. Cells gained from muscle biopsies have been expanded *in vitro* for 13 days. After baseline imaging to assess imaging data from healthy TA muscles, mice received therapeutic intervention and were monitored for up to 21 days.

Figures

Fig. 2:

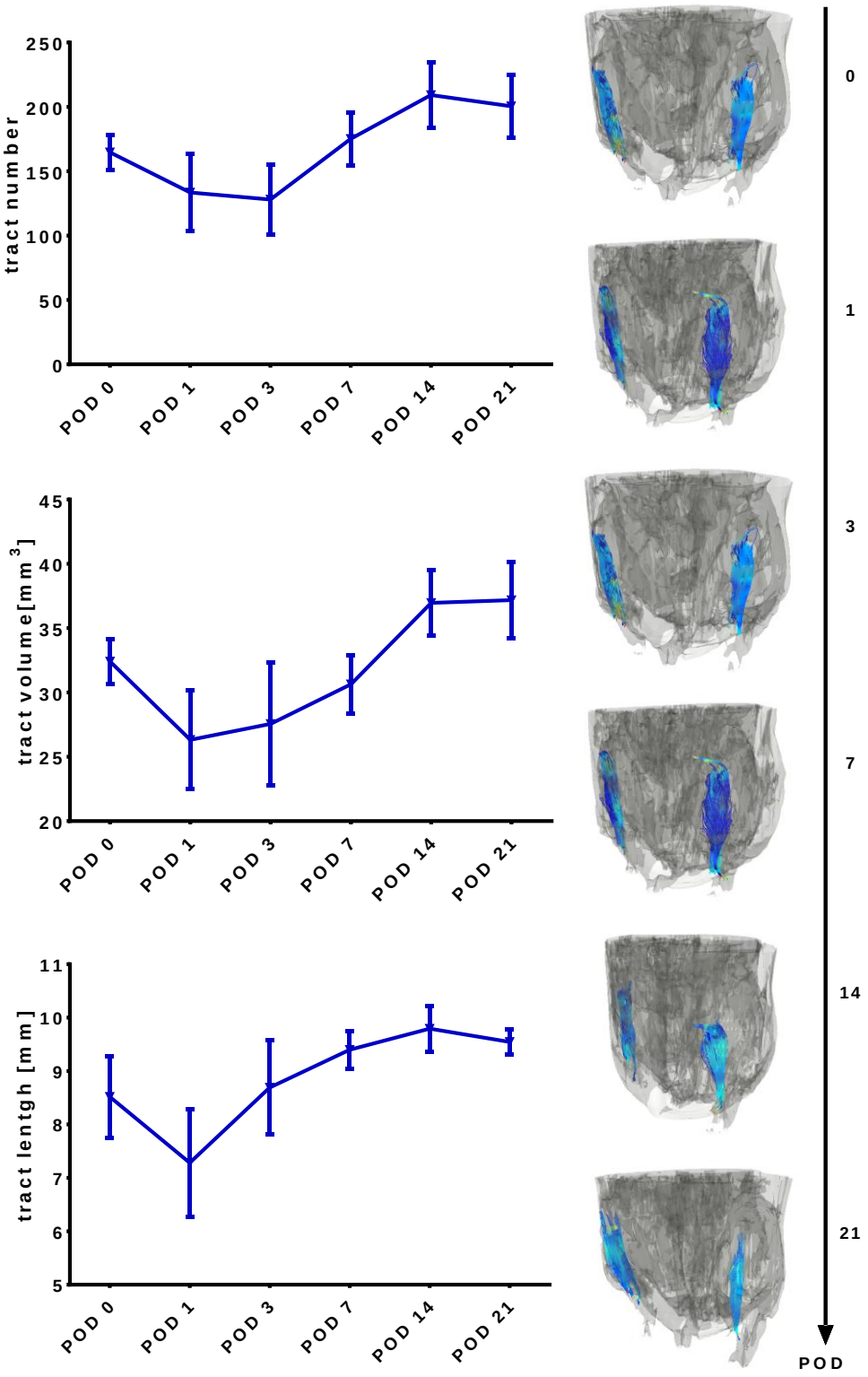

Representative sample showing changes in tract volume, tract number and tract length during the period of regeneration. Below is the computed tractography of the same individual animal showing tractography of aSSC-supported tissue regeneration.

Figures

Fig. 3:

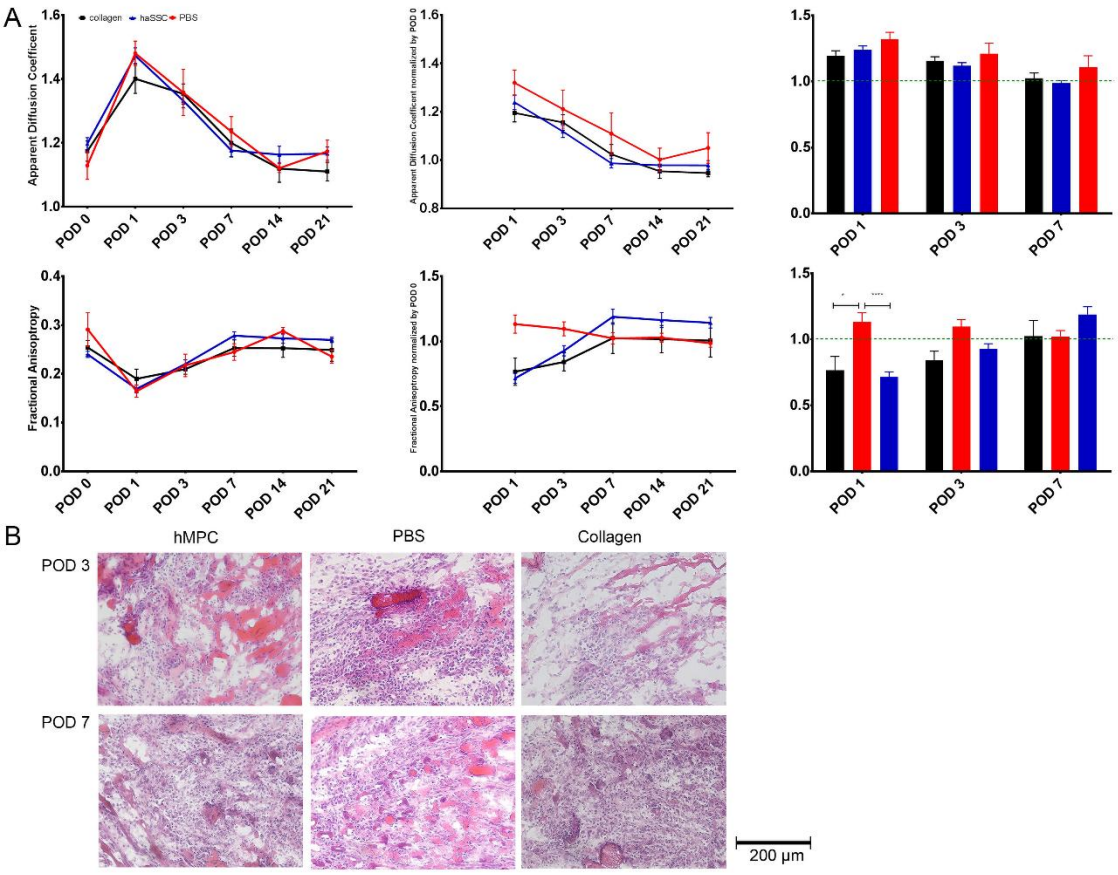

A) Changes in MR indexes before and during the timespan of muscle regeneration after intervention. Data are mean values of the experimental groups (collagen: n = 3, PBS: n = 3, haSSC: n = 9). ADC (in x 10-3 mm^2/sec) and FA are shown as original data, normalized by the baseline value of the uninjured TA of every animal prior to injury and therapeutic intervention. B) Representative images of H&E staining show the myogenic differentiation of the TA on POD 3 and 7 after MTT haSSCs in a collagen-carrier, respectively with the injection of collagen and PBS alone. Whilst haematoxylin stained nuclei appear blue, eosin stains proteins non-specifically pink.

Figures

Fig. 4:

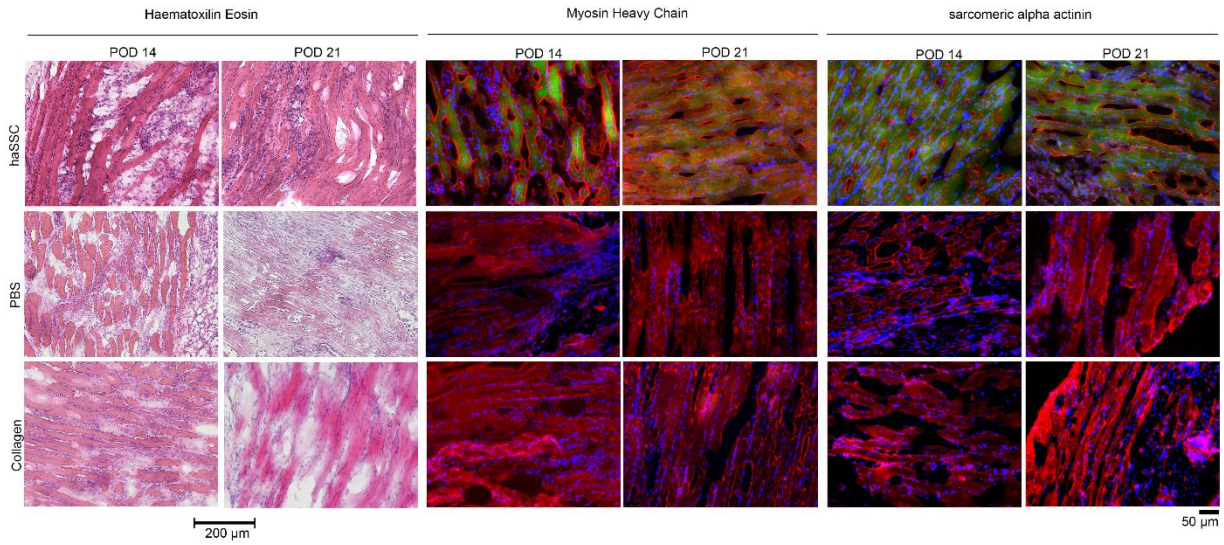

The development myofibers after injury and treatment with haSSCs, PBS and collagen respectively over the time span of 21 days were visualized with haematoxylin / eosin staining (nuclei appear blue, proteins in pink), revealing newly formed myofibers at the site of injury after 14 and 21 days of regeneration (The scale bar is 200 µm). Expression of skeletal muscle associated contractile proteins (middle panel) and sarcomeric actinin (right panel) via cyanine-3 conjugated secondary antibody is shown in red signal. Nuclei are stained by DAPI appear in blue signal whilst haSSCs pre-labelled with prior cell transplantation are visible through a green signal. Expression of both, sarcomeric alpha actinin and Myosin Heavy Chain after MTT at POD 14 and 21 is similar to the expression after self-regeneration of host tissue (treatment with PBS or collagen) (The scale bar is 50 µm.)

Figures

3 T1 -, T2 - relaxometry and magnetization transfer MRI permit non-invasive monitoring of stem cell supported skeletal muscle regeneration on a murine tibialis anterior crush injury model

Submitted to PlosOne. The manuscript is currently under revision by the journal.

Christian Eberhardt[1,] Daniel Keller[1,2,3], Sarah Nötzli[2,] Deana Haralampieva[2],

Cristina Rossi[1], Daniel Eberli[2] and Andreas Boss[1]

*1 Institute of Diagnostic **and** Interventional Radiology, UniversityHospital Zurich, Rämistr. 100, 8091 Zurich, Switzerland;*

2 Department of Urology, UniversityHospital Zurich, Frauenklinikstr. 10, 8091 Zürich, Switzerland;

3 Zurich Center for Integrative Human Physiology (ZIHP), University of Zurich, Winterthurerstr. 190 8057 Zurich Switzerland

CE, DK and AB contributed to the conception and design of research. CE and DK performed the experiments. CE and DK analyzed the data. CE interpreted the results and prepared the figures. DK wrote the animal license application. CE wrote the manuscript. DK and DE contributed to the ethical license application. AB and DK have proof-read the manuscript. AB and DE acquired research funding and are guarantors of integrity of the entire study. All authors approved final version of the manuscript.

3.1 Abstract

Stress Urinary incontinence (SUI) has a profound impact on the quality of life in a vast number of patients and urethral sphincteric deficiency represents the fundamental etiology. Preclinical investigations on autologous muscle stem cell transplantation for treating SUI emphasized the need for non-invasive imaging modalities tracking the differentiation of MPCs into muscle fibers for an early therapeutic evaluation. This study assessed muscle regeneration by multiparametric magnetic-resonance imaging (MRI) on a murine hind limb *tibialis anterior* (TA) muscle crush model (n=18 mice), followed by an injection of collagen embedded human muscle precursor cells (MPCs) isolated from the *rectus abdominis* from 4 different donors (n=12 mice) respectively of collagen only (n=3) or PBS injection (n=3) serving as control. MRI assessment of the hind limb using a 4.7T MR Scanner prior to surgery and on post-operative day (POD) 1, 3, 7, 14 and 28 quantified longitudinal and transverse relaxation times, and the magnetization-transfer ratio (MTR) of the regenerating TA muscle. Tissue specimens were histologically examined by hematoxylin-eosin staining and immunohistochemistry.

Neither collagen embedding of human MPCs during stem cell transplantation, nor collagen alone as widely applied scaffold in stem cell research did influence the retrieved MRI parameters delineating muscle regeneration of the TA with increasing longitudinal and transverse relaxation times as well as decreasing MTR. Histological examination proved that all study groups concluded TA regeneration, suggesting that murine MPCs cells contributed significantly to the muscle restoration. Our results show, that this murine TA crush model, ideally with radiation depleted satellite cells, does lend itself for advancing MR methodology for monitoring of stem cell therapy as possible treatment for SUI.

3.2 Introduction

Stress urinary incontinence (SUI), describing the involuntary leakage of urine, is a prevalent disorder affecting worldwide 200 million, mostly middle-aged and elderly people [1]. Besides creating enormous healthcare costs, this common urogenital disease poses a severe burden on the patient's life quality [2,3]. For women, pregnancy and subsequent vaginal delivery and for men, radical prostatectomy represent the major risk factors for developing SUI, generally caused by insufficient detrusor contraction due to weakened muscles of the urethra and the pelvic floor [4,5]. Currently, there are several therapeutic options available and yet, they are either of limited success or associated with complications as a consequence of invasive procedures [5,6].

Therefore the autologous transplantation of muscle stem cells at the site of impaired or inadequate muscle regeneration has been extensively investigated as a potential treatment of SUI [7]. Satellite cells residing beneath the basal lamina of muscle fibers represent the main reservoir for muscle regeneration [8,9]. After trauma or damage, quiescent satellite cells start to proliferate and differentiate, then also called muscle precursor cells (MPCs) or myoblasts [10], and fuse later on to form new myofibres [11], which were shown to contribute to the regeneration process of the striated urethral sphincter in a murine model [12,13].

Consequently, within the last decade a number of preclinical and clinical trials have been conducted assessing the feasibility of autologous muscle stem cell transplantation for reconstructing damaged urethral sphincter musculature and thereby restoring sphincter muscle function. The results hold great promise to establish stem cell therapy as a future treatment of SUI [14-20]. Especially the one year – respectively the two year follow-up studies delivered very encouraging results [16,17]. However, it is a much-debated question in stem cell research as to whether or not transplanted stem cells for tissue regeneration should be embedded in scaffolding materials. There are certain disadvantages associated with the injection of cells devoid of biomaterials, such as poor long-term cell survival and lack of control over the location of the cells after implantation. This could be circumvented by the minimal invasive injection of hydrogel scaffolding materials such as collagen in combination with the transplanted stem cells, providing structural support, restraining the cellular motility and further protecting transplanted cells from adverse effects of the inflammatory response at the injured environment [21].

Clearly, assessing the therapeutic success within regenerative medicine restricts or even precludes invasive measures such as tissue biopsies. Nevertheless, in view of evolving stem cell-based regenerative therapies, it is indispensable and crucial, though likewise challenging, to repeatedly evaluate non-invasively the therapeutic progress by monitoring muscle tissue regeneration [16]. As magnetic resonance imaging (MRI) has proofed capable to provide detailed anatomical visualization of soft tissue [22-24], it therefore lends itself as non-invasive outcome measure for muscle tissue regeneration. Several previous studies using MRI unraveled a significant amount of information on structural characteristics of the musculature examining the regeneration after injury in mice [25,26] and rats [27,28] Furthermore, MRI has been successfully applied to assess viability and differentiation of stem cells in mouse [29-31] and rat [32-34]. Thereby, MRI characterized the dynamic changes of muscle tissue differentiation by measuring the relaxation time, diffusion properties or magnetization transfer, the latter describing a detectable MR contrast meditated by proton exchange between the macromolecularly bound protons, mainly associated to proteins, and the free waterous fluid pool of protons upon a saturation prepulse set deliberately at a given off-

resonance frequency distinct from the water resonance frequency. And albeit all mentioned MR parameters closely reflect the course of the muscle tissue maturation, especially the diffusion properties and the magnetization transfer reveal rather structural, hence likely functional characteristics, of the developing muscle by delineating the fiber content and orientation as detected by diffusion weighted (DW-) MRI and the content of predominantly proteinaceous macromolecules in the maturing musculature as measured by magnetization-transfer (MT-) MRI.

A consecutive appraisal of the quality of the regenerated musculature is important for estimating its future function and thus, reliable and non-invasive markers reflecting the regenerative state of the developing musculature are needed for translating such a cell therapy approach into a clinical application. This study addressed two questions, (i) if MRI is suitable to non-invasively delineate the myogenic differentiation upon traumatic muscle injury on a murine tibialis anterior (TA) muscle crush model, mimicking damage inflicted during childbirth, in combination with a concurrent injection of muscle precursor cells, resembling a real scenario of stem cell-based regenerative therapies, and further to that, (ii) if collagen as commonly used hydrogel scaffolding material, providing the carrier matrix for cell therapies, interferes with the retrieved MR parameters. For that aim, we retrieved the T1- and T2 -relaxation as well as the MTR of mice that underwent TA muscle crush with subsequent injection of collagen embedded MPCs isolated from the *rectus abdominis* muscle of consented volunteers respectively collagen (control) and saline (control) alone.

3.3 Materials and Methods

Study design

This study on female athymic mice (CD-1 nude mice, Crl:CD1-Foxn1^{nu}; Charles River Laboratories, MA, USA) was approved by the local veterinary authorities (Veterinary Office of the Canton of Zurich, license no. 99/2013). Mice (n_{Total} =54; 23-28 g) at the age of 8-10 weeks were kept under standardized conditions in accordance with the institutional animal care guidelines with a 12-hour day-night cycle and unlimited access to standard diet and water. Research staff conducting experiments has received special education and training accredited by the Federation of Laboratory Animal Science Associations (FELASA).

This study comprised essentially two cohorts of mice with one cohort for non-invasive MRI monitoring of myogenic differentiation within the crushed TA in a longitudinal study design, while the other cohort requiring tissue harvest for histological examination of the myogenic differentiation at corresponding time points of the MRI experiments was assessed in a cross-sectional study design after TA muscle crush.

The cohort of mice dedicated to multiparametric MRI assessment (n_{MRI} = 18 mice) consisted of three subgroups examining the regenerating TA crush injury followed by: (i) the injection of collagen-embedded human muscle precursor cells (MPCs) isolated from the *rectus abdominis* from 4 different donors (n=12 mice), (ii) the injection of collagen (n=3) and (iii) the injection of PBS (n=3), respectively, serving as control. MRI assessment of the hind limb was performed one day prior to surgery and on post-operative day (POD) 1, 3, 7, 14 and 21. All tissue specimens were harvested for immunohistochemical analysis on POD 21 after completing all MRI experiments.

The other cohort providing the correspondent histological examination ($n_{Histology}$ = 36 mice) for each MR measurement assessed myogenic differentiation of TA muscle crush followed by: (i) the injection of collagen-embedded human muscle precursor cells (MPCs) (n=12), (ii) the injection of collagen (n=12) and (iii) the injection of PBS injection (n=12) on POD 3, 7, 14 and 21 with each three animals per time point.

Cell Culture

Human MPCs were extracted according to established protocols [35,36] from *rectus abdominis* muscle specimens obtained from informed and consented female patients undergoing abdominal surgery in the age 55±5 years (n=4). This procedure was approved by the local ethics committee (Ethics Committee of the Canton of Zurich, license no. StV 01/2008 and 2016-02171. In brief, muscle biopsy samples were minced and digested for 40 min at 37°C and 5% CO_2 in Dulbecco's Modified Eagle's Medium with F12 nutrient mixture (DMEM/ F12 growth medium) (Gibco, Grand Island, NY, USA) supplemented with 0.4% dispase (Gibco) and 0.2% collagenase type I (Worthington Biochemical, Lakewood, NJ, USA). In order to eliminate fast-adhering fibroblasts, digested samples were centrifuged, filtered, and seeded on collagen type I coated six-well dishes for 24 hours before transferring the supernatant containing human MPCs to fresh collagen type I coated six-well dishes. The cells were further cultured in DMEM/ F12 growth medium supplemented with 18% fetal bovine serum (FBS) (Gibco), 1% penicillin and streptomycin (Gibco), 10 µg/ml human epidermal growth factor (Sigma-Aldrich, Buchs, Switzerland), 1 µg/ml human basic fibroblast growth factor (Sigma-Aldrich), 10 µg/ml human insulin (Sigma-Aldrich), and 0.4 µg/ml dexamethasone (Sigma-Aldrich) in standard tissue culture polystyrene dishes at 37°C and 5% CO_2. For MPC aided muscle regeneration, cells were subcultured four times after initial isolation having reached 80%–90% confluency, washed in phosphate buffered saline (PBS) (Gibco) and the cell membrane was labelled with PKH-67 dye (Sigma-Aldrich) for cell tracking according to manufacturer instructions. For that purpose, 6 x 10^7 MPCs were resuspended in 3 ml 0.08% (v/v) PKH-67 and incubated for 5 min at room temperature. After quenching the reaction with

FBS, cells were washed twice with PBS and resuspended in 1 ml collagen carrier matrix in Minimum Essential Media (MEM) (2.7 mg rat tail collagen type I / ml MEM) (BD Biosciences, Bedford, MA; USA), and if needed, pH was readjusted to 7.2 with sterile $NaHCO_3$.

Animal Surgery

For analgesia, 0.1 mg/kg bodyweight (BW) buprenorphine (Temgesic, Indivior, UK) was administered subcutaneously 30 min prior start of any surgical intervention. Subsequently, anaesthesia was induced by 5% (v/v) isoflurane supplemented oxygen (Attane, Minrad I, Buffalo, NY) in an enclosed container. After applying eye ointment, animals were fixed and anaesthesia was maintained with 2-4% (v/v) isoflurane supplemented oxygen administration via small nose cone during surgical intervention. After lateral incision on the hind limb the TA muscle was carefully inserted between the jaws of an artery forceps and the crush injury was induced by pressing the forceps until reaching a defined mark on the holders. After removing the forceps, 30 µl MPC-collagen suspension containing 1.8 x 10^6 MPCs was applied at the site of injury and the wound was closed with Ethikon Vicryl 5-0 resorbable suture material. The crush injury was applied to both hind limbs of the mouse. Having completed the surgical procedure, animals recovered in a warmed cage and if needed, buprenorphine (0.1 mg/kg BW, s.c.) was readministered within 3 hrs, thereafter analgesia with buprenorphine (0.1 mg/kg BW, s.c.) was repeated on POD 1 and 2 if signs of pain occurred.

Histology

A separate cohort of mice were sacrificed for histological examination of regenerating TA on POD 3, 7, 14 and 21 after crush injury. The muscles specimens were excised, snap frozen and cryosections (8 µm) underwent hematoxylin-eosin (H&E) staining. Cryosections were rinsed after haematoxylin staining with acidified ethanol and placed into eosin solution, dehydrated through a series of graded alcohols, cleared in Xylol and sealed under coverslip with Pertex (Histolab, Goteborg, Sweden). For immunohistochemistry, dried cryosections were fixed in 4% PFA, permeablized in 0.1% Triton X-100 solution, blocked with 3% bovine serum albumin (BSA) and incubated with primary mouse antibodies against myosin heavy chain (MyHC) (1:1) (NA4 DHSB (Developmental Studies Hybridoma Bank)) respectively against α-Actinin (sarcomeric) (1:1) (A7811 Sigmal-Aldrich) (4°C, 12 hrs). The secondary indocarbocyanine Cy3-labelled antibody (rabbit anti-mouse IgG $F(ab')_2$ fragment–Cy3) (1:1000) (**C2181** Sigma-Aldrich) was incubated together with DAPI (1:100) (2-(4-Amidinophenyl)-6-indolecarbamidine dihydrochloride) (RT, 1hr). Samples were mounted with mounting media for fluorescent imaging and a cover slip.

Magnetic resonance imaging

The animals were subjected to MR imaging the day before muscle crush injury and then on POD 1, 3, 7, 14, 21 measuring longitudinal and transverse relaxation times and the magnetization transfer ratio. For that purpose, mice were placed in prone position on a respiratory sensor (SA Instruments, Stony Brook, NY, USA) located in a plastic holder with nose cone, providing air supplemented with 1.5% isoflurane (Attane, Minrad I, Buffalo, NY), and covered by a warming pad to maintain the body temperature. Ophtalmic ointment was used averting dryness of the eyes during the imaging process. Experiments were performed on a 4.7T small animal MRI system (Pharmascan 47/16 US; Bruker BioSpin MRI GmbH, Ettlingen, Germany) equipped with a linear polarized hydrogen whole-body mouse transmit-receive radiofrequency coil.

After a gradient-echo localizer scan in three spatial directions, the imaging protocol included an axial and sagittal T2-weighted, two-dimensional fast spin-echo sequences (2D-RARE) with time-to-echo (TE) = 33ms/ time-to-repetition (TR) = 2500 ms, number of averages (AVG) = 2, receiver bandwidth (BW) = 50000 Hz, echo train length = 8, echo spacing = 11.0 ms, field of view (FoV) = 40 x 40 mm, slice thickness = 1.5 mm, matrix 256 x 256, voxel size = 0.156 mm x 0.156 mm x 1 mm were recorded to cover the leg in 20 slices. The duration of the scan was 1 min 20 sec.

A further axial T2-weighted MR measurement was performed with a two-dimensional fast spin-echo sequence (2D-RARE) possessing the same geometry as applied for subsequent sequences measuring magnetization transfer. This scan was conducted with following parameters: TE = 33ms, TR = 6232 ms, AVG = 2, BW = 50000 Hz, echo train length = 8, echo spacing = 11.0 ms, FoV = 30 x 30 mm, slice thickness = 0.5 mm, matrix 128 x 128, voxel size = 0.234 mm x 0.234 mm x 0.5 mm were recorded to cover the leg in 60 slices. The duration of the scan was 4 min 20 sec.

Longitudinal and transverse relaxation times (T1 and T2 times) were determined by a 2D-RARE sequence with 5 different echo times and 6 repetition times: TE = 11, 33, 55, 77 and 99 ms, TR = 200, 400, 800, 1500, 3000 and 4500 ms, RARE factor = 2, AVG = 1, BW= 50 000 Hz, FoV 30 x 30 mm, slices = 1, slice thickness = 1.0 mm, matrix size = 128 x 128, voxel size = 0.234 cm x 0.234 cm x 1.0mm. The acquisition time was 12 min 10 sec.

Magnetization-transfer (MT) was measured with three-dimensional spoiled gradient-echo sequences (3D-FLASH). Sequence parameters were: TE = 4.7 ms, TR = 20.4 ms, AVG = 2, FA = 12°; BW = 50 000 Hz, sinc excitation pulse = 1 ms, FoV 30 x 30 mm x 30 mm (slice thickness = 30 mm), matrix size = 128 x 128 x 60, voxel size = 0.234 mm x 0.234 mm x 0.5 mm, acquisition time = 5 min 35 sec. Measurements were performed with a MT pre-pulse of Gaussian pulse shape for each TR under systematic variation of the off-resonance frequency

covering 50 Hz – 37 500 Hz, FA = 800°, MT pulse length = 10.9 ms, MT pulse bandwidth = 250 Hz, MT interpulse delay 0.01 ms, no dummy pulses. A reference scan for MTR quantification was acquired using the same sequence without any MT prepulse. Applying the same sequences used for imaging the hind limb on the lower abdomen on the urine-filled mouse bladder allowed to determine of the off-resonance frequencies saturating directly the water-bound protons due to the absence of macromolecules within the urine.

Quantification of MR imaging parameter

For all fitting procedures, non-linear least square fits to the signal intensities were performed based on the Levenberg-Marquardt-Algorithm (Matlab "lsqcurvefit") in a pixel-by-pixel manner.

For calculation of T1 time, the signal intensities of the RARE sequence were fitted to the equation

$$S(TR_i) = S_0(1 - INV * e^{-\frac{TR_i}{T1}}) \qquad (1)$$

with TR_i representing the applied repetition times.

The T2 time was calculated from the RARE sequence by fitting the equation

$$S(TE_i) = S(0) * e^{-\frac{TE_i}{T2}} + N \qquad (2)$$

to the signal intensities of the different echo times TE_i with N meaning the noise.

The MTR values (in %) were calculated from the MT sequences with and without MT prepulse in the following manner:

$$MTR = \frac{M_0 - M_{sat}}{M_0} \qquad (3)$$

with M_0 meaning the signal intensity without MT prepulse and M_{sat} the signal intensity with MT prepulse.

Definition of a region-of-interest (ROI)

Applying custom-written Matlab scripts (MathWorks, Natick, MA, USA) a region-of-interest (ROI) analysis was performed with manually drawn ROIs on anatomical images of the respective sequences. Three independent polygonal ROIs were drawn on each of three consecutive slices depicting the regenerating muscle areas. The image noise was determined in a ROI positioned outside the body in the upper left hand corner in the background of the image and corrected by squared subtraction according to Gudbjartsson [37].

Statistical evaluation and image post-processing

For descriptive analysis, mean values and standard deviations of the regenerating musculature, the T1 and T2 times and MTR were calculated and numeric data are presented as mean ± standard deviation. Statistical evaluation of the acquired parameters between the study groups was performed by two-way analysis of variance (ANOVA) with Bonferroni correction using GraphPad Prism 5 software (GraphPad Software, Inc., La Jolla, CA, USA). Generally, a P-value of less than 0.05 was considered significant.

Parametric maps of the regenerating TA were obtained by voxel-wise computation of the T1 relaxation time, T2 relaxation time and the magnetization transfer ratio, followed by a twofold interpolation and Gaussian filtering (FWHM = 0.55 mm).

3.4 Results

There are notable morphological alterations over the time course of muscle regeneration as depicted by representative H&E stainings of serial cryostat sections of the TA (**Fig. 1**), but with overall subtle differences between the three study groups. Besides the muscle damage clearly visible in the images from POD 3-14, tissue specimens on POD 3 and POD 7, to a lesser extent on POD 14, are generally characterized by an infiltration of mononuclear cells being present in fairly large numbers in the injured musculature. The sections on POD 14 display already elongated, rod-shaped cells and aligned regenerated muscle fibers, which are fully matured and densely aligned on POD 21 and by eventually reaching the structural characteristics of uninjured musculature the regeneration concluded in all study groups throughout the given time course of 3 weeks. A representative H&E stained tissue section of untreated, healthy TA is provided as control (**suppl. Fig. 3**).

To further characterize the progress of myogenic differentiation supported by injected collagen, with and without transplanted human MPCs, versus PBS injection alone, immunohistochemical characterization of TA was conducted on POD 14 and on POD 21 by doublestaining either sarcomeric α-actinin or myosin heavy chain (hc) by a Cy3-labeled secondary antibody (red signal) and the nuclei of cells by DAPI (blue signal). Engrafted human MPCs pre-labeled with PKH-67 prior cell transplantation are directly discernable (green signal) and demonstrate the contribution of transplanted human MPCs to the overall regeneration process (**suppl. Fig. 1, 2**). Again, an equally immunohistochemically assessed tissue section of untreated, healthy TA is provided as control (**suppl. Fig. 3**).

The immunofluorescent images of all study groups show an assembly of multinucleated myofibers positive for sarcomeric α-actinin (**suppl. Fig. 1**) and positive for myosin heavy

chain (**suppl. Fig. 2**) at both assessed timepoints, and in the case of engrafted human MPCs, the green-fluorescent PKH-67 membrane dye applied for *in vivo* cell tracking of the MPCs colocalizes with the observed myofibers. Already on POD 14, the myofibers demonstrate a well-defined sarcomeric organization of both proteins being involved in muscle contractility, thus representing markers of myogenic differentiation. Moreover, there was no significant overlap between the DAPI-stained myonuclei and Cy3-stained contractile proteins within the myofibers. Nevertheless, the state of sarcomeric organization as well as the abundance of the assessed muscle proteins is indistinguishable within the three study groups.

Muscle regeneration upon crush injury with subsequent transplantation of human MPCs versus injection of collagen respectively PBS alone was monitored by several MR parameters such as longitudinal and transversal relaxation times, T1 and T2, and the MTR (**Fig. 2**). Both, the T1 time and the T2 time increase as consequence of the crush injury, which is as relative mean T1 time for all groups approximately 120% of its initial relaxation time on POD 1, 3, and 7 (POD 1, 121.8±7.2%; POD 3, 122.3±6.8%; POD 7, 121.2±10.0%. Then, relative mean T1 time for all groups approaches respectively converges to baseline values on POD 14 and 21 (POD 14, 104.8±6.3%; POD 21 100.8±2.6%). There was no statistical significance comparing all the study groups. The relative mean T2 time prolongs for all three groups in average to 185 – 215% of its initial relaxation time on POD 1, 3, and 7 (POD 1, 184.7±58.7%; POD 3, 213.5±62.8%; POD 7, 202.6±76.7% and regresses to baseline values on POD 14 and 21 (POD 14, 111.5±18.5%; POD 21, 101.9±4.4%). Again, there was no statistical significance between the study groups.

While imaging the hind limb, same MT sequences were inevitably applied on the lower abdomen and hence the frequently urine-filled mouse bladder was imaged as well allowing consequently to measure the off-resonance frequencies saturating directly the water-bound protons, as the urine is devoid of any macromolecules. The off-resonance frequency avoiding direct saturation of water-bound protons could be determined with ≥2.500Hz (data not shown). In contrast to the relaxation times, the MTR inferred from measurements with an off-resonance frequency at 2500Hz shows a remarkable decline upon muscle injury and throughout the subsequent muscle regeneration, with a relative mean MTR for all groups decreasing gradually to 84.2±5.1% on POD1, to 73.1±6.0% on POD3 and to 67.7±13.0% on POD7 of its initial MTR value. Then again, the relative mean MTR increases gradually to the initially measured baseline values with 89.7±9.9% on POD14 and reaches 97.4±3.9% on POD21. The study groups did not differ significantly regarding their MTR values while regenerating the TA musculature.

Absolute mean values and standard deviation of the longitudinal and transversal relaxation times, T1 and T2 both in [ms], and the MTR in [%] for all study groups prior crush injury and on POD 1, 3, 7, 14, and 21 are given (**Tab. 1**). Furthermore, retrieved MR images depict the morphologic appearance of the TA musculature and representative parametric maps for T1 - and T2 relaxation and MTR retrieved for pre-surgical measurements and for all subsequent PODs demonstrate alterations regarding the assessed MR parameters in the course of muscle regeneration supported by the transplantation of human MPCs embedded in collagen (**Fig. 3**).

3.5 Discussion

In the wake of evolving stem cell therapies hopes are rising for a wide-ranging arsenal of therapeutic options to permanently reinvigorate damaged sphincter muscle tissue for SUI [5] and thus, demanding a sensitive, non-invasive evaluation measure for monitoring therapeutic success that can be readily translated into human clinical trials. Here, T1- and T2-relaxometry as well as MT-MRI imaging were tested for evaluating myogenic differentiation in a murine TA muscle crush model facilitating muscle regeneration by MPCs injected in combination with collagen as scaffolding material and this investigation shows, that multimodal MRI allows for a detailed assessment of the regenerative process in musculature despite of the use of collagen embedding the injected MPCs. All three phases of muscle regeneration [21,38], as further supported by histological examination of muscle tissue, are mirrored by the retrieved MR parameters.

The acute mechanical insult to the detrusor muscle, be it as consequence of vaginal delivery or prostatectomy, is causative for developing SUI and hence, in this study, a traumatic muscle crush injury was preferred for damaging the hind limb mimicking the actual onset of SUI over inflicting a nontraumatic damage by the intramuscular injection of myotoxins such as $BaCl_2$ [25] or Notexin [27], especially as the myotoxin induced muscle injury models resemble rather conditions like muscular dystrophies [27].

Initially, injured musculature enters within shortest time the inflammatory and degenerative phase (< POD 1), which is characterized by an initiation of the satellite cell proliferation and furthermore, by necrosis of ruptured myofibers leading to a strong inflammatory response, accompanied by an activation and infiltration of mononucleated cells such as neutrophils, macrophages [39]. Having induced muscle injury by Notexin injection, also Mattila [27] describes the muscle necrosis as a process releasing intracellular, degraded macromolecules into the basal lamina cylinders and leading to a local accumulation and retention of fluids due to osmotic effects. Thus, this local inflammation, combined with the interstitial edema due to

vascular and myofiber leakage as a direct result of the crush injury [40], might consequently account for the instant increase of T1 and T2 values and to the decline of MTR values, which were also very prominent in other studies assessing muscle regeneration upon damage [25,27]. Within the subsequent repair phase (POD 1-7), which is mainly characterized by the removal of cellular debris of necrotic muscle fibers by infiltrating macrophages, the MTR values gradually decrease further delineating the additional loss of fibrous protein matrix, whereas the T1 and T2 parameters remain at the high level as already observed on POD 1. Also a study on Duchenne muscular dystrophy emphasizes that both degenerating and regenerating muscle fibers with their elevated muscle water content due to interstitial edema account for increased T1 relaxation times [41,42].

Eventually, the remodeling phase (POD 14-21) comprises the reorganization and fusion of newly formed myotubes with existing myofibers resulting in complete muscle recovery and therefore the relaxation times and the MTR parameters converge towards baseline values retrieved prior crush injury, which again is in line with previous studies assessing the myogenic differentiation of MPCs subcutaneously injected into a murine model by T1 – and T2-relaxometry [30] and by magnetization transfer MRI [29].

For all study groups, the immunofluorescent images depict myofibers positive for sarcomeric α-actinin (**suppl. Fig. 1**) and positive for myosin heavy chain (**suppl. Fig. 2**) at both assessed timepoints, and in the case of transplanted human MPCs, the presence of the green-fluorescent PKH-67 membrane dye within those myofibers, initially applied for *in vivo* cell tracking of the human MPCs expanded *in-vitro*, confirmed the contribution of human MPCs to the myotube formation. In addition, these images clearly show the sarcomeric organization of the contractile proteins. Evidently, in the course of myogenic differentiation isolated human MPCs have evolved and fused with myofibrers as indicated by the green appearance of fully differentiated myofibers on POD 14 and 21 (**suppl. Fig. 1**).

Nevertheless, the TA of young laboratory mice provides a highly regenerative biological background possibly obscuring the effects of the muscle regeneration driven by the injected human MPCs which might have been discernable otherwise in a background with restricted or even abrogated muscle regeneration [43,44]. Moreover, there is an increasing amount of evidence showing that isolated MPCs lose their regenerative capacity in the course of *in-vitro* expansion after a few passages [9,44,45], probably aggravated by the fact that the MPC donors were patients in the age 50 – 60 years with a therefore age-related compromised regeneration potential [46]. This might have led to an overall mitigated regeneration of the injured TA muscle mediated by transplanted MPC in this mouse model. Additionally, satellite

cells feature different properties depending on the origin of the muscle [47] which might have further influenced the observed regenerative effects of transplanted MPCs [48,49].

In light of promising stem cell therapies helping in rebuilding urethral sphincter musculature, the rapid cell clearance of injected proliferating myoblasts, probably due to the adverse inflammatory environment created at site of injury, has to be averted by embedding MPCs into hydrogels of extracellular matrix (ECM) proteins such as collagen [21]. Common ECM proteins, like collagen or fibrin have so far been extensively used in tissue engineering for providing the required scaffold for myoblast differentiation [38]. The objective of this study was to further assess if non-invasive evaluation of muscle restoration is still feasible despite injecting fibrous ECM proteins as MPC carrier matrix and the direct comparison of MR parameters of all study groups proved that ECM application does not mask any of the myogenic restoration events amenable to MRI.

Within the framework of this ethical approval obtained for the conducted animal experiments, it was unfortunately not possible to advance and refine this mouse model by radiation depletion of mouse satellite cells prior muscle crush injury and subsequent myoblast injection to fully observe the contribution of transplanted human MPCs to the overall regeneration process [43,44]. This in fact represents a limitation of this study.

Although there are additional studies required to eventually anchor non-invasive MR monitoring for the evaluation of myogenic differentiation in the context of stem cell therapies helping in rebuilding urethral sphincter musculature, these observations show that all stages of muscle restoration are amenable to multimodal MR imaging despite using ECM scaffolding materials. The application of fabricated protein scaffolds, allowing for a much higher degree of alignment and organization of the regenerating myofibers in combination with mouse models deficient in autologous satellite cells would be a logical and important next step of investigation.

3.6 References

1. Norton P, Brubaker L. Urinary incontinence in women. *Lancet.* 2006;367(9504):57-67.
2. Holroyd-Leduc JM, Straus SE. Management of urinary incontinence in women: scientific review. *Jama.* 2004;291(8):986-995.
3. Wilson L, Brown JS, Shin GP, Luc KO, Subak LL. Annual direct cost of urinary incontinence. *Obstetrics and gynecology.* 2001;98(3):398-406.
4. Kim JC, Cho KJ. Current trends in the management of post-prostatectomy incontinence. *Korean J Urol.* 2012;53(8):511-518.
5. Lin CS, Lue TF. Stem cell therapy for stress urinary incontinence: a critical review. *Stem Cells Dev.* 2012;21(6):834-843.

References

6. Zhou S, Zhang K, Atala A, et al. Stem Cell Therapy for Treatment of Stress Urinary Incontinence: The Current Status and Challenges. *Stem Cells Int.* 2016;2016:7060975.
7. Nikolavasky D, Stangel-Wojcikiewicz K, Stec M, Chancellor MB. Stem cell therapy: a future treatment of stress urinary incontinence. *Seminars in reproductive medicine.* 2011;29(1):61-70.
8. Peault B, Rudnicki M, Torrente Y, et al. Stem and progenitor cells in skeletal muscle development, maintenance, and therapy. *Mol Ther.* 2007;15(5):867-877.
9. Shadrach JL, Wagers AJ. Stem cells for skeletal muscle repair. *Philos Trans R Soc Lond B Biol Sci.* 2011;366(1575):2297-2306.
10. Charge SB, Rudnicki MA. Cellular and molecular regulation of muscle regeneration. *Physiol Rev.* 2004;84(1):209-238.
11. Murphy MM, Lawson JA, Mathew SJ, Hutcheson DA, Kardon G. Satellite cells, connective tissue fibroblasts and their interactions are crucial for muscle regeneration. *Development.* 2011;138(17):3625-3637.
12. Yiou R, Yoo JJ, Atala A. Restoration of functional motor units in a rat model of sphincter injury by muscle precursor cell autografts. *Transplantation.* 2003;76(7):1053-1060.
13. Yiou R, Lefaucheur JP, Atala A. The regeneration process of the striated urethral sphincter involves activation of intrinsic satellite cells. *Anatomy and embryology.* 2003;206(6):429-435.
14. Chancellor MB, Yokoyama T, Tirney S, et al. Preliminary results of myoblast injection into the urethra and bladder wall: a possible method for the treatment of stress urinary incontinence and impaired detrusor contractility. *Neurourology and urodynamics.* 2000;19(3):279-287.
15. Stangel-Wojcikiewicz K, Majka M, Basta A, et al. Adult stem cells therapy for urine incontinence in women. *Ginekol Pol.* 2010;81(5):378-381.
16. Stangel-Wojcikiewicz K, Jarocha D, Piwowar M, et al. Autologous muscle-derived cells for the treatment of female stress urinary incontinence: a 2-year follow-up of a Polish investigation. *Neurourology and urodynamics.* 2014;33(3):324-330.
17. Carr LK, Steele D, Steele S, et al. 1-year follow-up of autologous muscle-derived stem cell injection pilot study to treat stress urinary incontinence. *International urogynecology journal and pelvic floor dysfunction.* 2008;19(6):881-883.
18. Carr LK, Robert M, Kultgen PL, et al. Autologous muscle derived cell therapy for stress urinary incontinence: a prospective, dose ranging study. *J Urol.* 2013;189(2):595-601.
19. Gras S, Klarskov N, Lose G. Intraurethral injection of autologous minced skeletal muscle: a simple surgical treatment for stress urinary incontinence. *J Urol.* 2014;192(3):850-855.
20. Peters KM, Dmochowski RR, Carr LK, et al. Autologous muscle derived cells for treatment of stress urinary incontinence in women. *J Urol.* 2014;192(2):469-476.
21. Qazi TH, Mooney DJ, Pumberger M, Geissler S, Duda GN. Biomaterials based strategies for skeletal muscle tissue engineering: existing technologies and future trends. *Biomaterials.* 2015;53:502-521.
22. McCully K, Shellock FG, Bank WJ, Posner JD. The use of nuclear magnetic resonance to evaluate muscle injury. *Med Sci Sports Exerc.* 1992;24(5):537-542.
23. Del Gaizo A, Silva AC, Lam-Himlin DM, Allen BC, Leyendecker J, Kawashima A. Magnetic resonance imaging of solid urethral and peri-urethral lesions. *Insights Imaging.* 2013;4(4):461-469.
24. Darwish HS, Habash MY. Magnetic resonance imaging of lower limb muscle injury. *Medical Imaging and Radiology.* 2017;5(1):2.
25. Feng S, Chen D, Kushmerick M, Lee D. Multiparameter MRI analysis of the time course of induced muscle damage and regeneration. *J Magn Reson Imaging.* 2014;40(4):779-788.

26. Zaccagnini G, Palmisano A, Canu T, et al. Magnetic Resonance Imaging Allows the Evaluation of Tissue Damage and Regeneration in a Mouse Model of Critical Limb Ischemia. *PLoS One.* 2015;10(11):e0142111.

27. Mattila KT, Lukka R, Hurme T, Komu M, Alanen A, Kalimo H. Magnetic resonance imaging and magnetization transfer in experimental myonecrosis in the rat. *Magn Reson Med.* 1995;33(2):185-192.

28. Winkler T, von Roth P, Matziolis G, et al. Time course of skeletal muscle regeneration after severe trauma. *Acta orthopaedica.* 2011;82(1):102-111.

29. Rottmar M, Haralampieva D, Salemi S, et al. Magnetization Transfer MR Imaging to Monitor Muscle Tissue Formation during Myogenic in Vivo Differentiation of Muscle Precursor Cells. *Radiology.* 2016;281(2):436-443.

30. Chuck NC, Azzabi Zouraq F, Rottmar M, Eberli D, Boss A. MR Imaging Relaxometry Allows Noninvasive Characterization of in Vivo Differentiation of Muscle Precursor Cells. *Radiology.* 2015;274(3):800-809.

31. Azzabi F, Rottmar M, Jovaisaite V, et al. Viability, differentiation capacity, and detectability of super-paramagnetic iron oxide-labeled muscle precursor cells for magnetic-resonance imaging. *Tissue Eng Part C Methods.* 2015;21(2):182-191.

32. Winkler T, von Roth P, Schuman MR, et al. In vivo visualization of locally transplanted mesenchymal stem cells in the severely injured muscle in rats. *Tissue engineering Part A.* 2008;14(7):1149-1160.

33. Madonna R, Delli Pizzi S, Di Donato L, et al. Non-invasive in vivo detection of peripheral limb ischemia improvement in the rat after adipose tissue-derived stromal cell transplantation. *Circ J.* 2012;76(6):1517-1525.

34. Madonna R, Delli Pizzi S, Tartaro A, De Caterina R. Transplantation of mesenchymal cells improves peripheral limb ischemia in diabetic rats. *Mol Biotechnol.* 2014;56(5):438-448.

35. Eberli D, Soker S, Atala A, Yoo JJ. Optimization of human skeletal muscle precursor cell culture and myofiber formation in vitro. *Methods (San Diego, Calif).* 2009;47(2):98-103.

36. Eberli D, Aboushwareb T, Soker S, Yoo JJ, Atala A. Muscle precursor cells for the restoration of irreversibly damaged sphincter function. *Cell transplantation.* 2012;21(9):2089-2098.

37. Gudbjartsson H, Patz S. The Rician distribution of noisy MRI data. *Magn Reson Med.* 1995;34(6):910-914.

38. Grasman JM, Zayas MJ, Page RL, Pins GD. Biomimetic scaffolds for regeneration of volumetric muscle loss in skeletal muscle injuries. *Acta Biomater.* 2015;25:2-15.

39. Tidball JG. Inflammatory processes in muscle injury and repair. *Am J Physiol Regul Integr Comp Physiol.* 2005;288(2):R345-353.

40. Dobek GL, Fulkerson ND, Nicholas J, Schneider BS. Mouse model of muscle crush injury of the legs. *Comp Med.* 2013;63(3):227-232.

41. Matsumura K, Nakano I, Fukuda N, Ikehira H, Tateno Y, Aoki Y. Proton spin-lattice relaxation time of Duchenne dystrophy skeletal muscle by magnetic resonance imaging. *Muscle & nerve.* 1988;11(2):97-102.

42. Matsumura K, Nakano I, Fukuda N, Ikehira H, Tateno Y, Aoki Y. Duchenne muscular dystrophy carriers. Proton spin-lattice relaxation times of skeletal muscles on magnetic resonance imaging. *Neuroradiology.* 1989;31(5):373-376.

43. Heslop L, Morgan JE, Partridge TA. Evidence for a myogenic stem cell that is exhausted in dystrophic muscle. *J Cell Sci.* 2000;113 (Pt 12):2299-2308.

44. Brimah K, Ehrhardt J, Mouly V, Butler-Browne GS, Partridge TA, Morgan JE. Human muscle precursor cell regeneration in the mouse host is enhanced by growth factors. *Hum Gene Ther.* 2004;15(11):1109-1124.

45. Montarras D, Morgan J, Collins C, et al. Direct isolation of satellite cells for skeletal muscle regeneration. *Science.* 2005;309(5743):2064-2067.

References

46. Cooper RN, Thiesson D, Furling D, Di Santo JP, Butler-Browne GS, Mouly V. Extended amplification in vitro and replicative senescence: key factors implicated in the success of human myoblast transplantation. *Hum Gene Ther.* 2003;14(12):1169-1179.

47. Collins CA, Olsen I, Zammit PS, et al. Stem cell function, self-renewal, and behavioral heterogeneity of cells from the adult muscle satellite cell niche. *Cell.* 2005;122(2):289-301.

48. Motohashi N, Asakura A. Muscle satellite cell heterogeneity and self-renewal. *Front Cell Dev Biol.* 2014;2:1.

3.7 Tables

Tab. 1: Muscle regeneration upon muscle crush injury followed by the injection of collagen, with and without transplantation of human MPCs, versus PBS injection alone was monitored by several MR parameters such as longitudinal and transversal relaxation times, T1 and T2 both in [ms], and the MTR in [%] for all study groups prior surgery and on POD 1, 3, 7, 14, 21.

POD	Longitudinal relaxation T1 [ms]			Transversal relaxation T2 [ms]			MTR [%]		
	hMPC	Collagen	PBS	hMPC	Collagen	PBS	hMPC	Collagen	PBS
0	1681.2± 36.2	1722.1± 16.7	1663.0± 34.0	30.4± 1.3	30.4± 0.9	31.1±0.8	56.3±1.7	56.2± 1.4	56.3±1.3
1	2041.5±135.5	2132.8± 87.6	2018.6± 51.1	55.6±18.8	63.8±22.4	51.7±5.1	47.4±2.3	44.9± 3.8	50.1±1.6
3	2052.7±113.9	2090.8±134.7	2064.5±114.2	66.0±22.3	66.3±12.8	60.2±8.3	41.6±2.9	40.3± 3.6	40.3±5.1
7	2034.6±153.9	2039.1±273.2	2078.2±106.8	64.3±26.6	55.2±20.6	58.2±7.7	38.2±6.3	39.9±10.8	35.9±8.0
14	1782.4±119.5	1706.5± 64.7	1763.1± 56.2	34.4± 6.9	33.4± 1.8	32.8±0.8	48.9±5.8	53.4± 1.8	54.0±4.6
21	1704.9± 48.9	1678.5± 21.4	1692.6± 39.5	31.0± 1.5	30.9± 0.5	31.4±1.5	54.3±2.3	55.4± 1.9	56.4±0.8

3.8 Figures

Fig. 1

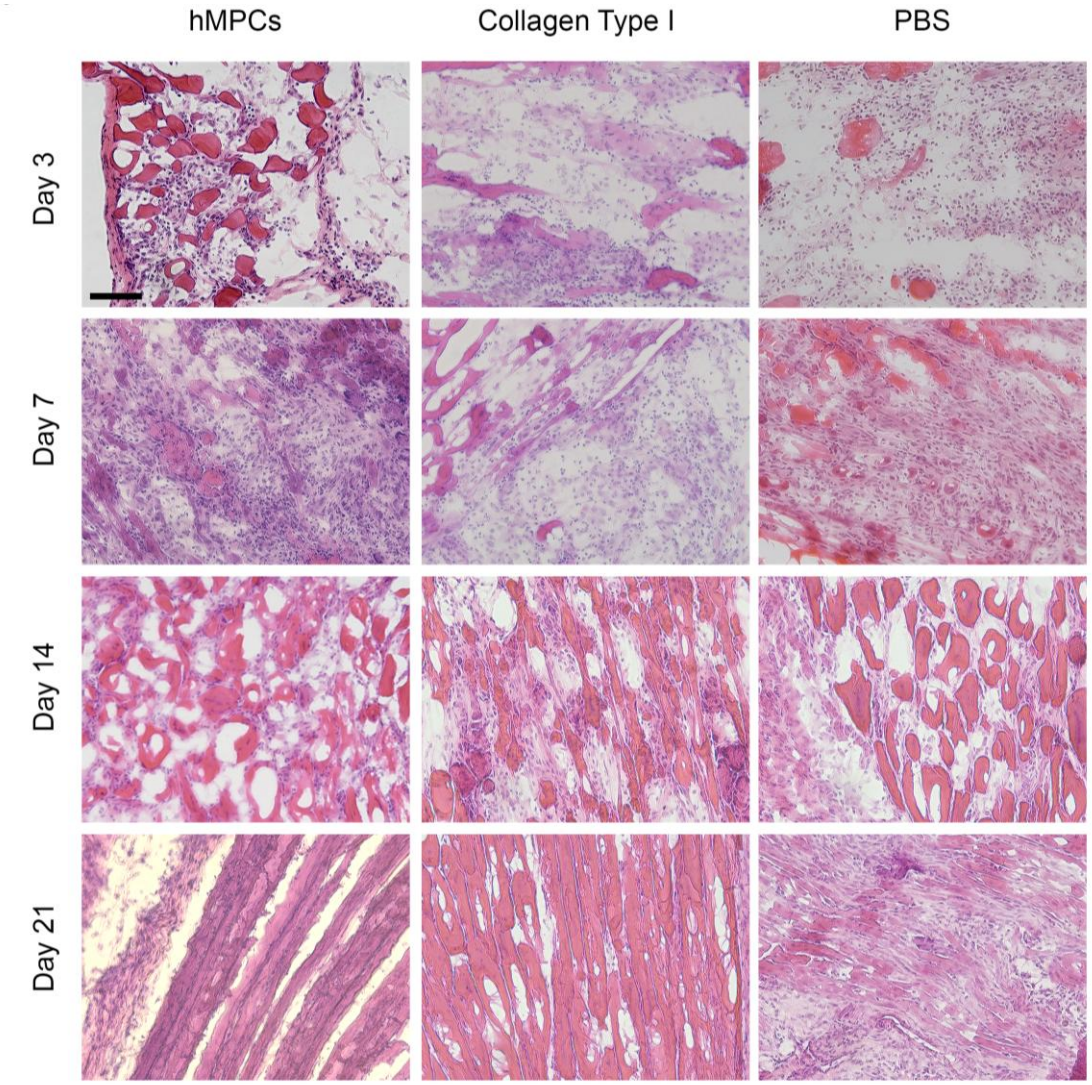

Representative images depicting H&E staining demonstrating the myogenic differentiation of the *tibialis anterior* musculature. Hematoxylin stained nuclei appear blue, whereas eosin stains proteins nonspecifically pink. The image shows cryosections of a *tibialis anterior* muscle specimens after muscle tissue after crush injury on POD 3, 7, 14, 21 with implantation of MPCs embedded in collagen, respectively with the injection of collagen and phosphate buffered saline alone. Scale bare, 100 µm.

Figures

Fig. 2:

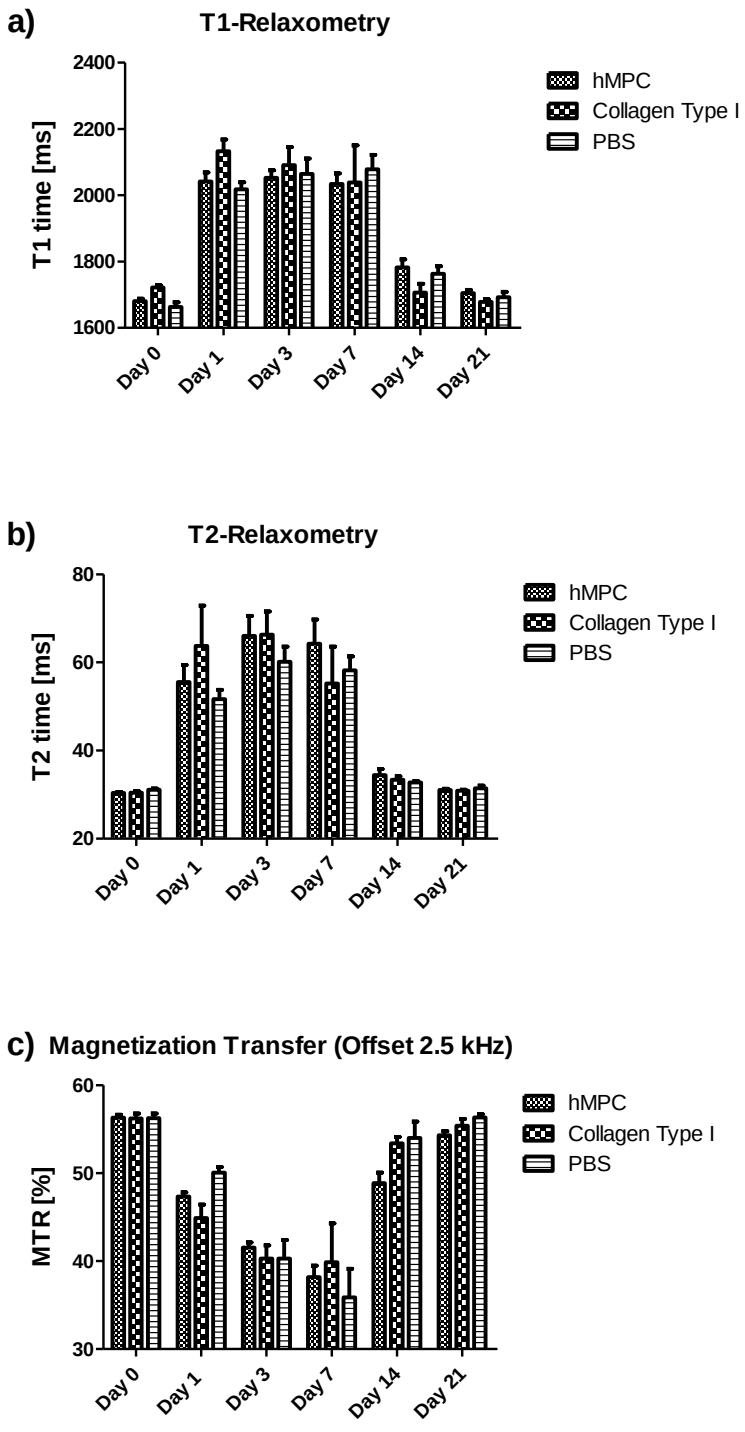

Muscle regeneration assessed by T1- and T2-relaxometry and MT-MRI, the latter with an off-resonance frequency 2500 kHz, depicting the myogenic regeneration of the *tibialis anterior* muscle after crush injury for animals having received an injection of human MPCs embedded in collagen, respectively the injection of collagen and phosphate buffered saline alone. The diagrams show the pre-surgical measurement and POD 1, 3, 7, 14 and 21 of the longitudinal T1 - a) and transverse T2 relaxation b) and magnetization transfer c) retrieved for the regenerating musculature.

Figures

Fig. 3:

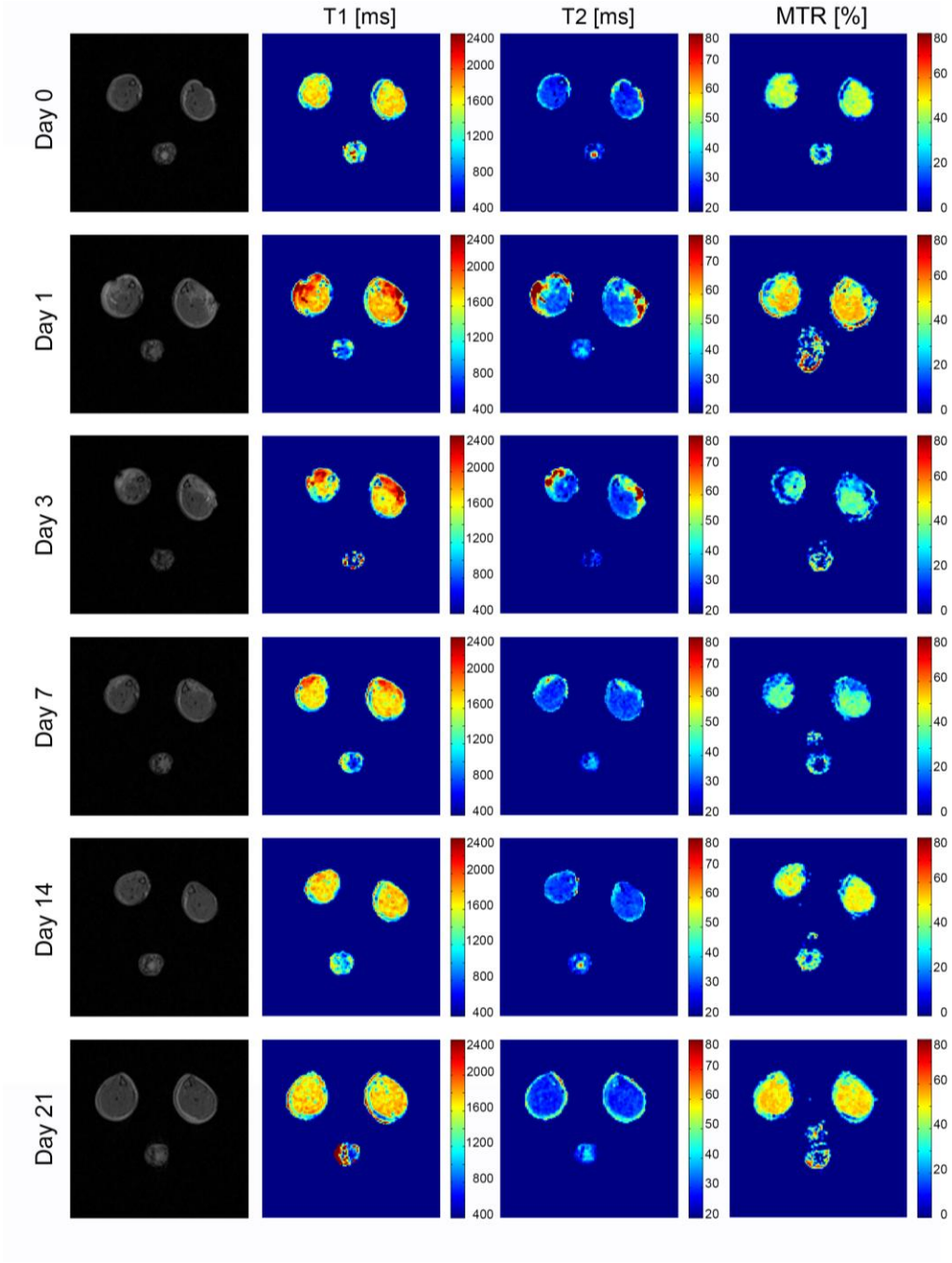

Representative axial MR images depicting the morphologic appearance and the correspondent parametric maps of the T1 relaxation time, the T2 relaxation time and the MTR for pre-surgical measurement (Day 0) and POD 1, 3, 7, 14 and 21 after muscle crush injury on the *tibialis anterior* muscle and subsequent injection of MPCs embedded in collagen as scaffolding material.

Figures

Suppl. Fig. 1:

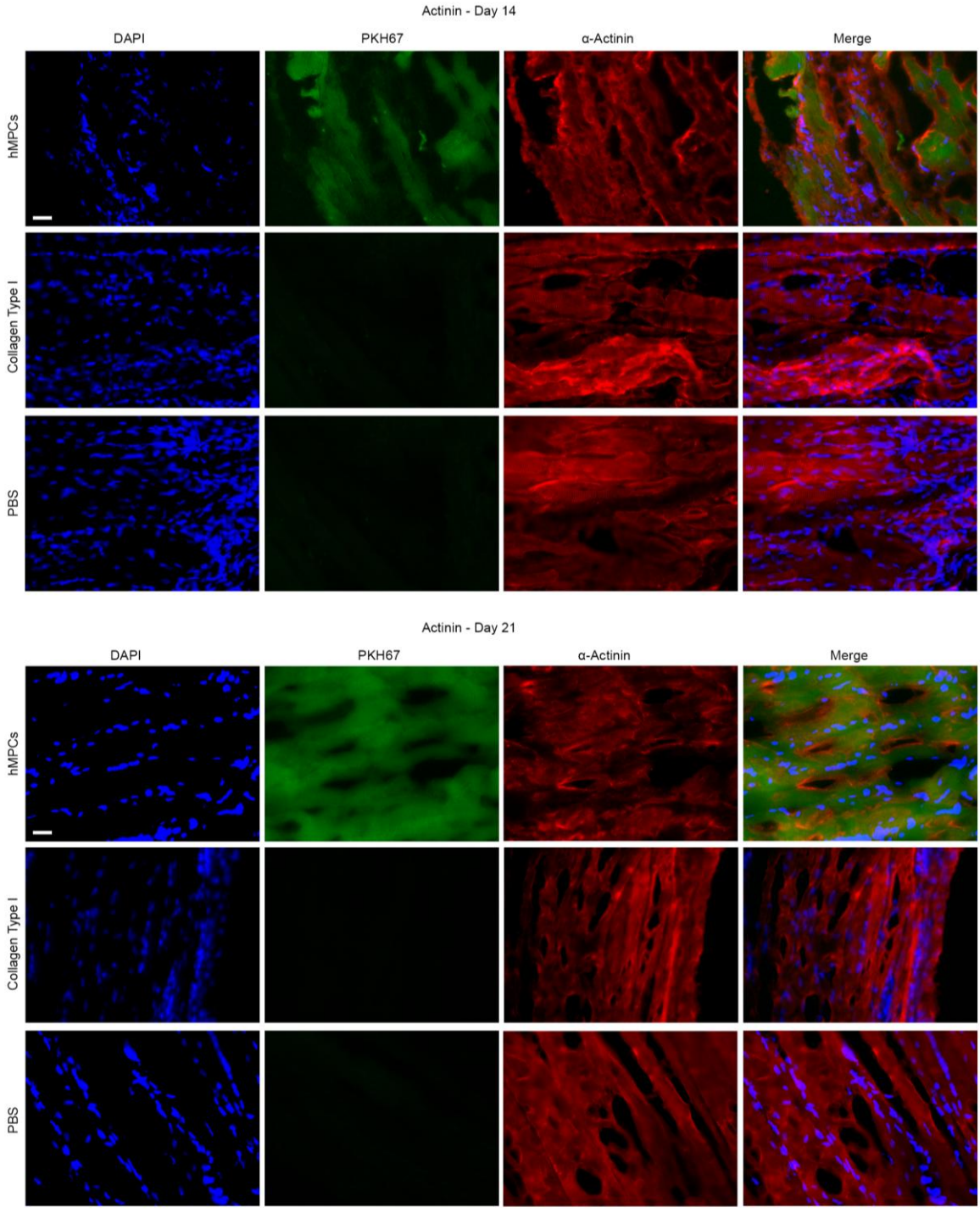

Immunofluorescent images detecting sarcomeric α-actinin during the myogenic differentiation of the *tibialis anterior* musculature on POD 14 (upper panel) and on POD 21 (lower panel). Nuclei are stained by DAPI (blue signal) and α-actinin by cyanine-3 conjugated antibody (red signal), whereas only injected MPCs pre-labeled with PKH-67 prior cell transplantation are directly visible (green signal). The right image shows superimposed pictures obtained for each fluorophore. Scale bar, 25 µm.

Figures

Suppl. Fig. 2:

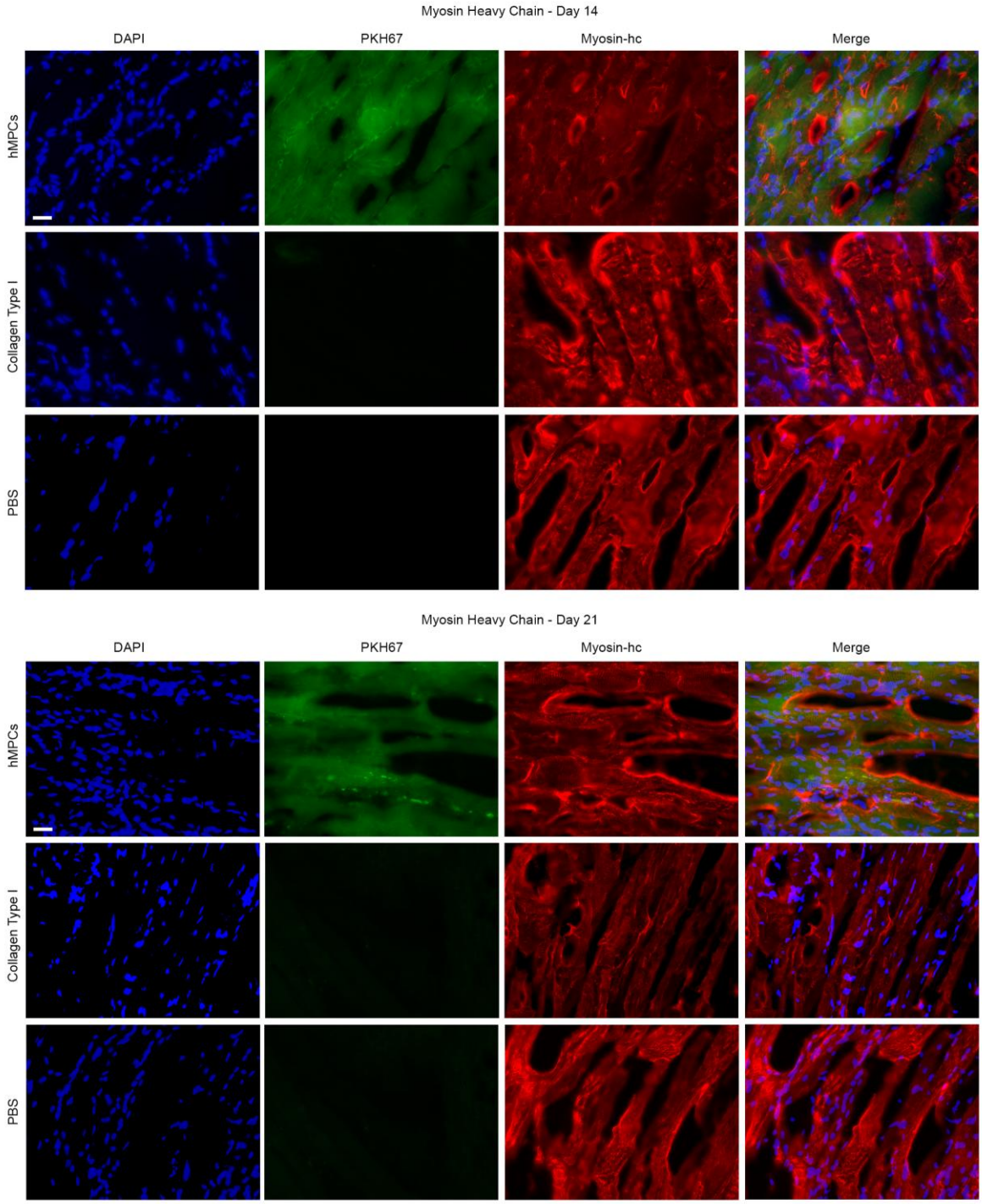

Immunofluorescent images detecting myosin heavy chain during the myogenic differentiation of the *tibialis anterior* musculature on POD 14 (upper panel) and on POD 21 (lower panel). Nuclei are stained by DAPI (blue signal) and myosin heavy chain (myosin-hc) by cyanine-3 conjugated antibody (red signal), whereas only injected MPCs pre-labeled with PKH-67 prior cell transplantation are directly visible (green signal). The right image shows superimposed pictures obtained for each fluorophore. Scale bar, 25 µm.

Suppl. Fig. 3:

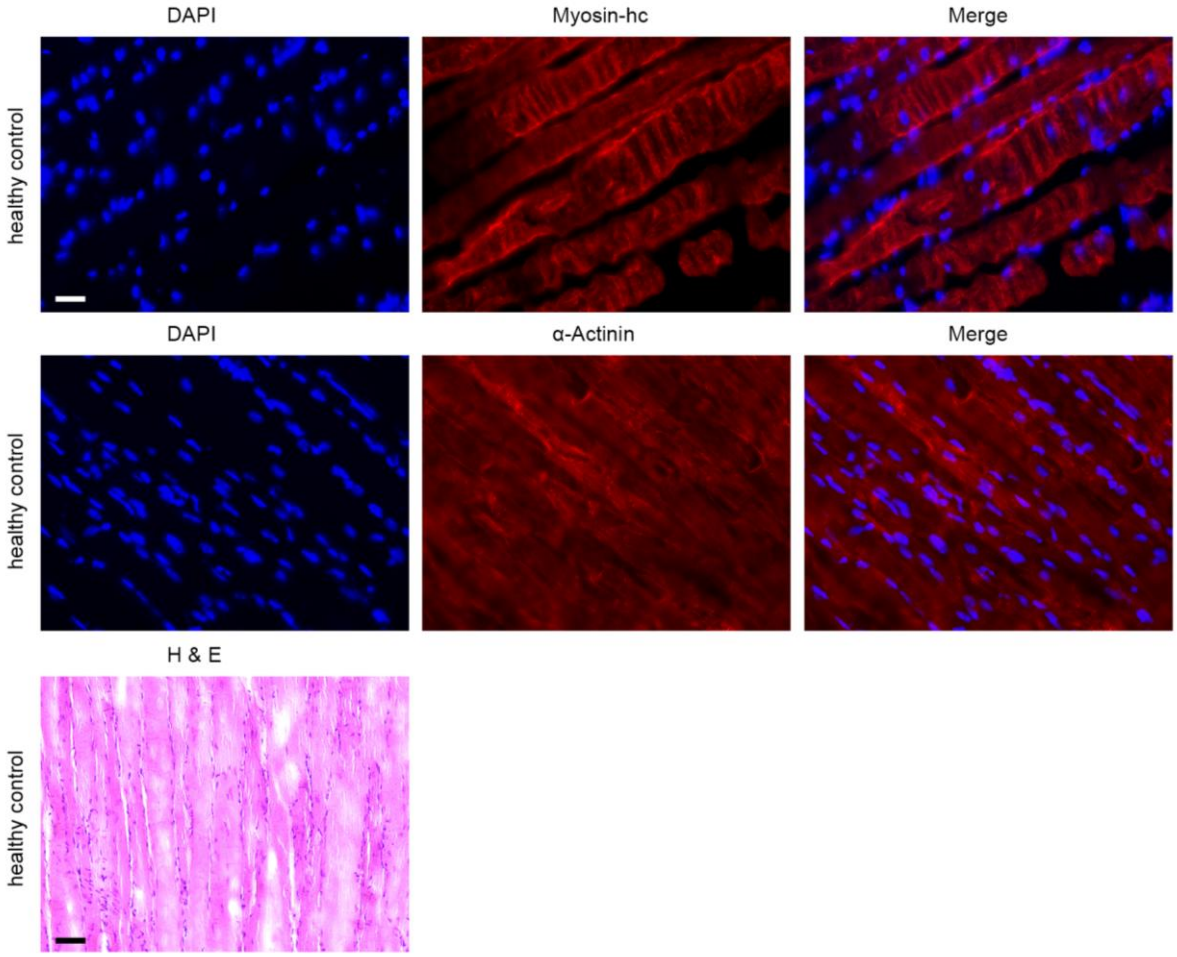

Immunofluorescent images detecting myosin heavy chain (upper panel) and sarcomeric α-actinin (lower panel) in a healthy *tibialis anterior* musculature serving as control tissue. Nuclei are stained by DAPI (blue signal) and myosin heavy chain (myosin-hc) by cyanine-3 conjugated antibody (red signal - upper panel) respectively α-actinin (red signal - lower panel). The right images show superimposed pictures obtained for each fluorophore. Scale bar, 25 µm.

The image below depicts the morphology of skeletal muscle on a representative H&E stained cryosection of healthy *tibialis anterior* musculature. Hematoxylin stained nuclei appear blue, whereas eosin stains proteins nonspecifically pink. The image shows of a *tibialis anterior* muscle specimens. Scale bar, 100 µm.

4 Curriculum Vitae

EDUCATION

2015 – 2018	***PhD*-studies** in Integrative Molecular Medicine Life Science Zurich Graduate School, University of Zurich
2013 – 2014	***Master of Science*** in Human *Biology* University of Zurich
2012 – 2013	***Bachelor of Science*** in Molecular Bioanalytics University of Applied Sciences Northwestern Switzerland FHNW
2010 – 2012	*Basic studies* in Biology and Environmental Sciences University of Zurich
2002 – 2008	***Matura / A-levels*** in Economics and Law Kantonsschule Zürcher Oberland KZO Wetzikon

EXPERIENCE

Work

01/2015 – 08/2018	**Research Associate**, University Hospital Zurich PhD-Thesis, Full Time Research Supervisors: Eberli Daniel MD PhD, Boss Andreas MD PhD
11/2013 – 11/2014	**Research Associate**, University Hospital Zurich Master Thesis, Full Time Research Supervisor: Salemi Souzan PhD, Eberli Daniel MD PhD
07/2013 – 08/2013	**Research Internship**, University Hospital Zurich Supervisor: Provenzano Maurizio MD PhD
04/2013 – 06/2013	**Research Associate**, University Hospital Zurich Bachelor Thesis, Full Time Research Supervisor: Provenzano Maurizio MD PhD, Gygax Daniel PhD
08/2012 – 09/2012	**Substitute Secondary School Teacher**, Sekundarschule Brugg
07/2012 – 10/2012	**Research Internship**, University of Applied Sciences Northwestern Switzerland Supervisor: Fent Karl PhD, Brun Nadja PhD
02/2011 – 06/2012	**Administrative Employee**, Swiss Federal Institute of Aquatic Science and Technology

Military (***Swiss Armed Forces***; Rank: Captain (NATO-Code: OF-2))

01/2018 – present	**Member of the Biosafety Level 3 Specialist Unit**, NBC laboratory battalion 1
08/2016 – 12/2017	**NBC specialist platoon leader / Deputy unit commander**, NBC laboratory unit 1/3
01/2016 – 12/2019	**Substitute judge**, Military court 6
01/2014 – 07/2016	**Quartermaster / staff officer** in a Airforce support brigade
03/2009 – 04/2010	**Compulsory Military Service** including Military Training School, senior non-commissioned officer school and logistic officer school